Title
miRNA-independent function of lnc-pri-miRNA loci

Author
He, Daniel

Publication Date
2021

Peer reviewed|Thesis/dissertation

miRNA-independent function of lnc-pri-miRNA loci

by
Daniel He

DISSERTATION
Submitted in partial satisfaction of the requirements for degree of
DOCTOR OF PHILOSOPHY

in

Developmental and Stem Cell Biology

in the

GRADUATE DIVISION
of the
UNIVERSITY OF CALIFORNIA, SAN FRANCISCO

Approved:

DocuSigned by:
Robert Blelloch
91DFF4C4A2FF4FC...

Robert Blelloch
Chair

DocuSigned by:
Daniel Lim

Daniel Lim

DocuSigned by:
Joseph Costello

Joseph Costello

DocuSigned by:
Barbara Panning
B18F20197C95417...

Barbara Panning

Committee Members

Acknowledgements

I am first and foremost extremely lucky and grateful to have family that is supportive of my academic endeavors throughout my life. As the first of my family to graduate college, I've learned the true value of hard-work, determination, and love through my parents. They continue to serve as inspiration for me to grow and become a better version of myself every day.

I am incredibly grateful to have had the opportunity to learn and grow as a scientist in the laboratory of Dr. Daniel Amos Lim. Dr. Lim has an unparalleled work-ethic that is motivating and inspiring for his students and mentees. I can truly say that I've never worked with a mentor that is so meticulously involved with the growth and success of his mentees. These past 5 years in Dr. Lim's lab will remain with me forever, and I will never forget the lessons I've learned about how to be a good scientist, and a good person.

Without a doubt, the academic environment within Dr. Lim's lab is mentally stimulating – where research spans from fine-grain detail of molecular biology, to broader impact health-care tools. I'd like to thank the lab members for all the help and invigorating discussions we've had. In particular, David Wu, a talented MSTP student in the lab was directly involved with my thesis project in the molecular dissection of *LOC646329*.

Outside of the lab, Dr. Aaron Diaz, Soren Muller, and Lin Wang were absolutely instrumental in my thesis project. Their knowledge and approaches from a computational biology standpoint really helped answer questions that elevated our findings and broadened the perspective of our work. I'd like to thank my thesis committee members, which was a team of extraordinary scientists whom I look up to. Dr. Robert Blelloch, Dr. Joe Costello, and Dr. Barbara Panning are all extremely accomplished scientists who gave invaluable guidance throughout my years at UCSF.

Prior to my graduate education, there are a number of academic mentors that have inspired and instilled the confidence I needed to become a graduate student. I'm extremely appreciative to have had the opportunity to learn from Dr. Stacey Harmer, and Dr. Peggy Farnham at UC Davis. As an undergraduate researcher in Dr. Harmer's and Dr. Farnham's lab, I was introduced to the world of academic science. This inspired me to continue working in academic science after my undergraduate education, where I continued to learn under Dr. Abby Dernburg at UC Berkeley. With Dr. Dernburg, I learned about what it meant to be a full-time scientist. This experience launched me into one of the most transformative experiences I've had since graduating from UC Davis. I worked with Dr. Benoit Bruneau at the Gladstone Institutes, where I was treated more like a graduate student with intellectual freedom, rather than a staff employee. It was in Dr. Bruneau's lab where I was truly inspired to become a graduate student myself. Without every single one of these people, and every single one of these events, I would not be where I am today – for that, I am truly grateful.

miRNA-independent function of lnc-pri-miRNA loci

Daniel He

Abstract

Among the large, diverse set of mammalian long noncoding RNAs (lncRNAs), long noncoding primary microRNAs (lnc-pri-miRNAs) are those that host miRNAs. Whether lnc-pri-miRNA loci have important biological function independent of their cognate miRNAs is poorly understood. From a genome-scale lncRNA screen, lnc-pri-miRNA loci were enriched for function in cell proliferation, and in glioblastoma (GBM) cells with *DGCR8* or *DROSHA* knockdown, lnc-pri-miRNA screen hits still regulated cell growth. To molecularly dissect the function of a lnc-pri-miRNA locus, we studied *LOC646329* (*a.k.a. MIR29HG*), which hosts the miR-29a/b1 cluster. In GBM cells, *LOC646329* knockdown reduced miR-29a/b1 levels, and these cells exhibited decreased growth. However, genetic deletion of the miR-29a/b1 cluster (*LOC646329-miR29Δ*) did not decrease cell growth, while knockdown of *LOC646329-miR29Δ* transcripts reduced cell proliferation. The miR-29a/b1-independent activity of *LOC646329* corresponded to enhancer-like activation of a neighboring oncogene (*MKLN1*), regulating cell propagation. The *LOC646329* locus interacts with the *MKLN1* promoter, and antisense oligonucleotide knockdown of the lncRNA disrupts these interactions and reduces the enhancer-like activity. More broadly, analysis of genome-wide data from multiple human cell types showed that lnc-pri-miRNA loci are significantly enriched for DNA looping interactions with gene promoters as well as genomic and epigenetic characteristics of transcriptional enhancers. Functional studies of additional lnc-pri-miRNA loci demonstrated cognate miRNA-independent,

enhancer-like activity. Together, these data demonstrate that lnc-pri-miRNA loci can regulate cell biology via both miRNA-dependent and miRNA-independent mechanisms.

Table of Contents

List of Figures

List of Tables

Chapter 1: Introduction

Summary

Long noncoding RNAs (lncRNAs) – transcripts longer than 200 nucleotides (nt) that have little evidence of protein coding potential – have been discovered to have critical biological roles, functioning through diverse molecular mechanisms. Given their broad definition, lncRNAs are comprised of a wide array of extremely diverse and heterogeneous transcripts. Based on differences in lncRNA transcript structure, processing, and the local genomic context, several major lncRNA subclasses can be identified. lncRNAs can be processed by different mechanisms, and therefore produce "non-traditional" transcripts – they can be capped with small nucleolar RNAs (sno-lncRNAs), derived from spliced intron lariats to form circular RNAs (circRNAs), or processed together with miRNA(s) to form lnc-pri-miRNA(s). Detailed studies of individual lncRNAs can shed light on shared molecular mechanisms potentially utilized by subclasses of lncRNAs with shared features. For each lncRNA subclass, it is important to experimentally define the various molecular mechanism(s) encoded by these loci. Thus, this introduction focuses on a few examples of these diverse lncRNAs that differ greatly according to their molecular features and genesis. Together, these examples demonstrate how the study of specific lncRNAs can inform us about the multifaceted complexity of lncRNA function in cellular biology.

Background

An increasing number of lncRNAs – transcripts longer than 200 nt that have little evidence of protein coding potential – have been discovered to have important biological roles, functioning via diverse molecular mechanisms (Djebali et al., 2012; Ulitsky and Bartel, 2013). Given their broad definition, lncRNAs are a particularly heterogeneous class of transcripts. However, based on differences in lncRNA transcript structure, processing, and the local genomic context, several major lncRNA subclasses can be defined (Wu et al., 2017). For each lncRNA subclass, understanding the differences that characterize each subclass may provide key insights into how this vast and complex part of the noncoding genome may function.

Most lncRNAs in the genome are biochemically identical to those of protein coding messenger RNAs (mRNAs) - they are transcribed by RNA Polymerase II, contain a 5' cap, spliced, and polyadenylated (Quinn and Chang, 2016). However, we have begun to discover that there are subsets of lncRNAs that do not possess these common features. lncRNA genes can have vast differences in RNA processing, which can lead to diverse transcript products. These differences include lncRNAs with small nucleolar RNA (snoRNA) caps, those that are derived from spliced introns to form circles, and those that are processed by canonical miRNA machinery. These diverse methods of processing may therefore reflect distinct mechanisms by which they function.

lncRNAs have been proposed to function through diverse mechanisms, including transcriptional regulation in *cis* or *trans*, organization of nuclear domains, and regulation of protein binding (Ulitsky and Bartel, 2013). Moreover, the assorted function of these lncRNA loci can be found embedded within the lncRNA gene itself (e.g. by harboring DNA regulatory

elements) rather than the lncRNA molecule (Engreitz et al., 2016; Groff et al., 2016). Recent findings have added another layer to this complexity by demonstrating that these functions may not be mutually exclusive. For example, antisense lncRNA transcription can regulate DNA elements in-*cis*, which in turn mediates protein binding in the mouse olfactory neurons to ensure proper enhancer-promoter contacts for Protocadherin gene expression (Canzio et al., 2019). Therefore, it is important to use tools and strategies directed at experimentally dissecting the function(s) of lncRNA loci.

In this chapter, I will focus on a couple of subclasses of lncRNAs defined by differences in lncRNA processing. By discussing lncRNAs from each of these subclasses, I hope to demonstrate how detailed investigation of each of these examples can provide insight into the common mechanism(s) of function of lncRNAs with shared features.

Sno-lncRNAs

One subclass of lncRNAs include those that are processed from snoRNA host genes (sno-lncRNAs). These sno-lncRNAs are flanked by snoRNAs, rather than the typical 5' cap and poly(A) tail. Utilizing deep RNA-sequencing of poly(A)+ and poly(A)- fractions, numerous stable intron-derived lncRNAs were identified as sno-lncRNAs (Yang et al., 2011). SnoRNAs carry out their function by forming complexes with specific protein components, forming ribonucleoprotein (RNP) complexes (Kiss, 2001). It was then demonstrated that sno-lncRNAs also had the capability to associate with such proteins, and mutations of the snoRNAs could result in reduced processing or even completely block sno-lncRNA generation (Yin et al., 2012). Notably, a cluster of sno-lncRNAs located on chromosome 15 – encompassing a 60kb region --

are deleted in patients with Prader-Willi Syndrome (PWS) (Cassidy et al., 2012), implicating these sno-lncRNAs in the molecular pathogenesis of PWS. Interestingly, knockdown of all 5 PWS region sno-lncRNAs using antisense oligonucleotides (ASOs) did not dramatically alter global gene expression.

In human embryonic stem (ES) cells, crosslinking followed by immunoprecipitation and sequencing (CLIP-seq) revealed that each of these sno-lncRNA transcripts from the PWS region bound the alternative splicing regulator, Fox2 (Yeo et al., 2009). Knockdown of these sno-lncRNAs resulted in splicing changes related to exons regulated by Fox proteins, while gene expression was not altered. Yin *et al*., therefore proposes that the binding of sno-lncRNAs to Fox2 act as a molecular sink to locally modulate splicing at specific sites within the nucleus.

Super-resolution structured illumination microscopy (SIM) demonstrated that a sno-lncRNA named *SLERT* interacted with the rRNA processing RNA helicase DDX21 specifically in the nucleolus (Sloan et al., 2015). *SLERT* has the ability to bind to and modulate the conformation of DDX21 proteins, which can subsequently change the size of DDX21 protein "ring-like" aggregates. These DDX21 conformation changes can lead to subsequent changes in pre-RNA transcription and rRNA processing (Xing et al., 2017). Notably, *SLERT* is another example of a sno-lncRNA that can bind to protein partners and function at site-specific regions within the cell. Although *SLERT* and PWS region sno-lncRNAs exhibit distinct cellular localization, which factors determine their post-transcriptional cellular localization is still unclear. However, based on studies of these sno-lncRNAs, it is suggested that these transcripts can partner with proteins and function at very site-specific regions within the cell.

Circular lncRNAs

Circular RNAs were first described in the 1970s as components of the viral genome (Sanger et al., 1976). Recent studies have suggested that some lncRNAs can indeed form circles (circRNAs). Due to their circular structure, circRNAs are more stable than their linear lncRNA counterparts, as they cannot be degraded by most RNA degradation machinery (Vicens and Westhof, 2014). These circRNAs are derived from lncRNAs that have failed intronic lariat debranching during canonical splicing (Zhang et al., 2013). Although circRNAs have been observed for many decades now, relatively little is known about the function of these odd ring-like shaped molecules.

Recent studies suggest a mechanism of function that is common amongst many circRNAs – in which circRNAs act as molecular sinks for sponging miRNAs. Although many circRNAs are found within the cell, some can be found in small membrane vesicles called exosomes in relatively abundant numbers (Li et al., 2015). In hepatocarcinoma cells, the circRNA circ-DB was found to sponge miR-34a, therefore de-repressing *USP7* (a target of miR-34a), promoting tumor growth (Zhang et al., 2019a). Similarly, the circRNA *ciRS-133* found in exosomes of gastric cancer cells can sponge miR-133, which activates PRDM16 to promote tumorigenesis (Zhang et al., 2019b). Although these are extracellular examples of circRNAs, evidence of intracellular circRNA function is similar.

In both the human and mouse brain, the antisense transcript of cerebellar degeneration-related protein 1 (*CDR1as*) is a circRNA found in the cytoplasm of neurons. *CDR1as* contains as many as 70 binding sites for miR-7 and one binding site for miR-671 (Memczak et al., 2013). However, unlike the traditional circRNAs acting as miRNA sponges, CDR1as knockout in the

mouse resulted in downregulation of miR-7, and upregulation of miR-7 target mRNAs – which in turn led to dysfunction of excitatory synaptic transmission (Piwecka et al., 2017). This finding was in contrast to the previously proposed miRNA sponge activity of CDR1as and brought to light the complex nature of circRNAs. It is proposed that CDR1as binds to miR-7 to stabilize it and translocate miR-7 to synapses (Piwecka et al., 2017). Whether circRNAs primarily function to promote or antagonize miRNA activity is still unclear. However, these stable RNA molecules are indeed capable of binding miRNAs to influence their activity.

Concluding remarks

Among the large, diverse set of long noncoding RNAs (lncRNAs) produced by mammalian cells, many have been initially described as non protein-coding mRNA-like transcripts. Recent studies revealed unique features – such as alternative forms of biogenesis and functional RNA domains -- of lncRNAs that can further distinguish them from mRNAs. Our recent understanding of lncRNA "subclasses" based on these unique features may be useful for studying these lncRNAs in "groups", where we can attempt to understand function that may be enriched within a specific sub-group. For example, many sno-lncRNAs seem to depend on the snoRNAs for transcript stabilization and RNP formation. With sno-lncRNAs having very specific localization within the cell, it's currently proposed that sno-lncRNAs serve as molecular "landing pads" for coordinated site-specific with protein complexes. However, the field is at its infancy, and only a select few sno-lncRNAs have been characterized.

Another subgroup of lncRNAs with an observed common mechanism of action are the circRNAs. Although these are relatively abundant and seemingly conserved throughout all

domains of life (Danan et al., 2012), we are still only starting to understand the full repertoire of regulatory function of these exotic molecules. A well-characterized circRNA such as CDR1as seems to contain many (up to 70) miRNA binding sites for miR-7 – this makes CDR1as a great lncRNA candidate to serve as a miRNA sponge or even a "vesicle" for miRNA transport. Although it is clear CDR1as can bind to miR-7, at this point in the field, it's not entirely clear why CDR1as is binding to miR-7. Although some circRNAs can indeed bind miRNAs, there have been reports of those that can bind proteins and act as scaffolds (Du et al., 2016; Li et al., 2019)

This chapter focused on a few examples of lncRNAs with unique features that can help distinguish one set of lncRNAs from another. With the current state of deep RNA-sequencing technology, we are rapidly discovering more lncRNA genes than we have thoroughly characterized. Whether or not the above lncRNAs all have a generalized mechanism common to their subclass comes down to rigorous characterization of each subclass of lncRNAs – perhaps by first using one as an example through a detailed molecular study. Moving forward, a combination of useful techniques for studying lncRNAs such as targeted genetic engineering using CRISPR, modulation of lncRNA transcription using CRISPRi or CRISPRa, along with techniques to probe transcript function by using antisense oligonucleotides (ASOs) and short hairpin RNAs (shRNAs) would be promising for dissecting lncRNA function. With the lncRNA field in its relative infancy, useful and innovative tools for interrogating lncRNA function will continue to grow and develop over time. The following chapters will now focus on our attempt at understanding a subclass of lncRNAs that produce miRNAs (lnc-pri-miRNAs), and how these lnc-pri-miRNAs may be enriched for dual function.

Chapter 2: lnc-pri-miRNA are at elevated levels in human glioblastoma and enriched for function

Summary

Glioblastoma multiforme (GBM) is the most common and deadly type of primary brain tumor. How lncRNAs may contribute to the pathogenesis of GBM is not known. One of the first steps to understanding how lncRNAs may contribute to this pathogenic process is through the profiling of lncRNA levels in GBM tissues. Here, we investigate lnc-pri-miRNA expression levels (compared to all other lncRNAs) in human GBM (166 patient samples) and low-grade glioma tumors (LGG, 530 patient samples). We find that lnc-pri-miRNAs are expressed at levels ~2-fold higher in GBM when compared to LGG. This trend was also observed when we examined patient-matched biopsies. Moreover, in a CRISPRi screen of 5,689 lncRNA loci in U87 GBM cells, lnc-pri-miRNAs were enriched for essential cellular function.

Introduction

An increasing number of long noncoding RNAs (lncRNAs) – transcripts longer than 200 nucleotides (nt) that have little evidence of protein coding potential – have been discovered to have important biological roles, functioning via diverse molecular mechanisms (Djebali et al., 2012; Ulitsky and Bartel, 2013). Given their broad definition, lncRNAs are a particularly heterogeneous class of transcripts. However, based on differences in lncRNA transcript structure, processing, and the local genomic context, several major lncRNA subclasses can be defined (Wu et al., 2017). For each lncRNA subclass, understanding how their expression and function are distinct from the larger set of lncRNAs may provide key insights into this vast and

complex part of the noncoding genome.

One lncRNA subclass is comprised of long noncoding primary microRNAs (lnc-pri-miRNAs) – transcripts that are processed to produce microRNAs (miRNAs) (Quinn and Chang, 2016). miRNAs are short (~22 nt) noncoding transcripts that regulate gene expression post-transcriptionally by promoting messenger RNA (mRNA) degradation and/or inhibiting translation (Treiber et al., 2019). miRNAs are generally derived from primary transcripts termed "pri-miRNAs," and while the majority of pri-miRNAs are transcribed from protein coding genes, approximately 600 miRNAs are produced from lnc-pri-miRNAs (Chang et al., 2015). Other than their inclusion of miRNA sequences, the features that distinguish lnc-pri-miRNAs from the broader set of lncRNAs has not been characterized. In this chapter, we focus on the transcriptomic levels of lncRNAs (lnc-pri-miRNAs vs all other lncRNAs) observed in GBM vs LGG.

Results

lnc-pri-miRNAs are enriched in high-grade glioma

We analyzed the transcriptomes of 530 low-grade glioma (LGG) and 166 glioblastoma (GBM) patient samples in The Cancer Genome Atlas (TCGA) (Ceccarelli et al., 2016) and found that lnc-pri-miRNAs were at levels approximately 2-fold higher in GBM as compared to LGG (**Fig. 2.1A, B**, **Table S2.1**). In contrast, neither the broader set of lncRNAs nor pri-miRNAs were significantly elevated in the higher-grade GBM brain tumors (**Fig. S2.1A, B**). Of note, lnc-pri-miRNA expression alone was sufficient to distinguish GBM and LGG patients (**Fig. 2.1C, D**).

To ask if there are shared features of lnc-pri-miRNA that may underlie their increased expression in GBM, we analyzed genomic regions encompassing the promoter (2kb upstream to 100bp downstream of TSS) of the lnc-pri-miRNAs and other lncRNAs. *SWI5* is the top ranked motif enriched in lnc-pri-miRNA promoters (~71% of lnc-pri-miRNA contained this motif), while *ZNF519* is the top enriched (~59%) motif in the set of "other" lncRNA promoters (**Fig. S2.1B**). The enrichment of the *SWI5* motif discovered in lnc-pri-miRNA promoters but not in "other" lncRNA promoters distinguish lnc-pri-miRNA from the broader set of lncRNAs, suggesting distinct regulation.

To more directly correlate lnc-pri-miRNA expression with glioma disease progression, we obtained patient-matched tumor biopsies (n=31 pairs) obtained from the initial diagnosis and after tumor recurrence. In recurrent glioma, 12 out of 16 lnc-pri-miRNAs were expressed at increased levels as compared to the primary tumor (**Fig. 2.1E**, **F**, **Table S2.2**). Consistent with the comparison of GBM and LGG, the broader set of lncRNAs was not elevated during glioma progression in individual patients (**Fig. 2.1E, F**). Similarly, pri-mRNAs were not any more

likely to be elevated in recurrent tumors as compared to protein coding genes (**Fig. S2.1C**). Thus, lnc-pri-miRNAs are a transcriptionally distinct subset of lncRNAs in human gliomagenesis.

Discussion

Taken together, our data suggest that increased lnc-pri-miRNA expression observed in patient-derived high-grade glioma tumors and the enrichment of cellular propagation function in U87 GBM cells (Liu et al., 2017) have functional relevance that may contribute to the progression of these aggressive brain tumors. However, we do not know exactly how each of these lnc-pri-miRNAs found in GBM may actually contribute to gliomagenesis. The well-studied oncogene MYC has been proposed to globally repress miRNA expression during tumorigenesis by occupying and regulating pri-miRNA promoters (Chang et al., 2008). Interestingly, miRNAs derived from protein-coding genes (pri-miRNAs) were not found at increased levels in GBM. Furthermore, our analyses of the promoter regions of lnc-pri-miRNAs with increased levels observed in GBM (**Fig. S2.1B**) revealed distinct transcription factor motifs than those of MYC – suggesting a different driver for the expression-level changes observed in GBM. Future work to carefully examine how lnc-pri-miRNA expression changes relate to gliomagenesis may reveal important biological function that is interwoven within complex loci such as lnc-pri-miRNAs.

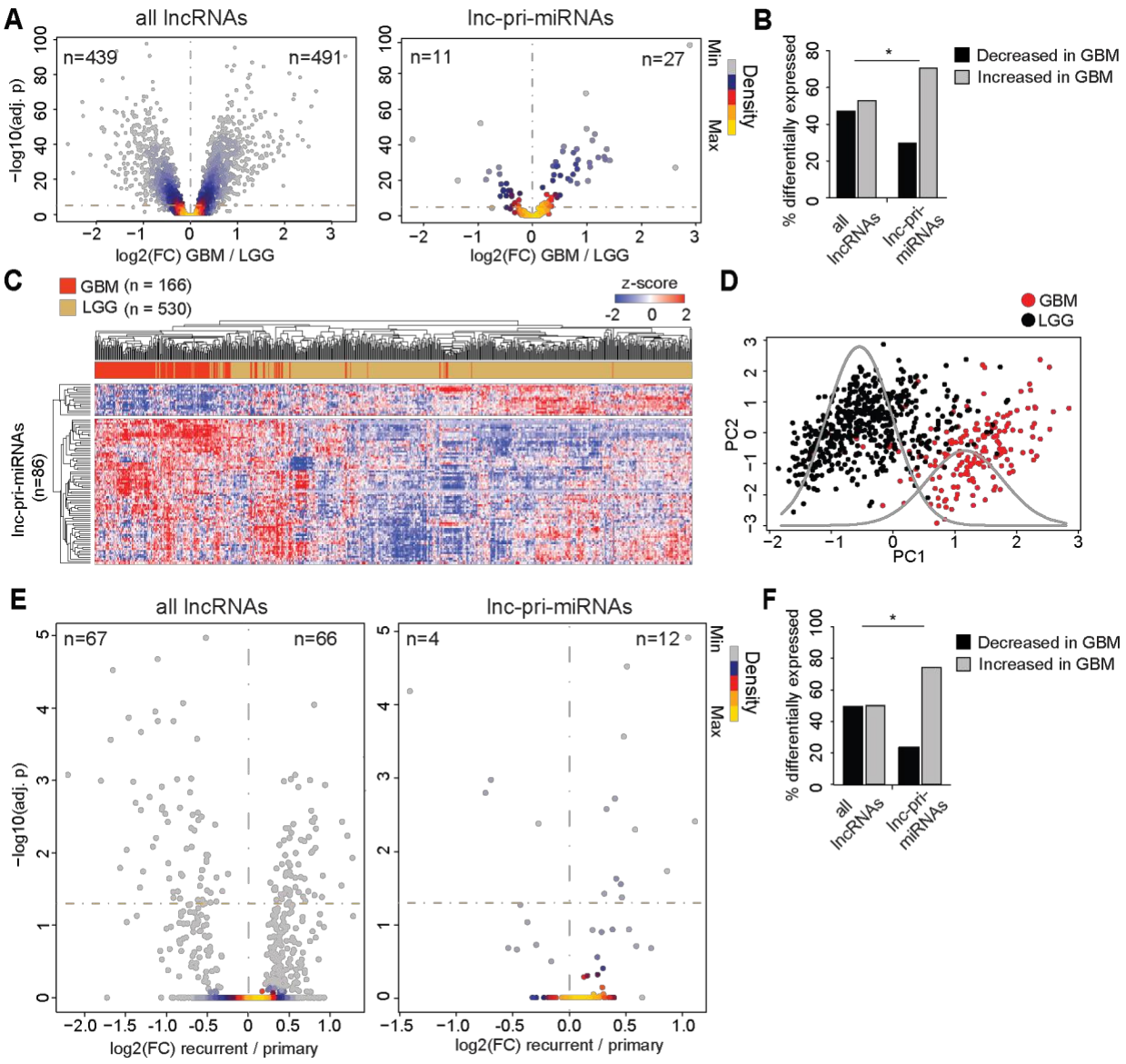

Figure 2.1 lnc-pri-miRNAs are a distinct subclass of lncRNA enriched in GBM.

(A) Volcano plots of lncRNA and lnc-pri-miRNA expression in GBM vs. LGG patient samples. Each dot represents a single lncRNA. (B) Quantification of differentially-expressed lncRNAs and lnc-pri-miRNAs. * *P-value* < 0.05, Fisher's exact test. (C) Unsupervised hierarchical clustering of lnc-pri-miRNA expression across all glioma samples. (D) Principle component analysis of GBM and LGG samples. (E) Volcano plots of lncRNA and lnc-pri-miRNA expression in patient-matched tumor biopsies from initial diagnosis and tumor recurrence. (F) Quantification of differentially-expressed lncRNAs and lnc-pri-miRNAs. * *P-value* < 0.05, Fisher's exact test.

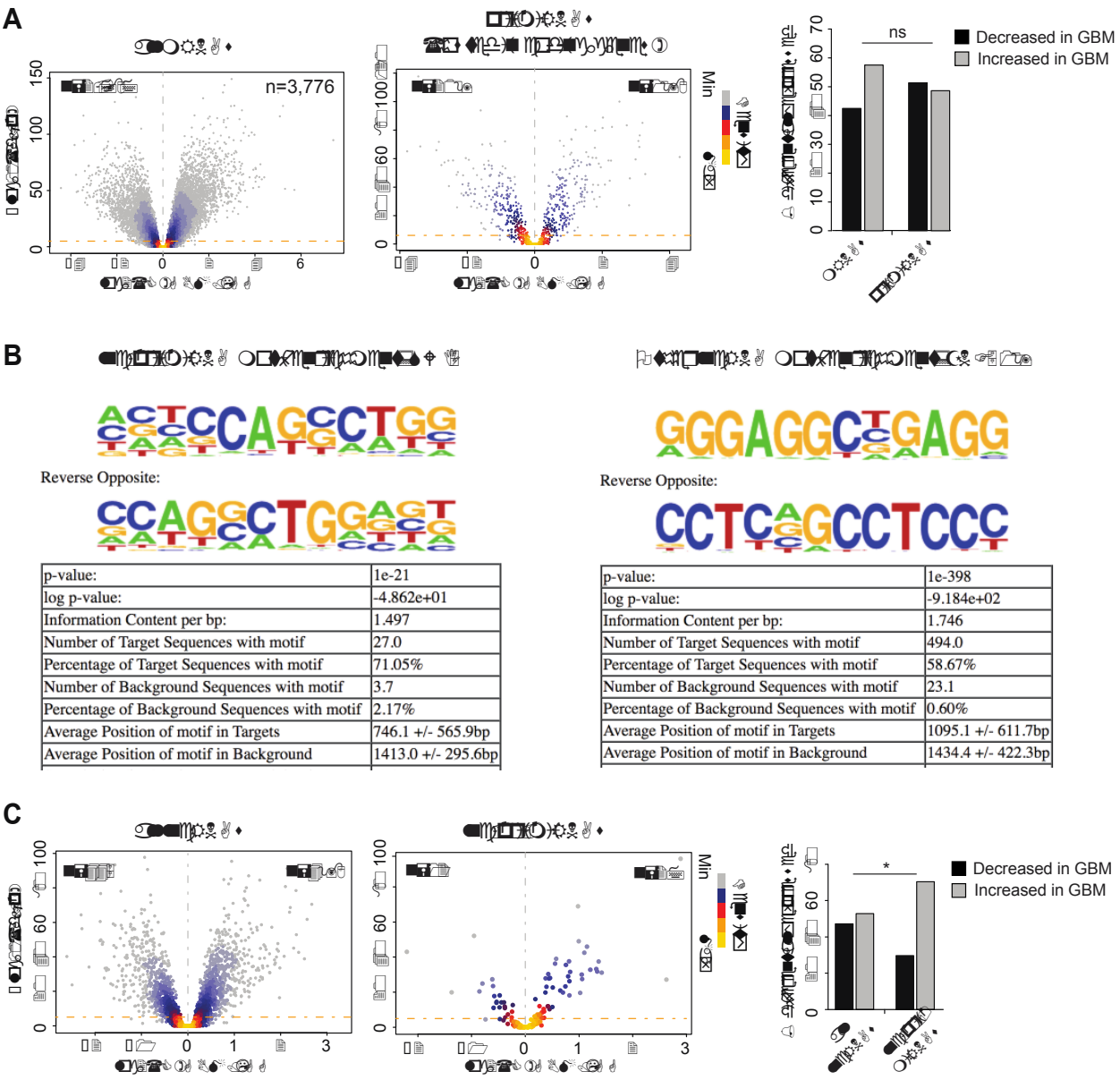

p-value:	1e-21
log p-value:	-4.862e+01
Information Content per bp:	1.497
Number of Target Sequences with motif	27.0
Percentage of Target Sequences with motif	71.05%
Number of Background Sequences with motif	3.7
Percentage of Background Sequences with motif	2.17%
Average Position of motif in Targets	746.1 +/- 565.9bp
Average Position of motif in Background	1413.0 +/- 295.6bp

p-value:	1e-398
log p-value:	-9.184e+02
Information Content per bp:	1.746
Number of Target Sequences with motif	494.0
Percentage of Target Sequences with motif	58.67%
Number of Background Sequences with motif	23.1
Percentage of Background Sequences with motif	0.60%
Average Position of motif in Targets	1095.1 +/- 611.7bp
Average Position of motif in Background	1434.4 +/- 422.3bp

Figure S2.2 Protein coding pri-miRNAs are not any more likely enriched in GBM.

(A) Volcano plots of mRNA and pri-miRNA expression in GBM vs. LGG patient samples. Right hand panel includes quantification of differentially-expressed mRNAs and pri-miRNAs. ns= not significant, Fisher's exact test. (B) HOMER2 motif analyses of the promoters (2kb upstream to 100bp downstream) of lncRNAs found elevated in GBM. Left panel shows lnc-pri-miRNA analysis, while the right panel shows "other lncRNA" analysis. (C) Volcano plots of lncRNA and lnc-pri-miRNA expression in GBM vs. LGG patient samples. Each dot represents a single lncRNA. Right hand panel includes quantification of differentially-expressed lncRNAs and lnc-pri-miRNAs. * P-value < 0.05, Fisher's exact test.

Table S2.1 GBM vs LGG

All lncRNAs GBM vs LGG (adj. p-value < 0.05)

ID	LogFC	adj. p
CYP17A1-AS1	-0.9327896	2.29E-98
AL139289.1	0.94436209	4.41E-96
AC062021.1	-1.5728563	4.97E-94
AC026785.2	2.14367766	5.82E-92
AC009227.1	-0.8676259	2.27E-91
AC125611.3	3.2939736	3.40E-91
AL355472.3	1.31160623	1.17E-87
AC008781.1	0.92822482	6.28E-86
AC096772.1	0.77576741	1.74E-85
AC112491.1	1.55141185	3.62E-85
AC134349.1	0.88034228	5.70E-83
AP005329.1	2.10401571	1.93E-81
NUCB1-AS1	1.26246779	8.79E-81
AL133415.1	2.33112658	4.03E-79
LINC02067	1.2282625	9.54E-79
PWAR5	-1.4427379	9.67E-79
SLC25A21-AS1	-1.8794974	2.13E-77
AC015540.1	-0.8042934	1.55E-76
AC021224.1	1.21033663	2.28E-74
AL031320.2	1.23423443	1.93E-73
AC069228.1	-0.7953576	3.07E-72
AC022167.2	0.97651442	9.82E-72
COL4A2-AS1	2.67210857	3.65E-71
AC011603.2	1.29527796	1.58E-70
LINC01943	2.20786945	2.62E-69
AL390195.1	0.78341244	8.91E-69
AL117339.4	-0.995604	2.86E-68
EPB41L4A-AS1	-0.9332238	5.46E-68
AC053503.1	-1.3526134	2.86E-67
AC135050.7	1.18015846	6.54E-67
VIM-AS1	2.19097219	1.41E-66
AC092162.3	-1.0010576	7.59E-66
AL118505.1	-2.301393	5.17E-65
AC020915.4	0.88047879	5.23E-65

Table S2.1 GBM vs LGG

All lncRNAs GBM vs LGG (adj. p-value < 0.05)

ID	LogFC	adj. p
AL391834.2	-0.7154538	2.01E-64
OLMALINC	-1.1686336	1.52E-63
LINC01579	2.57179861	1.87E-62
AL049749.1	-0.8462948	2.33E-61
Z94057.1	-1.8904107	3.45E-61
AC010273.1	0.78389427	4.90E-61
AC113133.1	-0.6395678	8.57E-61
DNMBP-AS1	-0.9575918	1.69E-60
AC091564.3	1.03170653	3.10E-60
AC026401.3	1.33148815	3.38E-60
GDNF-AS1	-1.6089725	8.28E-60
AC009102.2	-1.2335617	1.33E-59
AP000688.1	1.58693847	2.75E-59
AC067969.2	-0.8753977	4.09E-59
AL645608.1	-1.5673575	4.75E-59
LINC01561	-1.4382709	5.01E-59
AC124312.2	-0.8803157	7.96E-59
AC245060.5	-0.9197516	1.70E-58
AC073864.1	-1.2373854	3.29E-58
WAC-AS1	-0.890104	3.62E-58
AC093673.1	1.48598475	7.16E-58
AL590385.2	1.81126778	7.27E-58
LINC00906	-1.1699312	3.51E-57
AL157700.1	-1.4174932	4.18E-57
AL022313.4	-2.2840149	4.76E-57
ARSD-AS1	1.36330377	7.65E-57
FAM201A	-1.1442172	9.72E-57
AC079907.1	0.79125347	1.13E-56
AC092069.1	1.14415054	1.18E-56
AP000721.2	-1.196417	1.70E-56
DGUOK-AS1	0.89718429	2.28E-56
AL445685.1	0.6512694	2.69E-56
AC073320.1	0.63618354	2.78E-56
AC007342.7	-0.7814649	3.10E-56
AL358334.3	1.49826933	3.22E-56

Table S2.1 GBM vs LGG

All lncRNAs GBM vs LGG (adj. p-value < 0.05)

ID	LogFC	adj. p
AP000879.1	0.7445333	2.81E-55
AL353796.1	-0.8707335	3.27E-55
AL445524.1	0.81713365	3.59E-55
AL031714.1	0.67175464	4.44E-55
MIR9-3HG	-0.9510548	5.01E-55
AL132656.4	-0.8963182	6.08E-55
LIPE-AS1	0.61393618	6.11E-55
AP000223.1	-0.5225137	1.02E-54
AP001486.2	-1.335009	1.12E-54
AL163636.1	1.39606621	1.15E-54
AC132872.3	0.6186064	2.00E-54
AL020996.3	0.67793892	2.08E-54
TMEM72-AS1	-0.5342093	3.62E-54
AL731533.2	-0.5642208	4.28E-54
AC106786.2	1.04237169	5.53E-54
AC008669.1	-0.8821919	6.07E-54
AC011489.1	0.86281726	6.11E-54
AC090617.4	0.75307458	8.95E-54
AC097460.1	1.03350569	9.53E-54
AC009902.2	2.33856699	1.48E-53
AC009090.3	0.81394769	2.36E-53
AL008726.1	1.06108693	3.00E-53
AC006064.4	1.08523562	4.37E-53
AL136964.1	-0.8591809	5.86E-53
AC080128.2	-0.9248364	6.52E-53
AC010542.5	1.04329908	7.71E-53
TBC1D3P1-DHX40P1	0.92405939	1.86E-52
AC010320.2	0.68199771	2.00E-52
AC027575.2	0.67992441	5.05E-52
AP001372.3	1.3114369	6.23E-52
AC007375.3	-1.1488866	6.30E-52
WDFY3-AS2	-1.1035666	8.75E-52
ADGRA1-AS1	-1.4552191	1.85E-51
AL137141.1	-1.2087282	2.06E-51
AC120036.5	-1.1776571	2.56E-51

Table S2.1 GBM vs LGG

All lncRNAs GBM vs LGG (adj. p-value < 0.05)

ID	LogFC	adj. p
AC104793.1	-1.082255	7.60E-51
C5orf66	0.58195395	1.00E-50
AC027130.1	-0.798741	1.01E-50
LINC00836	-1.8752437	1.29E-50
AC022148.1	-0.9830061	1.63E-50
LINC00900	1.24147666	2.88E-50
AP000766.1	-0.8191252	3.47E-50
Z94160.2	-1.8935596	4.58E-50
AL445231.1	0.67563437	4.74E-50
AC011405.1	0.75208513	4.76E-50
C1RL-AS1	1.15455543	5.82E-50
DRAIC	-0.7702934	8.71E-50
AL139260.2	0.72812856	9.55E-50
AC080100.1	-1.2521492	1.06E-49
AL035458.2	0.99442686	1.14E-49
AP001029.2	-0.8901596	1.67E-49
PWAR6	-1.831007	2.95E-49
AC090425.2	0.97139	3.17E-49
AC145207.3	1.00751557	4.65E-49
SGMS1-AS1	-0.8904642	5.07E-49
AC073167.1	-0.8780667	6.51E-49
AL139274.2	-0.7273582	7.77E-49
AL365259.1	-0.8979846	1.45E-48
CD44-AS1	1.93962983	1.94E-48
AL133481.1	-0.9873041	2.06E-48
AD001527.2	0.86935818	2.56E-48
CARD8-AS1	1.03159166	2.81E-48
AC010536.3	-1.1736979	4.45E-48
AC008894.2	0.66263976	5.14E-48
AL049838.1	-1.2452646	5.49E-48
AC005696.4	-1.8446159	5.81E-48
AC008760.1	0.73221877	7.30E-48
STEAP3-AS1	1.64054613	1.12E-47
AL731571.1	-0.7484486	1.23E-47
AL391834.1	-0.6099569	1.24E-47

Table S2.1 GBM vs LGG

All lncRNAs GBM vs LGG (adj. p-value < 0.05)

ID	LogFC	adj. p
AC254562.3	-0.6085268	1.53E-47
AC012629.2	0.51453435	1.61E-47
AL451070.1	0.79597626	1.61E-47
AC020978.3	0.72360142	1.90E-47
LINC00641	-1.5961409	2.57E-47
AP006333.1	-1.3792287	2.63E-47
AC046143.1	0.59844174	4.63E-47
AL161668.3	-1.0382873	8.29E-47
IGFBP7-AS1	1.66827538	1.10E-46
AL137025.1	-0.7230774	1.15E-46
NALCN-AS1	-1.2005961	1.18E-46
AC022028.2	-0.9623695	1.39E-46
AC011511.2	0.75678392	1.50E-46
PPP3CB-AS1	-1.1002699	1.66E-46
AC023024.2	-1.196898	2.15E-46
AC025162.1	1.05017106	2.38E-46
AC007744.1	-1.5462191	4.92E-46
LACTB2-AS1	0.90904382	4.93E-46
AL355974.2	2.28104915	9.19E-46
AC068831.3	0.65750656	1.03E-45
AC006262.1	-1.0098899	1.41E-45
AC010655.2	1.56676276	1.45E-45
AC099850.3	0.8589958	1.46E-45
AC105036.3	0.64177872	1.55E-45
AC008894.3	1.21161788	2.08E-45
CNOT10-AS1	0.45782169	2.19E-45
AL078612.1	1.04000258	4.26E-45
FP671120.4	1.92145286	4.38E-45
AC002398.2	1.68488835	5.66E-45
AC009630.2	0.9954402	8.24E-45
TMEM220-AS1	1.03441688	8.45E-45
AL023806.1	-0.7412196	9.10E-45
AC008569.1	1.32414042	1.07E-44
AC004067.1	0.60330662	1.35E-44
AL133406.2	0.47386172	1.40E-44

Table S2.1 GBM vs LGG

All lncRNAs GBM vs LGG (adj. p-value < 0.05)

ID	LogFC	adj. p
AC079742.1	0.75912875	3.39E-44
AP003469.4	-1.1804244	4.65E-44
AL354740.1	-0.8410269	4.75E-44
AC064875.1	1.95181584	5.23E-44
AC010226.1	0.72812769	5.46E-44
AL132855.1	-0.8954522	6.63E-44
AC091133.1	0.54686525	7.98E-44
AC018511.2	-0.4844649	9.94E-44
AC005703.6	1.11625675	1.11E-43
ATP1A1-AS1	0.83163515	1.21E-43
AL139095.4	0.68599728	1.22E-43
AC055713.1	0.71261935	1.58E-43
TMEM5-AS1	0.48316429	1.68E-43
AC022201.2	0.43320706	1.73E-43
AL731569.1	-0.5494528	1.82E-43
AC007938.1	-0.9810639	2.03E-43
AC125257.2	0.69891528	2.17E-43
AL136131.3	2.38853238	2.71E-43
LAMTOR5-AS1	0.78429082	3.23E-43
AC010642.2	0.85928343	5.05E-43
AC022167.1	0.95188544	5.05E-43
AC011447.3	0.72478	5.77E-43
AC097382.2	-0.566349	1.03E-42
MIF-AS1	1.19825854	1.24E-42
AL512353.1	0.76320871	1.48E-42
ID2-AS1	-0.7465673	1.58E-42
CRNDE	1.76140246	1.87E-42
GK-AS1	0.63104018	2.25E-42
AC087071.2	0.76274639	2.31E-42
AL031595.3	0.94310161	2.46E-42
LINC00665	0.84483417	2.47E-42
TYMSOS	1.07772602	2.54E-42
AC004803.1	-0.8035526	2.74E-42
LRP4-AS1	-1.1882339	3.02E-42
AC092718.4	0.88683568	4.30E-42

Table S2.1 GBM vs LGG

All lncRNAs GBM vs LGG (adj. p-value < 0.05)

ID	LogFC	adj. p
AL662797.3	1.01825008	5.06E-42
PRC1-AS1	1.28330823	7.27E-42
AL591848.4	-0.7962548	8.43E-42
AP4B1-AS1	0.51340753	9.71E-42
DGCR9	-1.3148125	1.03E-41
CFLAR-AS1	0.60561841	1.32E-41
AC004158.1	-1.1596718	1.54E-41
Z99129.4	-1.0745685	1.70E-41
AC089999.2	0.41987346	1.81E-41
AC018648.1	-0.4632648	2.31E-41
LINC01426	1.22826979	3.03E-41
Z98884.1	-0.8481725	3.04E-41
AL355075.3	0.96361254	3.04E-41
AL050343.1	0.50066749	4.45E-41
AC020656.1	2.07723646	4.48E-41
AC073389.3	-0.5438846	4.65E-41
AL117332.1	0.64121478	5.30E-41
AC134772.1	0.8366657	5.47E-41
FLJ16779	-2.6086899	6.26E-41
AP002490.1	-1.5857565	6.96E-41
FAM181A-AS1	1.38017809	7.13E-41
AL662795.2	-1.1135953	8.06E-41
AC022445.1	0.38000989	8.23E-41
WDFY3-AS1	-0.7097423	8.90E-41
AC231981.1	0.79306532	9.32E-41
AC147651.3	1.01451297	1.12E-40
AC007938.2	1.90942505	1.23E-40
KCNIP2-AS1	-1.3475488	2.01E-40
AC023796.2	0.95613228	2.98E-40
AC003101.3	-1.3068566	3.04E-40
AC011481.2	0.66594212	3.17E-40
AC021739.5	-0.5891499	3.99E-40
AL391845.2	-0.6791655	4.34E-40
ACTA2-AS1	1.65299029	5.72E-40
AC020900.1	0.84740017	6.66E-40

Table S2.1 GBM vs LGG

All lncRNAs GBM vs LGG (adj. p-value < 0.05)

ID	LogFC	adj. p
AC007406.5	-0.7390933	7.37E-40
AP000911.1	-1.0250479	7.59E-40
AC020763.4	-1.319282	7.61E-40
AC079414.3	-0.5521859	7.75E-40
OTUD6B-AS1	-0.6061852	8.10E-40
AC098617.1	-0.9615393	8.73E-40
AC008870.3	1.13994312	9.06E-40
SNHG18	1.54931593	9.40E-40
AP003419.1	0.5999042	9.68E-40
AC104316.1	0.49278653	1.15E-39
AL109804.1	0.50267324	1.24E-39
HOXA-AS3	2.51465332	1.51E-39
BHLHE40-AS1	0.89222124	1.56E-39
AL590133.2	0.69104574	1.58E-39
ELFN2	-0.9162454	2.14E-39
AL020996.1	0.93660209	2.28E-39
AC016876.2	0.73031794	2.67E-39
KCNK4-TEX40	-1.1213579	2.67E-39
AL139099.2	0.60348712	2.71E-39
AC103974.1	-0.6188833	2.78E-39
AC023421.1	-0.8297221	3.06E-39
AC078883.1	0.65386118	3.08E-39
AC093484.1	0.56411414	3.60E-39
AP001107.6	0.97255887	3.66E-39
ADAMTSL4-AS1	1.16992649	4.26E-39
AC008440.2	1.04865522	4.30E-39
AC010761.1	0.83039123	4.96E-39
AC010618.3	0.690929	4.98E-39
AC002546.1	-0.9230669	5.15E-39
AC012073.1	0.54626792	5.50E-39
TTC3-AS1	-1.0272099	5.52E-39
AL603756.1	-0.6809963	5.54E-39
HOTAIRM1	1.86695788	5.71E-39
AL589765.7	0.54224665	5.86E-39
AC005070.3	-0.6842414	6.90E-39

Table S2.1 GBM vs LGG

All lncRNAs GBM vs LGG (adj. p-value < 0.05)

ID	LogFC	adj. p
AL157871.4	1.01550798	8.28E-39
AC006449.7	-0.7693649	1.21E-38
AL391839.2	-0.422285	1.77E-38
AC130324.3	0.71939032	2.47E-38
SIAH2-AS1	0.47645988	2.87E-38
GNG12-AS1	0.80447213	3.06E-38
TMEM147-AS1	0.63253574	3.35E-38
AC018730.2	-0.5262035	3.71E-38
RRM1-AS1	0.67688677	4.40E-38
AL441992.1	0.65482275	4.64E-38
AC079203.2	-0.5089708	5.66E-38
AC022613.1	1.07669891	6.55E-38
AC233723.2	-0.8243481	7.65E-38
AC099805.1	-0.6888483	1.08E-37
AC008870.1	-1.1012767	1.47E-37
AC093297.3	-0.7896763	1.67E-37
AL137782.1	0.58419332	1.73E-37
PYCARD-AS1	1.03062094	2.13E-37
AL162586.1	0.97350332	2.36E-37
AL359643.3	0.53336367	2.55E-37
GPR158-AS1	-0.8328969	2.70E-37
AC069209.1	-0.7119587	3.16E-37
AL354919.2	1.88773131	3.43E-37
AC064852.1	-0.5100506	3.62E-37
AC083862.2	0.59144652	3.64E-37
AC084116.4	-1.0546693	3.90E-37
AC090510.1	-0.7706913	4.68E-37
AC100782.1	1.30740373	4.73E-37
AL445309.1	-0.5308392	5.36E-37
AL133215.1	-0.4080558	5.53E-37
AC063977.6	1.08083656	5.79E-37
NAPA-AS1	0.49097054	6.92E-37
AC096586.1	-0.4689458	7.95E-37
AL121985.1	1.22220135	8.93E-37
AC112503.1	-0.913513	9.75E-37

Table S2.1 GBM vs LGG

All lncRNAs GBM vs LGG (adj. p-value < 0.05)

ID	LogFC	adj. p
AC048382.5	-0.5665906	1.51E-36
AL451085.2	1.08967629	1.52E-36
AP001107.2	0.50259562	1.52E-36
ADPGK-AS1	0.53977318	1.56E-36
AC006449.3	-0.8710821	1.67E-36
AC127024.6	0.35362915	1.90E-36
AC012100.2	0.56333276	1.96E-36
BAIAP2-AS1	-0.9534706	2.24E-36
AL162231.2	0.85656118	2.26E-36
HOXA-AS2	1.87101954	2.47E-36
MAPT-AS1	-1.2472702	2.81E-36
MAP3K20-AS1	0.65267229	3.57E-36
AL604028.1	0.48490934	5.10E-36
AC092849.2	0.73123795	5.30E-36
AC145207.2	0.54288598	5.31E-36
PIK3CD-AS2	0.93597734	6.72E-36
AC067838.1	-0.3998698	6.96E-36
AC011484.1	-1.3228696	7.13E-36
AC012640.4	0.59619658	7.42E-36
AC016722.2	0.66798633	8.90E-36
AC007036.3	-1.4856437	9.15E-36
NRAV	0.87389903	1.05E-35
AL022322.2	-0.8728317	1.19E-35
AC090607.1	0.66082845	1.44E-35
AP000662.2	-0.5869386	1.47E-35
AC011511.5	1.60889191	1.49E-35
AP006216.1	-0.4246137	1.50E-35
AC068580.3	0.9387276	1.62E-35
AL158151.1	1.11134487	1.74E-35
AP000350.5	-0.4261098	1.80E-35
AC020659.1	0.71400049	1.99E-35
ZNF710-AS1	-0.9060315	2.17E-35
AC011472.3	0.75658899	2.21E-35
AP003486.1	-0.8726354	2.25E-35
AC007563.2	1.71779189	2.27E-35

Table S2.1 GBM vs LGG

All lncRNAs GBM vs LGG (adj. p-value < 0.05)

ID	LogFC	adj. p
AL162171.3	-0.5726883	2.34E-35
AL731577.2	-0.7322458	2.38E-35
AL136988.1	0.81719059	2.63E-35
DPYD-AS1	0.99403538	2.64E-35
AL162258.1	1.4117539	3.18E-35
AC011944.1	-0.9938525	3.42E-35
AP001189.1	0.61011874	3.98E-35
AC087163.3	0.41201181	4.79E-35
AL590094.1	1.38958494	5.18E-35
AC117503.2	0.82002512	5.74E-35
SLC16A1-AS1	0.73231697	5.81E-35
CPB2-AS1	-0.8266731	6.97E-35
AC093484.4	0.88622081	8.56E-35
AC009041.2	-2.1308696	8.66E-35
ADD3-AS1	-0.7502928	9.02E-35
AL513534.1	-0.752184	9.15E-35
AC020931.1	0.76175287	9.20E-35
AC020909.2	-0.7517845	1.23E-34
AP001148.1	-0.7257391	1.26E-34
AL031846.2	-1.1367625	1.54E-34
TNFRSF14-AS1	0.83357692	1.58E-34
P4HA2-AS1	0.9784251	1.73E-34
AL157392.3	-0.9465739	1.73E-34
AC079329.1	1.05502092	1.89E-34
AC012513.3	-0.8509246	2.17E-34
HLA-DQB1-AS1	1.61817112	2.69E-34
PCOLCE-AS1	1.98327674	2.69E-34
AP000547.3	-1.7510988	3.17E-34
TGFB2-OT1	1.51321417	3.67E-34
AP001453.1	0.5699342	3.80E-34
AL590999.1	-1.7848861	4.02E-34
LMO7-AS1	0.46525727	4.23E-34
POLR2J4	0.67222363	4.44E-34
TRHDE-AS1	-0.9280348	4.60E-34
AC104825.2	-0.7831307	6.38E-34

Table S2.1 GBM vs LGG

All lncRNAs GBM vs LGG (adj. p-value < 0.05)

ID	LogFC	adj. p
APOBEC3B-AS1	0.75066052	9.47E-34
AP003392.3	0.55050922	1.07E-33
BTG3-AS1	0.70576248	1.08E-33
LINC01532	-1.4040602	1.20E-33
AC138956.1	0.48112696	1.40E-33
AC009690.2	0.80888826	1.41E-33
AC108516.2	0.62077866	1.69E-33
LBX2-AS1	0.95050862	1.81E-33
AC023024.1	-1.7110085	2.49E-33
AC108002.1	-1.0608705	2.62E-33
AC012613.2	-0.6157452	2.63E-33
AL391121.1	-0.5207752	2.89E-33
COL4A2-AS2	1.00322448	3.04E-33
AC004947.2	-1.1386475	5.03E-33
AC002398.1	0.60684665	5.29E-33
AC018797.2	0.44839205	5.39E-33
AC080038.3	1.47781565	5.43E-33
HOXB-AS1	1.53189297	5.65E-33
AC073107.1	0.4537922	7.62E-33
AC079313.1	0.77588996	7.85E-33
LINC00844	-1.7563286	7.93E-33
AL133355.1	-0.4743516	8.23E-33
AC139769.2	-1.0641545	8.53E-33
AC100793.2	0.5410021	9.86E-33
AC091564.2	0.65387391	1.24E-32
RUNDC3A-AS1	-1.4166537	1.27E-32
LINC01503	1.18797663	1.36E-32
AC104350.1	-0.5700889	1.50E-32
AC117503.5	0.41376361	1.67E-32
AL365277.2	0.65186499	1.82E-32
SNHG14	-0.8685724	2.17E-32
Z84488.1	0.93506328	2.30E-32
DNAJC27-AS1	-0.6535098	2.50E-32
AL645608.3	-0.7798373	2.77E-32
LOXL1-AS1	1.24107077	2.94E-32

Table S2.1 GBM vs LGG

All lncRNAs GBM vs LGG (adj. p-value < 0.05)

ID	LogFC	adj. p
AC008264.2	-0.6682781	4.26E-32
AC005339.1	0.65897651	4.49E-32
AL356652.1	0.78063669	5.30E-32
AC008124.1	-0.7371571	6.01E-32
AC002116.1	0.51280718	6.01E-32
AC084398.2	0.65486961	8.95E-32
C20orf203	-0.6549191	9.18E-32
AC099676.1	0.4789165	9.40E-32
MEOX2-AS1	1.76371505	1.02E-31
AC011451.1	0.37837053	1.41E-31
AC093677.2	0.6188517	1.50E-31
AL135960.1	-0.5861302	1.53E-31
AC024909.3	1.17205885	1.54E-31
AL121694.1	0.51889183	1.61E-31
AL139099.5	1.7663285	1.87E-31
AC068643.1	-0.5634618	1.99E-31
AP003396.3	-0.664644	2.10E-31
AL355802.3	0.52760249	2.11E-31
AC095057.3	-0.6509519	2.47E-31
AL450306.1	-0.8014274	2.60E-31
AC090772.4	0.47805026	2.66E-31
AC091180.3	0.60413257	3.86E-31
TNK2-AS1	-0.6726155	3.93E-31
AL121748.2	1.09026181	3.94E-31
PPP1R12A-AS1	-0.5174295	4.07E-31
AC023509.1	0.47430903	4.31E-31
AC104109.4	0.44806781	4.61E-31
AC005899.4	-0.6923668	4.76E-31
AC135048.4	0.81221368	5.38E-31
AC073896.2	0.4728229	5.63E-31
SGO1-AS1	0.75647738	8.39E-31
AL391684.1	-0.6123496	8.63E-31
TSPOAP1-AS1	0.52885819	1.09E-30
RNF219-AS1	-0.8675179	1.11E-30
NDUFA6-AS1	-0.5646191	1.17E-30

Table S2.1 GBM vs LGG

All lncRNAs GBM vs LGG (adj. p-value < 0.05)

ID	LogFC	adj. p
Z82188.2	0.87015355	1.46E-30
AC114271.1	0.51280284	1.54E-30
AC127070.3	-0.777297	2.00E-30
INHBA-AS1	-0.7046013	2.06E-30
AL355916.2	-0.9637133	2.23E-30
AC084876.1	0.41044653	2.25E-30
LINC00346	0.96664025	2.37E-30
TMEM254-AS1	-0.699316	2.82E-30
MANEA-AS1	-0.5085588	3.08E-30
AC020909.3	0.6412279	3.87E-30
AC093535.2	-1.1841862	3.93E-30
AC020651.1	-0.507132	4.41E-30
AC067750.1	-0.5892058	4.73E-30
LINC02328	0.6299635	5.11E-30
AL023653.1	0.82176138	5.18E-30
AP001318.3	0.37688984	5.63E-30
AC010185.1	0.7446149	6.02E-30
AC096636.1	-1.4196613	8.41E-30
JMJD1C-AS1	-0.5874787	9.67E-30
AC010230.1	-0.7927271	9.94E-30
AC107081.2	0.54063614	1.12E-29
AC061992.1	0.77202115	1.13E-29
AP001972.5	-1.332151	1.35E-29
AC010973.2	0.82058569	1.46E-29
AC080038.1	0.87429148	1.46E-29
AC005954.2	0.37717198	1.52E-29
AP003465.1	-0.5093245	1.53E-29
AC011455.2	0.59059793	1.58E-29
AC008277.1	-0.5236719	1.62E-29
NORAD	-0.5551648	1.89E-29
AC012309.2	0.43367421	1.96E-29
AP000777.3	0.51092278	2.23E-29
AC104985.1	-0.5642061	2.37E-29
AC092117.1	-1.0258436	2.61E-29
AL360182.2	-0.4295815	2.66E-29

Table S2.1 GBM vs LGG

All lncRNAs GBM vs LGG (adj. p-value < 0.05)

ID	LogFC	adj. p
SMIM25	1.18551249	2.98E-29
AP003068.1	-0.5325001	3.12E-29
SLX1A-SULT1A3	0.5024262	3.99E-29
AL157838.1	0.57980967	4.08E-29
SLC12A5-AS1	1.57005894	4.30E-29
AC005696.2	-0.5733334	4.88E-29
PAXIP1-AS2	0.69292711	4.95E-29
AL136295.2	0.50233688	5.52E-29
TTC28-AS1	-0.6801786	5.57E-29
AL118558.3	-0.5593318	6.03E-29
AC011005.4	0.73769098	6.24E-29
AC016705.2	-0.8471886	6.59E-29
AC009403.1	0.49163114	6.65E-29
AC055811.1	-0.430969	6.96E-29
AC110285.1	-1.1214393	7.09E-29
AL391425.1	-0.5202055	7.93E-29
AL590714.1	0.46273161	9.15E-29
LINC02440	-0.7878878	1.01E-28
HOXA10-AS	1.60687343	1.04E-28
AC107027.3	-0.4111537	1.22E-28
Z95115.1	-0.6679518	1.27E-28
AL596330.1	0.99018342	1.41E-28
AC135507.1	0.36279423	1.44E-28
AC018557.1	-0.6130887	1.53E-28
AC007608.1	-0.4923245	1.55E-28
UG0898H09	-1.8026894	1.68E-28
SOCS2-AS1	1.46028935	1.80E-28
AC092849.1	0.53497016	1.82E-28
AL358790.1	-0.4033625	1.85E-28
WWTR1-AS1	1.15743626	2.12E-28
AC053503.4	0.909129	2.46E-28
AC008149.1	0.68744106	2.85E-28
AC093458.2	-0.4305533	3.39E-28
AC127502.2	0.80300996	3.49E-28
HCP5	1.35177277	3.54E-28

Table S2.1 GBM vs LGG

All lncRNAs GBM vs LGG (adj. p-value < 0.05)

ID	LogFC	adj. p
U91328.3	0.5134802	3.71E-28
LINC02525	0.73757656	3.90E-28
AP001469.3	-0.6736817	4.36E-28
AL450326.1	-0.3995582	5.34E-28
AC069544.1	-0.4166098	6.00E-28
NDUFB2-AS1	0.56243441	6.77E-28
AC010834.3	-0.4156531	7.39E-28
AC004080.6	1.60943216	7.65E-28
AP003032.2	1.03260494	7.89E-28
AC083799.1	0.60901639	8.25E-28
AL596244.1	-0.8159472	8.42E-28
AD000864.1	0.94618915	8.73E-28
AC090197.1	0.98933286	1.03E-27
AC004707.1	0.55519745	1.39E-27
PCBP1-AS1	0.26436315	1.39E-27
AL158212.2	-0.427449	1.81E-27
PSMB8-AS1	1.05263726	2.01E-27
Z99716.1	-1.0384032	2.02E-27
AC145098.1	0.51834465	2.05E-27
AC005264.1	0.58067419	2.20E-27
AL139317.3	0.44603017	2.41E-27
UBE2Q1-AS1	0.39850808	2.72E-27
LINC00893	0.61687674	3.33E-27
AC022762.2	-0.4747846	3.62E-27
AL160270.1	-1.394731	3.88E-27
LINC01759	0.69169167	3.98E-27
LINC01358	0.81078442	4.13E-27
AC009318.2	-0.3295493	4.41E-27
AP000280.1	1.54518619	5.33E-27
AC005056.1	1.10914091	5.84E-27
MIR124-2HG	-1.2418991	6.22E-27
AC006153.1	0.59206891	7.24E-27
FOXD3-AS1	1.3010907	7.69E-27
AC004448.5	-0.7257091	8.08E-27
FLNC-AS1	1.11035105	8.67E-27

Table S2.1 GBM vs LGG

All lncRNAs GBM vs LGG (adj. p-value < 0.05)

ID	LogFC	adj. p
AC092645.1	1.02312933	9.48E-27
AC022306.2	-0.3120075	1.05E-26
AC107375.1	-0.8281564	1.07E-26
AC023301.1	-1.5058706	1.07E-26
AC092378.1	0.55688218	1.12E-26
AP000593.3	0.28535184	1.25E-26
PRRT3-AS1	0.44900113	1.52E-26
LINC00334	0.55961769	1.53E-26
AC114947.2	-0.9055578	1.85E-26
TUG1	-0.7032587	2.12E-26
LINC01137	0.62209743	2.20E-26
MKNK1-AS1	0.53376227	2.27E-26
BX537318.1	0.47966584	2.35E-26
AC007743.1	-0.516305	2.37E-26
AC005609.5	-0.5616386	2.48E-26
AC022211.2	0.52794773	2.50E-26
AC090984.1	-0.4000678	2.60E-26
WDR11-AS1	-0.9624982	2.72E-26
RALY-AS1	0.39586858	3.09E-26
AC092115.2	0.74852087	3.10E-26
AC011511.3	0.48525742	4.64E-26
BISPR	1.18749336	4.65E-26
AC109587.1	0.35686204	4.72E-26
AC136475.2	-0.4905641	4.99E-26
AC068700.1	-0.667009	5.06E-26
AC006460.2	-0.3699049	5.12E-26
DNAJC3-AS1	-0.6513721	6.78E-26
AC002347.2	0.26317631	6.80E-26
PCED1B-AS1	1.11065638	7.99E-26
AP001793.2	0.38783007	1.10E-25
AC027228.2	0.64971658	1.21E-25
GTSE1-AS1	-0.4348591	1.22E-25
AC007319.1	0.7287176	1.26E-25
AC007336.3	1.21974706	1.41E-25
AL031670.1	0.32544997	1.65E-25

Table S2.1 GBM vs LGG

All lncRNAs GBM vs LGG (adj. p-value < 0.05)

ID	LogFC	adj. p
AC093726.1	0.78386601	1.71E-25
AC018761.4	0.50828286	1.89E-25
BX322557.1	-0.7860409	2.06E-25
WISP1-OT1	1.33725675	2.25E-25
AC105020.2	0.51485896	2.25E-25
AL109955.1	0.58593819	2.28E-25
AP000442.2	0.44384904	2.36E-25
TSC22D1-AS1	-0.7993215	2.40E-25
AC011466.3	0.65801802	2.58E-25
AC010531.7	-0.4651688	2.69E-25
AL357060.2	0.55048615	2.89E-25
LEF1-AS1	0.71711989	2.89E-25
SRD5A3-AS1	0.48813733	3.32E-25
AF106564.1	-1.6602668	3.95E-25
AC009163.1	0.75327596	4.31E-25
AC005614.2	0.31835474	4.39E-25
AC138207.1	0.67675023	4.44E-25
AC015909.5	-0.3729655	5.10E-25
MYCBP2-AS1	-0.8343605	5.53E-25
LINC00324	0.58125779	5.83E-25
AC124016.2	-0.6835229	5.99E-25
RAD21-AS1	-0.3751526	6.13E-25
AL031587.5	-0.5974098	6.39E-25
AC092691.1	-0.6259204	6.80E-25
AC092720.2	-0.6873638	7.23E-25
LINC01602	-1.1696301	7.51E-25
AC007364.1	0.41524302	7.56E-25
AC048382.6	-0.4156102	8.14E-25
AC019197.1	-1.0271656	8.50E-25
AC078909.1	-0.5017589	1.09E-24
AC027307.3	-0.3412422	1.11E-24
AC004824.1	0.66541895	1.13E-24
AP000763.3	-0.7841268	1.17E-24
AC099518.5	0.68742333	1.20E-24
AC012321.1	-0.6043313	1.26E-24

Table S2.1 GBM vs LGG

All lncRNAs GBM vs LGG (adj. p-value < 0.05)

ID	LogFC	adj. p
HDAC2-AS2	-0.4617258	1.35E-24
LINC00928	-0.6573546	1.40E-24
CDR1	-1.3773697	1.54E-24
AC003681.1	-0.5915719	1.56E-24
AC092958.1	1.42189134	1.65E-24
LINC01024	-0.4112149	1.72E-24
LINC00689	-2.496011	1.85E-24
AC008105.2	0.49601681	1.91E-24
AC068587.6	-1.2115976	2.04E-24
AC078795.1	0.52157245	2.07E-24
LIMD1-AS1	0.73918156	2.07E-24
AC107398.3	-1.6202406	2.19E-24
AC026771.1	0.48038314	2.24E-24
AC124798.1	-0.7869021	2.47E-24
AC008770.1	0.49622465	2.49E-24
AL049780.1	0.39090788	2.56E-24
AC016717.2	-0.9090859	2.75E-24
RRN3P2	0.4995275	2.92E-24
ELOA-AS1	0.35647024	3.40E-24
SNHG11	0.75639655	3.51E-24
AC091729.3	0.77670507	3.91E-24
AC114546.3	-0.5323607	3.99E-24
AL121987.2	-0.7181072	4.12E-24
RBPMS-AS1	0.64042012	4.16E-24
AD000671.3	0.4088752	4.21E-24
AC024267.6	0.85463136	4.30E-24
AL022311.1	-0.548729	4.38E-24
AC037198.1	1.30061928	4.77E-24
AL118558.1	-0.543254	5.19E-24
AL080276.2	0.43848058	5.20E-24
AC096677.2	0.76370296	5.26E-24
ZEB2-AS1	-0.6963245	5.29E-24
AC069287.2	0.41935948	5.84E-24
DKFZp779M0652	-0.5267673	6.10E-24
AC027237.3	0.3752275	7.90E-24

Table S2.1 GBM vs LGG

All lncRNAs GBM vs LGG (adj. p-value < 0.05)

ID	LogFC	adj. p
AL355338.1	0.54193581	9.90E-24
BX284668.5	0.87935194	1.02E-23
ADAMTS9-AS2	0.55155839	1.04E-23
AC008522.1	-0.8679384	1.09E-23
AC018362.1	0.53973696	1.16E-23
AL512590.3	-0.8024845	1.21E-23
Z97989.1	-0.9246975	1.21E-23
LINC01521	-0.5629481	1.33E-23
AL109811.2	0.34004492	1.34E-23
AL139807.1	0.57526799	1.42E-23
AL110504.1	-0.6171713	1.47E-23
AC122129.1	-0.6405027	1.67E-23
AL139021.1	0.39003811	1.68E-23
AL162231.4	0.88248346	1.73E-23
NNT-AS1	-0.509059	1.82E-23
AC025171.1	0.59736972	1.85E-23
AC002456.1	0.72677341	1.90E-23
AC005726.5	-1.3775493	2.10E-23
AC010624.3	0.33544541	2.22E-23
AL133304.3	-0.4818798	2.27E-23
AL158834.2	-0.3888064	2.37E-23
DTX2P1-UPK3BP1-PMS2P11	0.37346623	2.40E-23
GRM5-AS1	-1.536222	2.53E-23
AL357055.3	-0.3913425	2.64E-23
AC005821.1	0.91339332	3.35E-23
AC093503.3	-0.5826923	3.54E-23
AL139260.1	0.41105834	3.82E-23
AL606760.2	0.37839972	3.99E-23
AC012645.1	-0.582874	4.04E-23
AL132780.4	-0.5569962	4.07E-23
PHKA2-AS1	0.48067384	4.19E-23
NAV2-AS2	-0.7111002	4.21E-23
SNHG9	0.71595408	4.56E-23
MRVI1-AS1	-0.4619097	5.12E-23
ST20-AS1	0.5625838	5.20E-23

Table S2.1 GBM vs LGG

All lncRNAs GBM vs LGG (adj. p-value < 0.05)

ID	LogFC	adj. p
AC021739.2	-0.5836669	5.83E-23
B4GALT4-AS1	0.38712533	7.20E-23
AL139022.1	0.36795239	7.64E-23
LINC02035	-0.5487965	9.45E-23
AC007040.1	0.34403678	9.67E-23
HLA-F-AS1	0.70417719	1.05E-22
AC096537.1	0.76529311	1.15E-22
AL160236.2	0.35584967	1.21E-22
AC012313.3	0.91301972	1.22E-22
AL589765.4	0.32639104	1.27E-22
AP001505.2	-0.5056967	1.50E-22
CD81-AS1	0.51034089	1.51E-22
LINC00294	-0.5685975	1.63E-22
AL359921.1	0.2872269	1.63E-22
CARS-AS1	0.47833988	1.68E-22
AC141928.1	-0.7376593	1.72E-22
AP005263.1	0.49461104	1.81E-22
LINC00092	0.94546295	2.00E-22
ZNF503-AS2	0.56944178	2.00E-22
AC005034.3	-0.4204345	2.05E-22
LINC02381	1.05431176	2.12E-22
AL356124.2	0.69982219	2.36E-22
AP000866.1	-0.5140043	2.50E-22
AL138781.2	-0.3970294	2.53E-22
AL358334.2	0.68684715	2.53E-22
AC092111.1	-0.9006638	2.70E-22
AC018362.2	0.40602082	2.86E-22
TOB1-AS1	-0.4833396	2.97E-22
AC009120.2	0.31978294	3.11E-22
AL035413.1	0.37295905	3.15E-22
AC007228.2	-0.4783414	3.55E-22
DPP9-AS1	0.46962351	3.59E-22
AC010761.4	0.84173159	3.63E-22
AC097461.1	-0.591316	3.75E-22
AC027277.1	0.92360288	4.32E-22

Table S2.1 GBM vs LGG

All lncRNAs GBM vs LGG (adj. p-value < 0.05)

ID	LogFC	adj. p
AL022476.1	-0.3897242	4.53E-22
AF131216.3	-0.9713358	4.55E-22
AC000068.2	0.52812572	5.10E-22
MORC2-AS1	-0.4744025	5.11E-22
AL162742.2	0.54197805	5.13E-22
AC026691.1	-0.6183213	5.41E-22
DCST1-AS1	0.48060965	6.18E-22
DICER1-AS1	-0.6718247	6.26E-22
AL671710.1	0.46258534	6.29E-22
AC009113.2	-0.3111639	6.30E-22
AL603832.1	0.49035343	6.47E-22
AL592424.1	-0.4020207	6.90E-22
AC006369.1	0.57923555	7.51E-22
CA3-AS1	1.21647985	7.78E-22
AC092718.2	0.44565864	7.85E-22
LINC00205	-0.678294	8.25E-22
AC009902.3	1.00773988	9.27E-22
AC073333.1	0.65638434	1.12E-21
AC013489.3	0.46614855	1.54E-21
AC015922.4	0.76928719	1.62E-21
AC087623.2	0.70520664	1.64E-21
AL391863.1	0.4429089	1.66E-21
AC007032.1	0.5003796	1.78E-21
AL355974.3	0.93400882	1.90E-21
AC002350.2	0.41593592	2.02E-21
TRAPPC12-AS1	-0.4016416	2.10E-21
AF129408.1	-0.3569377	2.12E-21
AC016825.1	-0.9032918	2.24E-21
AL359918.2	-0.5725473	2.51E-21
AC022400.1	-0.7068491	2.92E-21
AC139768.1	-0.4487007	2.92E-21
AC006453.2	0.86140434	2.94E-21
AP000648.3	-0.4725778	2.95E-21
AC105383.1	-0.6855541	3.31E-21
AC009139.2	-0.4158622	4.02E-21

Table S2.1 GBM vs LGG

All lncRNAs GBM vs LGG (adj. p-value < 0.05)

ID	LogFC	adj. p
AC022858.1	-0.7004147	4.36E-21
AL158151.2	0.41235003	4.55E-21
AC007382.1	-0.4802444	5.67E-21
LINC01224	0.98511783	6.87E-21
AL133243.2	-0.4242403	7.54E-21
AC073611.1	0.33815785	7.85E-21
AL356481.1	0.3138268	8.09E-21
AD000090.1	1.29356986	8.21E-21
SNAI3-AS1	-0.5281526	9.56E-21
AL807752.3	-1.1620206	1.02E-20
LINC01105	-1.3651323	1.02E-20
AF287957.1	-0.4739467	1.02E-20
AL163051.2	-0.2693173	1.06E-20
OIP5-AS1	-0.499648	1.10E-20
UXT-AS1	0.523771	1.18E-20
OXCT1-AS1	-0.556243	1.24E-20
AC105345.1	-0.4939756	1.37E-20
AC011899.2	0.75644901	1.38E-20
ADGRL3-AS1	-0.4274028	1.41E-20
HOTAIR	1.23035293	1.41E-20
AC010168.2	0.46042879	1.46E-20
TGFB3-AS1	0.62611516	1.55E-20
AP001350.2	-0.403461	1.65E-20
ZNF571-AS1	-0.7475396	1.66E-20
AC087500.1	0.42251218	1.71E-20
AL109811.1	0.48350238	1.73E-20
CR769775.4	-0.565785	1.86E-20
LINC02283	-1.3844804	1.97E-20
AL021453.1	-0.4967189	2.08E-20
AC022400.8	-0.3610011	2.13E-20
DCTN1-AS1	-0.5490139	2.13E-20
RMRP	1.32531474	2.15E-20
AL122058.1	-0.4863268	2.23E-20
AL139398.1	0.47736552	2.26E-20
AL138963.3	0.69426604	2.34E-20

Table S2.1 GBM vs LGG

All lncRNAs GBM vs LGG (adj. p-value < 0.05)

ID	LogFC	adj. p
AC008686.1	0.68074558	2.53E-20
AL133230.1	0.47160001	2.59E-20
AC025259.1	0.39044068	2.64E-20
AFAP1-AS1	-0.6422763	2.79E-20
PTPRD-AS1	-0.8183319	3.05E-20
AP000943.3	0.38565435	3.19E-20
ZNF667-AS1	0.53635313	3.29E-20
AC090692.1	1.02123015	3.44E-20
AL109615.3	0.65156156	3.78E-20
AL035530.2	-0.4072722	4.28E-20
AC010636.2	0.41253223	4.33E-20
Z94721.2	0.45273091	5.01E-20
HOXD-AS2	0.8250856	5.29E-20
AC007314.1	0.34641826	5.74E-20
AC138207.4	0.49236924	6.07E-20
AL450384.2	-0.5334971	6.55E-20
AL807752.2	-0.8988615	6.94E-20
AC093627.4	0.55973058	7.70E-20
AC013391.3	-0.9568906	7.76E-20
LINC02308	0.68876779	7.88E-20
AC007163.1	0.49431655	8.59E-20
AC007608.3	-0.6985323	8.88E-20
AL158151.3	0.69436156	9.44E-20
TUBA3FP	-0.3366974	9.46E-20
AL356489.2	-0.7362985	1.07E-19
AC131159.2	0.41004764	1.11E-19
AC010536.1	-0.446095	1.14E-19
AC130343.2	-0.3281156	1.17E-19
AC093620.1	-0.371962	1.23E-19
AC084024.3	0.43428904	1.33E-19
AL356481.3	-0.5159738	1.34E-19
LRP1-AS	-0.678771	1.37E-19
LINC00941	0.77123193	1.41E-19
AL158850.2	0.6270747	1.42E-19
DENND6A-AS1	0.25590219	1.48E-19

Table S2.1 GBM vs LGG

All lncRNAs GBM vs LGG (adj. p-value < 0.05)

ID	LogFC	adj. p
AC073896.4	-0.4521751	1.68E-19
AL021368.2	-0.5535621	1.76E-19
AC009113.1	-0.5980476	1.81E-19
AC100827.3	-0.3684673	1.96E-19
BX890604.1	-0.7418087	1.97E-19
AC091271.1	-0.5467485	2.05E-19
LINC01679	0.5469959	2.27E-19
ARHGEF7-AS2	-0.4557853	2.39E-19
ITFG1-AS1	0.3422378	2.46E-19
TMEM246-AS1	-0.4900192	2.48E-19
AC080112.2	0.71523249	2.49E-19
AL049829.2	-0.6398295	2.58E-19
AC009065.1	-0.4860038	2.70E-19
AC012306.2	0.38529868	3.14E-19
AL590627.2	0.29707889	3.25E-19
AC092368.3	0.29075612	3.26E-19
AC245052.4	0.44038632	3.34E-19
TNRC6C-AS1	-0.8116017	3.73E-19
AL445686.2	0.614613	4.01E-19
AC087439.1	0.33717394	4.35E-19
MED4-AS1	0.34438537	4.72E-19
SATB1-AS1	-0.7174963	4.91E-19
AC018761.2	0.51692563	4.92E-19
AC022007.1	0.46462703	4.98E-19
AL035446.1	0.99786578	5.27E-19
LINC00599	-1.3854239	5.28E-19
AC011498.3	0.47146577	5.57E-19
AC135050.6	0.38357365	5.93E-19
AC104836.2	-0.4863239	6.94E-19
AC104938.1	-0.3620839	7.03E-19
AC025164.2	0.51528626	8.07E-19
AL162511.1	-0.8766775	8.32E-19
KDM4A-AS1	0.39016251	8.86E-19
AC034228.3	-0.6459328	9.11E-19
AC106869.1	-0.613606	9.51E-19

Table S2.1 GBM vs LGG

All lncRNAs GBM vs LGG (adj. p-value < 0.05)

ID	LogFC	adj. p
AL161747.2	-0.5947865	1.14E-18
AC091948.1	-0.3688111	1.16E-18
AC026369.1	-0.6417351	1.16E-18
LINC01198	1.02429762	1.19E-18
AC006059.1	-0.6759188	1.23E-18
AC005899.8	0.33049467	1.42E-18
AL391422.3	0.6988293	1.46E-18
AL365273.1	-0.2510297	1.49E-18
AC005165.1	0.67224335	1.61E-18
LIFR-AS1	-0.6196654	1.61E-18
AC004551.1	0.92636556	1.84E-18
AL078581.3	0.36793365	1.93E-18
AL513315.1	0.68879529	2.05E-18
RGMB-AS1	-0.4712007	2.17E-18
AC009087.1	0.38647128	2.43E-18
AC048344.1	0.35865084	2.47E-18
AL353708.3	-0.4713919	2.60E-18
AC083809.1	-0.3801844	2.64E-18
BAALC-AS1	1.03185154	2.65E-18
AC008011.2	0.49962247	2.91E-18
AL049597.2	0.36830167	2.94E-18
AC099329.1	0.56316613	3.20E-18
AL139339.2	0.33871152	3.33E-18
AP000924.1	0.7528957	3.73E-18
AC009126.1	-0.3854577	3.79E-18
AC114490.1	0.40187865	3.87E-18
AC012065.4	-0.4602674	4.02E-18
AC005277.1	-0.7583181	4.06E-18
AL365181.3	-1.0771954	4.40E-18
AL591845.1	0.70260777	4.41E-18
AC103858.1	0.3896701	4.46E-18
PRAL	1.1543025	4.77E-18
AC022098.1	-0.4610714	5.63E-18
AL033528.2	0.39034192	6.01E-18
AP003396.1	0.35452226	6.42E-18

Table S2.1 GBM vs LGG

All lncRNAs GBM vs LGG (adj. p-value < 0.05)

ID	LogFC	adj. p
AC020913.2	0.55711011	7.79E-18
AC087286.3	-0.452103	8.45E-18
PITRM1-AS1	-0.4524475	8.68E-18
AC105446.1	0.73231939	8.75E-18
AP001610.1	1.15091191	9.19E-18
AC015922.3	0.5269442	9.46E-18
AL662797.2	0.74775568	9.49E-18
AL391807.1	-0.9123722	1.10E-17
CBR3-AS1	0.542351	1.10E-17
AC109826.1	0.42773373	1.23E-17
AL591721.1	-0.4020851	1.25E-17
AC008655.1	-0.9597049	1.26E-17
LINC01852	0.32746634	1.35E-17
AC102953.2	-0.6588448	1.36E-17
AC006487.1	0.71950088	1.47E-17
AC010336.5	0.36046342	1.57E-17
AC007485.2	-0.4784144	1.63E-17
LINC01116	1.31819224	1.64E-17
AC139713.2	-0.7171036	1.66E-17
AL159169.2	-0.4697411	1.71E-17
AC010319.4	0.35203551	1.73E-17
AC010336.1	0.70889853	1.77E-17
AC104083.1	-0.7871118	1.90E-17
FLJ31104	-0.3341967	2.05E-17
AC097534.1	0.39491593	2.09E-17
AL031963.1	0.38754847	2.12E-17
AC079781.5	0.53068887	2.23E-17
RFPL1S	-1.2421608	2.36E-17
AC004477.2	0.40987404	2.41E-17
SLC7A11-AS1	-0.6252806	2.55E-17
C17orf102	-0.4756684	2.66E-17
AC027097.1	0.25425423	2.67E-17
AC007786.1	-0.2904846	2.97E-17
MIR325HG	-0.6059343	3.20E-17
AC093305.1	-0.6575042	3.85E-17

Table S2.1 GBM vs LGG

All lncRNAs GBM vs LGG (adj. p-value < 0.05)

ID	LogFC	adj. p
AC007405.2	-0.6949058	4.03E-17
AP000753.2	0.32667113	4.09E-17
AC138207.5	0.45464642	4.16E-17
AC138150.2	-0.3601039	4.20E-17
DLGAP1-AS1	0.59783245	4.22E-17
AL592078.1	-0.7659611	4.28E-17
AP001267.3	-0.3811087	4.46E-17
GNAS-AS1	1.97630414	4.51E-17
AC010649.1	-0.9582736	4.54E-17
AC006960.3	-0.4989005	4.58E-17
RPARP-AS1	-0.4466486	4.81E-17
AL512791.1	0.44519481	5.12E-17
SNHG17	0.70509966	5.42E-17
AL033527.2	-0.4335628	5.67E-17
AL442663.3	-0.3127347	6.00E-17
AC010336.6	-0.6236061	6.09E-17
ZNF252P-AS1	-0.2540574	6.43E-17
LINC01023	0.49026411	6.79E-17
AP000763.4	0.36732616	6.89E-17
AP004609.3	-0.4623588	7.11E-17
LINC00863	-0.5331733	7.39E-17
AC005329.2	-0.4461008	7.42E-17
AC000068.3	-0.33713	7.54E-17
AL031056.1	-1.2822937	7.61E-17
FOXN3-AS1	0.409502	7.80E-17
AC010336.3	-1.0003897	7.83E-17
AC004854.2	0.38707579	9.39E-17
AL845472.1	-0.6410224	9.57E-17
AC060766.7	0.48542344	9.83E-17
AL356599.1	-0.399897	1.06E-16
AL137186.2	-0.3324498	1.08E-16
PROX1-AS1	-0.4873869	1.09E-16
LINC00632	-0.8102162	1.11E-16
LINC01088	-1.5929703	1.24E-16
LINC01918	-0.4005294	1.36E-16

Table S2.1 GBM vs LGG

All lncRNAs GBM vs LGG (adj. p-value < 0.05)

ID	LogFC	adj. p
AC091563.1	-0.3959407	1.46E-16
NCAM1-AS1	-0.8533324	1.67E-16
AC026356.2	0.36887108	1.75E-16
HLTF-AS1	-0.3192084	1.84E-16
AL136295.7	-0.440999	1.89E-16
RHPN1-AS1	0.37333272	1.94E-16
ILF3-AS1	-0.5657014	1.97E-16
STX18-AS1	-0.3097458	2.12E-16
AP003476.1	-0.5335798	2.15E-16
AC021078.1	0.28661603	2.15E-16
UBA6-AS1	0.42442303	2.21E-16
AC004241.1	-0.5210678	2.24E-16
AC022211.4	0.39986848	2.31E-16
AC097641.1	-0.3925102	2.51E-16
AC023283.1	0.56953672	2.64E-16
AC100778.4	0.53851585	2.65E-16
FAM13A-AS1	-0.4629779	2.86E-16
AC091060.1	0.28587347	2.95E-16
AL355312.2	0.35273631	2.96E-16
AC096992.2	-0.3690643	3.02E-16
ARHGEF26-AS1	-0.8247668	3.47E-16
AL161772.1	-0.7297677	3.93E-16
DGCR5	-0.6931209	3.97E-16
ZSWIM8-AS1	-0.4390217	4.71E-16
AC011498.6	0.29167332	5.05E-16
FOXD2-AS1	0.7492014	5.22E-16
AP000757.1	-1.0033258	5.29E-16
AP003550.1	0.35548751	5.67E-16
AC087289.2	0.34702718	5.80E-16
AL355816.2	0.36391883	5.89E-16
AL513190.1	-0.444509	5.98E-16
AC006213.1	0.34339675	6.05E-16
AC009812.1	-0.4039503	6.44E-16
AL049795.2	0.26258537	6.49E-16
AC006116.10	0.54570871	6.52E-16

Table S2.1 GBM vs LGG

All lncRNAs GBM vs LGG (adj. p-value < 0.05)

ID	LogFC	adj. p
DLGAP1-AS2	0.60116337	6.94E-16
AC110015.1	0.5694973	7.04E-16
AC007750.1	0.84528273	7.63E-16
VSTM2A-OT1	-0.7713772	9.28E-16
AC008622.2	0.70311287	9.29E-16
AC092134.1	-0.5902995	9.95E-16
AC004623.1	-0.5199687	1.02E-15
AC106707.1	0.37661589	1.03E-15
AC010503.1	-1.471501	1.10E-15
AC012170.3	0.28014125	1.31E-15
CASC2	-0.5372247	1.31E-15
PAN3-AS1	-0.369176	1.45E-15
AL117209.1	-0.4634583	1.47E-15
AC006538.1	-0.4528835	1.59E-15
AL033384.2	-0.4319082	1.62E-15
AC244517.2	0.85572985	1.64E-15
AC108451.2	-0.6679248	1.65E-15
AC010761.5	0.8032598	1.78E-15
AP001972.2	-0.5377674	1.87E-15
LINC00886	0.59200138	2.15E-15
AL590666.2	-1.3571313	2.31E-15
AC007383.3	-0.3265257	2.40E-15
AC099343.3	0.48330656	2.41E-15
AC087292.1	-0.4155057	2.52E-15
AC068987.2	-0.6096755	2.63E-15
NKILA	0.45220086	2.66E-15
AC016588.1	0.38869286	2.69E-15
AC012358.3	-0.5058094	2.76E-15
AC009005.1	0.49596591	2.99E-15
AP003108.3	0.40170477	3.07E-15
AP000350.6	-0.437574	3.14E-15
AC138028.6	0.29217073	3.37E-15
MGC16275	-0.5481585	3.48E-15
PKP4-AS1	-0.5420292	3.54E-15
AC116535.1	-0.3435805	3.65E-15

Table S2.1 GBM vs LGG

All lncRNAs GBM vs LGG (adj. p-value < 0.05)

ID	LogFC	adj. p
AC016747.1	0.54972129	4.20E-15
U47924.1	0.32986396	4.23E-15
AC109361.2	0.63506379	4.39E-15
AL020993.1	0.33011868	4.53E-15
AC025287.1	0.59211593	4.63E-15
AC022532.1	0.64765901	4.70E-15
AC125611.4	0.77427934	4.86E-15
AC018647.1	-0.7701545	5.13E-15
AL645465.1	0.34911813	5.58E-15
AC011474.1	-0.5093297	6.54E-15
AL669831.5	0.30006509	6.88E-15
AC020558.1	0.3312753	7.26E-15
AC126407.1	-0.5531386	7.47E-15
AC091564.5	0.6669846	7.64E-15
MYCNOS	-0.5835735	7.64E-15
AC079834.2	0.4403315	7.77E-15
AC002401.1	-0.4739997	8.18E-15
AC021097.1	0.47949628	8.31E-15
AL356019.2	-0.3595207	8.85E-15
FOXD1-AS1	0.83343175	8.96E-15
AL359198.1	-0.6005625	9.12E-15
AC007728.2	0.35474311	9.57E-15
AC025262.3	0.35852083	1.02E-14
AC138811.1	-0.37683	1.09E-14
AC022558.3	0.33652828	1.10E-14
AL359075.2	0.56773662	1.14E-14
AL118556.1	-0.3552089	1.15E-14
AC074212.1	0.66222424	1.26E-14
TGFB2-AS1	0.5088314	1.35E-14
AC011825.3	0.276314	1.43E-14
AC087276.3	0.4004776	1.46E-14
PCAT19	0.49403823	1.49E-14
AC138466.4	-0.6603476	1.53E-14
AC073052.2	0.23186768	1.90E-14
MCCC1-AS1	0.27829403	1.99E-14

Table S2.1 GBM vs LGG

All lncRNAs GBM vs LGG (adj. p-value < 0.05)

ID	LogFC	adj. p
AL513327.1	0.51013943	2.10E-14
AC107068.1	-0.340293	2.21E-14
AC005740.3	0.32465607	2.24E-14
AC005330.1	-0.567788	2.32E-14
AL353763.1	-0.3175802	2.35E-14
AL133367.1	-0.5216511	2.46E-14
AL731563.3	-0.2946227	2.50E-14
AC073548.1	0.37049746	2.53E-14
AC099778.1	-0.3869119	2.59E-14
AC100786.1	-0.6250559	2.60E-14
AP000438.1	-0.7005787	2.66E-14
AL731563.2	0.43726972	2.68E-14
AC107067.1	-0.6171111	2.72E-14
LINC02449	-0.3427824	2.78E-14
SPON1-AS1	-0.9534956	3.28E-14
AL354813.1	-0.8384524	3.44E-14
APTR	0.38357593	3.58E-14
SP2-AS1	-0.3057781	4.20E-14
MCF2L-AS1	0.38506002	4.30E-14
AC244502.1	1.14734587	4.92E-14
DLGAP4-AS1	0.38483639	5.13E-14
AC064836.3	-0.343795	5.15E-14
AC025569.1	-0.4307921	5.23E-14
AC006547.3	0.35623877	5.38E-14
AL358115.1	0.31734336	5.43E-14
HHATL-AS1	-0.3866509	5.52E-14
STXBP5-AS1	-0.4766141	5.73E-14
AC108002.2	0.41303228	5.74E-14
AL512329.2	0.58353304	6.00E-14
MIR100HG	0.73811026	6.00E-14
AL592430.1	-0.672495	6.15E-14
AC008738.5	0.64216398	6.61E-14
AC026356.1	0.37888637	7.13E-14
SNHG19	-0.6350877	7.82E-14
MAP3K14-AS1	0.39797688	7.99E-14

Table S2.1 GBM vs LGG

All lncRNAs GBM vs LGG (adj. p-value < 0.05)

ID	LogFC	adj. p
LINC01778	0.62820965	8.08E-14
AC007666.1	-0.7086391	8.18E-14
AL928654.3	-0.5282808	8.18E-14
AC005253.1	0.34095268	8.18E-14
AC239868.2	-0.6811362	8.22E-14
AC005229.4	0.36357181	8.71E-14
AC006942.1	0.42285356	9.18E-14
AC037198.3	0.77615529	9.56E-14
AC245100.8	0.43099034	1.04E-13
Z92544.2	-0.3729077	1.06E-13
CTD-2201I18.1	0.87736272	1.12E-13
LINC01138	0.46950816	1.19E-13
STARD4-AS1	0.60879739	1.20E-13
AL355001.2	0.46491022	1.23E-13
FAM66C	-0.415811	1.34E-13
SNHG12	0.53381756	1.45E-13
AL008729.2	-0.6920205	1.85E-13
HAS2-AS1	0.4865548	2.00E-13
AC127459.1	-0.387236	2.01E-13
LINC00475	0.85092048	2.08E-13
AL133417.1	-0.3564233	2.20E-13
LINC01515	0.51343041	2.27E-13
SOX21-AS1	-0.5852858	2.33E-13
AC008581.1	-0.4994132	2.38E-13
AC083964.1	0.20497776	2.44E-13
AL161452.1	0.30606003	2.48E-13
AC067852.1	0.35033395	2.65E-13
EDRF1-AS1	-0.2639021	2.73E-13
AL450263.1	-0.349006	2.84E-13
AP006621.1	0.40496705	2.96E-13
AC005775.1	0.43390282	3.05E-13
AC011558.1	0.80233379	3.11E-13
AL158066.1	-0.459398	3.14E-13
AC107959.1	-0.4547711	3.50E-13
AC008738.3	0.70614665	3.56E-13

Table S2.1 GBM vs LGG

All lncRNAs GBM vs LGG (adj. p-value < 0.05)

ID	LogFC	adj. p
AP003064.1	-0.6140382	3.95E-13
AC002310.2	-0.3901657	3.99E-13
AL138762.1	-0.2589209	4.05E-13
AC022400.9	-0.3278517	4.10E-13
AC025917.1	-0.3021586	4.55E-13
AC022916.1	-0.3886103	4.67E-13
AL035587.1	0.25608853	4.91E-13
AC010883.1	0.2697392	5.24E-13
AL022326.2	-0.2937523	5.29E-13
AC123912.4	0.55500067	5.58E-13
SEPT4-AS1	-0.714026	5.61E-13
AC022034.2	0.66460323	5.70E-13
AC012157.1	-0.4398407	5.85E-13
AC026801.3	0.4469527	5.95E-13
CKMT2-AS1	-0.3398398	6.00E-13
CEBPB-AS1	0.37256427	6.02E-13
ODF2-AS1	0.38118283	6.08E-13
TMPO-AS1	0.57270597	6.08E-13
AC009563.1	0.23568061	6.44E-13
DLEU1	0.52280398	7.73E-13
OSTM1-AS1	0.66438533	7.90E-13
CYB561D2	-0.4752604	7.93E-13
AC083798.2	0.23249232	7.96E-13
AL122010.1	0.23841432	8.26E-13
PRKCZ-AS1	-0.4534873	8.34E-13
AC010655.4	0.35645831	8.54E-13
AC007938.4	-0.6062264	8.59E-13
AL096701.3	-0.2955668	8.95E-13
AC010501.1	-0.4603384	9.38E-13
EPB41L4A-AS2	0.3274617	9.45E-13
AC092140.1	0.41303735	9.87E-13
AC006027.1	0.44617007	1.03E-12
AC010503.2	-1.0645777	1.04E-12
LINC01534	0.22612764	1.05E-12
AC009831.1	-0.2648099	1.07E-12

Table S2.1 GBM vs LGG

All lncRNAs GBM vs LGG (adj. p-value < 0.05)

ID	LogFC	adj. p
AL139125.2	-0.4353759	1.09E-12
AC022154.1	0.28090792	1.10E-12
AL009172.2	-0.9749647	1.22E-12
AC073324.2	0.92340047	1.22E-12
AC104986.2	-0.4134377	1.24E-12
AL355140.1	-0.5820419	1.31E-12
AP000317.2	0.45599373	1.32E-12
AC010533.1	0.58883208	1.32E-12
AL139246.5	-0.4319893	1.33E-12
LINC00403	-0.6276346	1.43E-12
AC023906.4	0.34314706	1.49E-12
AC008543.1	0.4104465	1.53E-12
AC024075.1	-0.3235768	1.62E-12
AC009501.1	0.4074728	1.68E-12
AL035252.3	-0.3502231	1.94E-12
SNHG22	0.36815885	1.95E-12
DDX11-AS1	0.29102756	2.06E-12
AC027031.2	0.56070267	2.09E-12
AL513218.1	0.26801428	2.14E-12
AL138828.1	0.37347206	2.15E-12
AL049796.1	-0.3214353	2.17E-12
AC105277.1	0.42477712	2.21E-12
AF111167.2	-0.4078413	2.23E-12
AC135048.1	0.28250407	2.45E-12
AC027796.4	0.29948719	2.48E-12
AP000282.1	-0.916245	2.60E-12
AC068724.2	0.34473228	2.71E-12
PTOV1-AS2	0.36247527	2.71E-12
LINC00839	-1.1310781	2.80E-12
SLC9A3-AS1	-0.7080288	2.90E-12
AC025423.4	0.97837489	2.93E-12
ZNF582-AS1	0.40554367	3.02E-12
AL645608.6	0.6065957	3.08E-12
AC119403.1	0.19630518	3.17E-12
AC025442.1	-0.2547873	3.19E-12

Table S2.1 GBM vs LGG

All lncRNAs GBM vs LGG (adj. p-value < 0.05)

ID	LogFC	adj. p
AC108449.1	-0.3656779	3.25E-12
AL355075.4	1.01865189	3.35E-12
AC105206.2	-0.2877805	3.77E-12
AC008840.1	-0.4640241	3.92E-12
AC244021.1	0.46699968	3.99E-12
AC074044.1	0.19792731	4.17E-12
MIAT	-1.1408653	4.28E-12
AC133065.6	0.58115996	4.32E-12
AL133465.1	-0.6167185	5.40E-12
AC008764.3	0.30183503	5.52E-12
AC092159.2	0.25814845	5.65E-12
AC079174.2	-0.3565582	5.84E-12
AC015688.8	-0.4498769	5.97E-12
CACNA1C-AS1	-0.4197899	6.07E-12
ERICH6-AS1	0.46713804	6.07E-12
AL354892.2	-0.3366965	6.61E-12
AC066613.2	-0.3253746	6.75E-12
AC027575.4	0.24621091	6.78E-12
LINC01089	-0.6622821	6.79E-12
AL117348.1	0.56834405	7.13E-12
AC010261.2	0.30881873	7.22E-12
SYP-AS1	-0.7687809	7.48E-12
AC132872.1	-0.4865269	8.17E-12
AL161729.1	-0.371647	8.31E-12
AC231533.1	0.31678378	8.65E-12
AC108451.1	-0.5057511	8.69E-12
AC093157.1	0.43696476	8.90E-12
AP003501.1	0.42644466	8.99E-12
AL023284.4	-0.3923388	9.02E-12
AP003068.3	0.28228775	9.04E-12
AC027601.2	-0.2335113	9.09E-12
AC087442.1	-0.4388805	9.63E-12
LINC01006	-0.8146084	9.80E-12
ATP2A1-AS1	0.40081179	1.01E-11
AC012615.3	0.38641322	1.02E-11

Table S2.1 GBM vs LGG

All lncRNAs GBM vs LGG (adj. p-value < 0.05)

ID	LogFC	adj. p
AC015563.2	-0.3713145	1.20E-11
RNASEH1-AS1	0.47321525	1.22E-11
AC026471.2	-0.3251795	1.27E-11
AP001010.1	-0.3455675	1.27E-11
LINC01102	-0.6870647	1.29E-11
AC004233.3	-0.5019836	1.29E-11
AC009511.2	-0.3696128	1.36E-11
AC013356.4	-0.5284828	1.36E-11
FO393401.1	-0.1984304	1.42E-11
TAF1A-AS1	0.35572362	1.50E-11
SLC25A5-AS1	0.35696837	1.54E-11
AL929472.2	0.31472865	1.58E-11
LINC01963	-0.4826298	1.72E-11
AC008945.2	0.7283544	1.77E-11
AC021092.1	0.40715289	1.84E-11
AL513550.1	-0.3681927	1.88E-11
UBL7-AS1	0.31025912	1.90E-11
AC018809.2	-0.2680244	2.03E-11
AC092675.1	0.43224218	2.05E-11
AC117503.3	0.20429241	2.06E-11
AC137723.1	-0.3329488	2.09E-11
CD27-AS1	-0.3894921	2.13E-11
PRICKLE2-AS1	-0.5695567	2.13E-11
AC008750.1	0.57222663	2.19E-11
LINC00237	-0.7733054	2.21E-11
ZNF561-AS1	0.34519033	2.30E-11
EMX2OS	-0.9546955	2.54E-11
AC010300.1	-0.4444762	2.62E-11
AC114811.2	-0.4228915	2.70E-11
AC020934.2	0.37059575	2.71E-11
AC004771.4	-0.3735507	2.80E-11
AL121830.1	-0.5536915	2.81E-11
AP001626.1	-0.4127841	2.82E-11
DPP10-AS1	-0.5356255	2.83E-11
DNAJC9-AS1	-0.2895164	2.98E-11

Table S2.1 GBM vs LGG

All lncRNAs GBM vs LGG (adj. p-value < 0.05)

ID	LogFC	adj. p
PINK1-AS	-0.3153679	3.02E-11
ZNF350-AS1	-0.4515887	3.06E-11
AC005104.1	0.35585967	3.20E-11
AC003991.2	0.47822133	3.36E-11
AC084125.4	0.46571955	3.61E-11
AL589935.1	-0.594044	3.66E-11
AC109446.3	-0.3787036	3.67E-11
AP001528.3	-0.383585	4.17E-11
AC008635.1	0.39896937	4.29E-11
AC012184.1	0.25621097	4.38E-11
MID1IP1-AS1	-0.3915367	4.46E-11
AF127577.1	0.36152258	4.56E-11
KIAA1614-AS1	0.34525955	5.35E-11
AC130456.5	0.26071664	5.37E-11
AC009163.7	-0.3728566	5.38E-11
AC008915.2	0.26540468	5.42E-11
AC103923.1	0.35099779	5.61E-11
AC022107.1	-0.4013793	5.76E-11
AC141586.3	-0.5415639	6.12E-11
ARHGAP5-AS1	-0.4842135	6.23E-11
AC120114.1	-0.3332448	6.85E-11
AC144652.1	-0.4766025	7.09E-11
ZNF674-AS1	0.36277614	7.54E-11
AP003306.2	-0.3972833	7.74E-11
AC026464.2	-0.3842128	8.39E-11
PTOV1-AS1	0.30171794	9.37E-11
B3GALT5-AS1	0.63592194	9.43E-11
AC008750.2	0.67916972	9.86E-11
AC012184.3	0.23637087	9.89E-11
AL662844.4	-0.404549	1.01E-10
AC098829.1	0.31308119	1.02E-10
AP003086.2	0.22874448	1.07E-10
AC124319.2	-0.4374989	1.07E-10
AC087501.5	0.31179015	1.08E-10
LINC01351	-0.5399558	1.09E-10

Table S2.1 GBM vs LGG

All lncRNAs GBM vs LGG (adj. p-value < 0.05)

ID	LogFC	adj. p
AC233702.10	-0.488211	1.19E-10
AL391244.3	0.35115923	1.21E-10
LINC01551	0.75850592	1.22E-10
AC024592.1	0.36907721	1.23E-10
AC005786.3	0.33134522	1.30E-10
AC005480.1	0.31614761	1.30E-10
AC009779.2	-0.3354011	1.33E-10
H1FX-AS1	0.41953717	1.33E-10
AC037459.3	-0.4062863	1.37E-10
AC009052.1	0.28884073	1.48E-10
AL049830.3	0.6357819	1.53E-10
EML2-AS1	-0.4537648	1.65E-10
AC117489.1	0.33971335	1.74E-10
AC012485.1	-0.2221175	1.80E-10
SNHG3	0.47770456	1.89E-10
AC092164.1	-0.4340643	1.90E-10
AC087164.2	0.4338859	1.95E-10
AL035563.1	-0.4011577	1.99E-10
CEBPA-AS1	-0.3197441	2.05E-10
AC132938.3	0.19176932	2.13E-10
IDI2-AS1	-0.4221334	2.22E-10
AC027290.1	0.44847711	2.25E-10
AC005944.1	0.39427901	2.27E-10
AC243829.1	-0.4572955	2.34E-10
AL513302.2	-0.3441665	2.34E-10
A2ML1-AS1	-0.2595578	2.41E-10
AC000068.1	-0.2716418	2.53E-10
AC092902.5	-0.4555395	2.56E-10
AC021188.1	-0.3566933	2.57E-10
AC090152.1	-0.5967764	2.64E-10
AL359397.2	-0.28077	2.66E-10
AC015961.2	-0.519531	2.67E-10
LINC00654	0.61710569	2.68E-10
C15orf59-AS1	-0.5048526	2.76E-10
LINC00174	0.46079334	2.78E-10

Table S2.1 GBM vs LGG

All lncRNAs GBM vs LGG (adj. p-value < 0.05)

ID	LogFC	adj. p
AC055811.4	-0.485969	2.97E-10
AC108863.1	0.29831684	3.12E-10
AL117335.1	-0.3689911	3.15E-10
AL161935.3	0.48966297	3.20E-10
ZSCAN16-AS1	0.37061014	3.35E-10
AC012645.3	0.43144102	3.40E-10
TMCC1-AS1	-0.3629485	3.41E-10
ZMYND10-AS1	0.58898541	3.51E-10
AC060780.1	-0.4243183	3.92E-10
AC008536.3	-0.2121581	4.06E-10
AC013472.3	0.21005524	4.13E-10
AC106820.5	0.35192963	4.26E-10
AC010127.1	-0.4158594	4.31E-10
AC127024.5	0.23474612	4.47E-10
AC108488.1	0.35097299	4.54E-10
AP001107.9	-0.3252635	4.73E-10
AP002893.1	-0.692067	4.84E-10
AC011446.2	0.5575926	5.16E-10
AC074117.1	0.27287553	5.39E-10
AC107464.1	0.80572627	5.74E-10
AC012254.3	-0.3181259	5.85E-10
AC002094.2	0.25567524	6.34E-10
AC012313.5	0.32744934	6.39E-10
AL049776.1	0.24943127	6.49E-10
DKFZP434K028	-0.4093753	6.96E-10
TMEM51-AS1	-0.6116889	7.45E-10
AC007495.1	-0.3368322	8.50E-10
AC011008.2	-0.4353729	8.71E-10
AC008735.2	0.32614046	8.72E-10
AC004520.1	-0.3733793	8.95E-10
GUSBP11	-0.5615074	9.01E-10
AC091078.1	0.24967798	9.22E-10
SMG7-AS1	-0.2486273	9.52E-10
AC034102.5	0.30065035	1.00E-09
AC009955.4	-0.4193038	1.01E-09

Table S2.1 GBM vs LGG

All lncRNAs GBM vs LGG (adj. p-value < 0.05)

ID	LogFC	adj. p
PEG13	-0.6529558	1.15E-09
AL158206.1	0.28477287	1.17E-09
AC044849.2	0.3477348	1.17E-09
AC110491.3	0.20674031	1.29E-09
AC016027.1	-0.2817325	1.30E-09
AC005332.6	-0.2685487	1.31E-09
SNHG16	0.38091476	1.43E-09
AC016727.1	0.24117386	1.45E-09
AC115618.1	0.34110273	1.45E-09
AC132872.4	0.24836013	1.48E-09
AC010978.1	0.34144064	1.49E-09
AC010653.2	-0.3828233	1.51E-09
AC009318.1	0.30228619	1.63E-09
U62317.3	0.31788789	1.65E-09
NEAT1	0.82377663	1.76E-09
AP000350.7	-0.1920353	1.82E-09
ATP13A4-AS1	-0.3840806	1.83E-09
AL590369.1	0.23265584	1.86E-09
USP2-AS1	0.38265527	1.86E-09
AL109659.2	0.49262018	1.96E-09
AC109347.1	-0.2686892	1.96E-09
AC010997.3	0.22891404	2.08E-09
AC079328.3	0.45648954	2.11E-09
AC008878.4	0.40051662	2.14E-09
AC073641.1	0.22781296	2.16E-09
AL161757.2	0.19549809	2.23E-09
AL359094.1	-0.4910956	2.48E-09
AL592146.1	0.48575582	2.51E-09
AC007292.3	0.15922495	2.59E-09
AL049629.1	-0.3546857	2.60E-09
AC097376.2	0.29782974	2.65E-09
AC010327.3	0.49364179	2.74E-09
AC113383.1	-0.492622	2.76E-09
AC012360.3	-0.3657745	2.84E-09
LINC00882	-0.4086388	2.84E-09

Table S2.1 GBM vs LGG

All lncRNAs GBM vs LGG (adj. p-value < 0.05)

ID	LogFC	adj. p
AC084036.1	-0.3615677	2.99E-09
AC005005.3	0.27354644	3.00E-09
AC024896.1	-0.3831813	3.05E-09
AC020904.3	-0.3943161	3.30E-09
AC104051.2	-1.0531308	3.47E-09
AC104758.2	0.30849745	3.50E-09
AL136309.4	0.27851857	3.61E-09
LINC00960	-0.5557008	3.61E-09
AC007308.1	-0.2508846	3.71E-09
AC005009.2	-0.5977515	3.76E-09
AC131097.3	-0.8401666	3.94E-09
DLG5-AS1	-0.2652788	3.95E-09
LINC00667	-0.289033	4.14E-09
PRKCQ-AS1	-0.473879	4.30E-09
AC124066.1	-0.4570302	4.47E-09
AC130304.1	0.45819875	4.50E-09
ITFG2-AS1	-0.2426222	4.63E-09
AP001350.1	-0.4019307	4.68E-09
N4BP2L2-IT2	-0.3169393	4.68E-09
AC018766.1	0.32405225	4.92E-09
AC010834.1	-0.2737781	5.34E-09
AP000802.1	-0.3688251	5.41E-09
AL022328.2	-0.292591	5.44E-09
AC105020.6	0.28812206	5.61E-09
LINCR-0001	-0.3211412	6.35E-09
AL132780.1	0.23185395	6.49E-09
AC018816.1	0.38661378	6.56E-09
MIATNB	0.23655347	6.76E-09
AC025165.2	0.68477587	6.79E-09
AC245297.3	0.38471587	6.87E-09
AL358781.2	0.27196434	6.87E-09
AC107068.2	0.17285619	6.94E-09
AP001107.4	-0.3324977	7.21E-09
AL137129.1	0.47907724	7.55E-09
AP006623.1	-0.3184441	7.69E-09

Table S2.1 GBM vs LGG

All lncRNAs GBM vs LGG (adj. p-value < 0.05)

ID	LogFC	adj. p
AC034102.6	0.20380049	8.19E-09
AC090971.1	0.33240852	8.38E-09
INTS6-AS1	-0.3259154	8.60E-09
AC132192.2	-0.3233174	8.81E-09
AC002070.1	0.20552436	9.57E-09
GAS6-AS1	0.42578717	9.69E-09
ADAMTS9-AS1	0.41168337	1.01E-08
AC245884.9	-0.4386264	1.04E-08
CCDC183-AS1	-0.3407328	1.12E-08
AC008906.1	0.36847363	1.14E-08
AC007920.2	-0.5302209	1.16E-08
LINC00310	-0.3519367	1.16E-08
LINC00327	0.35539851	1.17E-08
AC009948.1	0.22957037	1.18E-08
AL133325.3	-0.6989779	1.33E-08
AC073525.1	-0.9514913	1.35E-08
AC138028.3	0.21187652	1.37E-08
AC008741.2	-0.4098262	1.43E-08
AL133520.1	-0.2137212	1.49E-08
OVCH1-AS1	0.16602049	1.49E-08
AC008537.4	0.32949419	1.50E-08
AC084125.1	0.36175577	1.51E-08
AC022893.1	-0.294762	1.61E-08
SAPCD1-AS1	0.40024289	1.70E-08
AL445183.1	-0.5525716	1.78E-08
AC090616.7	-0.271084	1.81E-08
ARAP1-AS2	-0.3175955	1.94E-08
AC004877.1	-0.448438	2.07E-08
LINC01232	0.41480335	2.18E-08
AL358781.1	-0.4121389	2.52E-08
AC107464.3	0.31834033	2.53E-08
AC000123.3	-0.2417219	2.53E-08
AC084757.3	0.3207849	2.54E-08
AC010761.2	0.23796673	2.59E-08
U47924.2	0.4517324	2.77E-08

Table S2.1 GBM vs LGG

All lncRNAs GBM vs LGG (adj. p-value < 0.05)

ID	LogFC	adj. p
AC097534.2	0.41046169	2.82E-08
AZIN1-AS1	-0.2703846	3.33E-08
AC117498.1	0.31685132	3.36E-08
AC087289.4	-0.2059833	3.36E-08
C8orf31	-0.2934903	3.40E-08
AC106782.6	0.19688198	3.40E-08
AL031587.2	0.23357414	3.51E-08
AC012640.2	0.32707142	3.53E-08
A1BG-AS1	0.3566726	3.63E-08
AC011603.3	-0.726919	3.67E-08
NRSN2-AS1	0.26038514	4.05E-08
AC009403.2	0.714439	4.16E-08
AC136604.2	0.19842547	4.18E-08
AF131216.4	-0.2043073	4.22E-08
AP000892.3	0.31575451	4.22E-08
AL049795.1	0.29639746	4.27E-08
AC109460.2	-0.2839591	4.37E-08
AL662799.1	-0.3680415	4.39E-08
AP004608.1	-0.3720333	4.57E-08
AC008403.2	0.25343931	4.65E-08
AC009060.1	-0.4344529	5.20E-08
AL031595.1	0.49520603	5.54E-08
AC012676.1	-0.4012062	5.58E-08
AL021395.1	-0.4757217	5.85E-08
Z99289.1	0.43337641	6.53E-08
AL355974.1	0.50633295	6.96E-08
AC127496.7	-0.2315871	7.46E-08
LINC01415	-0.3627173	7.49E-08
AC012146.1	0.42017127	7.89E-08
SNHG25	0.31715868	8.35E-08
SNHG21	-0.1948041	8.36E-08
AC125807.2	0.45037215	8.41E-08
AC012313.1	0.35584126	8.74E-08
AC025576.1	-0.3613024	9.11E-08
LINC00623	0.34807556	9.16E-08

Table S2.1 GBM vs LGG

All lncRNAs GBM vs LGG (adj. p-value < 0.05)

ID	LogFC	adj. p
AC007193.3	0.26542276	9.58E-08
AC034228.1	-0.3450037	9.70E-08
LINC00663	-0.2788511	9.77E-08
AP001062.3	-0.2756548	1.06E-07
AC005021.1	0.50013131	1.09E-07
PITPNA-AS1	0.2850224	1.16E-07
AC055720.2	-0.3296611	1.17E-07
SMIM15-AS1	0.22045941	1.28E-07
AC096667.1	-0.2655141	1.28E-07
RORA-AS1	-0.1800943	1.46E-07
HAND2-AS1	0.599398	1.48E-07
STARD7-AS1	0.26942099	1.49E-07
AC005586.1	0.35053572	1.57E-07
AL645941.3	-0.3840222	1.62E-07
AC007191.1	-0.2704089	1.62E-07
AC008074.3	0.19945782	1.62E-07
AL645608.8	-0.5288892	1.64E-07
Z98882.1	-0.2738446	1.78E-07
AC004771.1	-0.2893586	1.86E-07
BDNF-AS	-0.3397025	1.86E-07
AC244517.4	0.59666288	1.88E-07
FLG-AS1	-0.5603329	2.02E-07
AC006064.2	-0.3580394	2.04E-07
AC074032.1	0.29826769	2.05E-07
AC137056.1	-0.3554505	2.06E-07
TRAF3IP2-AS1	-0.3739051	2.12E-07
KMT2E-AS1	0.31846442	2.15E-07
AC007566.1	0.36661729	2.16E-07
AC087289.5	0.50762322	2.21E-07
RAMP2-AS1	-0.53709	2.23E-07
AC109449.1	-0.1523656	2.23E-07
AP000777.2	0.20716922	2.29E-07
AL359915.2	0.28261844	2.33E-07
DUXAP8	0.55283898	2.43E-07
AC009407.1	-0.4500863	2.45E-07

Table S2.1 GBM vs LGG

All lncRNAs GBM vs LGG (adj. p-value < 0.05)

ID	LogFC	adj. p
AC011504.1	-0.5576685	2.58E-07
AC010326.3	0.2942239	2.58E-07
HEIH	0.22726437	2.80E-07
AC095055.1	-0.297887	2.99E-07
AC104365.3	0.19965963	3.19E-07
AP001258.1	0.30240024	3.20E-07
AC126773.2	-0.6481636	3.26E-07
GSEC	0.25231778	3.87E-07
AC067930.6	-0.3172023	3.88E-07
LINC00652	-0.4417473	4.00E-07
AC007192.2	-0.4971686	4.10E-07
LINC01159	0.33998661	4.75E-07
AC110285.2	-0.6633527	4.76E-07
AC009088.2	-0.3463841	4.82E-07
LINC00342	-0.5324868	5.46E-07
AC079315.1	-0.2899998	5.46E-07
AL352979.2	-0.222546	5.47E-07
AC066613.1	-0.2909977	5.54E-07
AC009549.1	0.57624218	5.65E-07
AC073111.4	-0.2277046	5.78E-07
AC105942.1	0.34427905	5.83E-07
AL035071.1	-0.3669887	6.21E-07
AL451165.2	0.22056213	6.46E-07
SERHL	-0.2949141	6.50E-07
EPHA5-AS1	0.36259469	6.90E-07
ZIM2-AS1	0.44039518	6.92E-07
SNHG4	0.32285653	7.16E-07
AP000942.2	0.54340746	7.35E-07
LMCD1-AS1	-0.2719672	7.60E-07
AC138430.1	0.68212576	7.69E-07
AP002449.1	0.18370888	7.84E-07
ASB16-AS1	0.30936537	8.04E-07
LINC01206	0.56918184	8.21E-07
AC091230.1	-0.5843917	8.31E-07
AC008105.3	0.32572017	8.45E-07

Table S2.1 GBM vs LGG

All lncRNAs GBM vs LGG (adj. p-value < 0.05)

ID	LogFC	adj. p
AL139011.1	-0.2698182	8.86E-07
AC079385.1	0.15430544	8.94E-07
FEZF1-AS1	0.6669948	9.29E-07
AL133453.1	0.34323348	9.64E-07
AL365203.3	0.27701057	9.64E-07
AC005076.1	0.28570342	9.78E-07
AC073195.1	-0.2606861	1.06E-06
LINC01485	-0.3809841	1.06E-06
AC008393.1	-0.2685049	1.07E-06
DUBR	0.2674993	1.07E-06
LINC02009	0.60987186	1.12E-06
AC037459.2	-0.1871209	1.15E-06
CADM3-AS1	-0.9646812	1.18E-06
AF127577.4	0.28668336	1.19E-06
AL645568.1	0.21123608	1.21E-06
AL590822.2	-0.484754	1.22E-06
AC005220.1	-0.3621337	1.27E-06
AL359715.3	-0.3508319	1.35E-06
LINC02482	0.24583684	1.36E-06
LINC01114	0.4405893	1.40E-06
LINC00957	0.50703501	1.54E-06
AC009237.14	0.43272753	1.59E-06
AC093673.2	0.30872848	1.60E-06
NUP50-AS1	0.35206466	1.64E-06
AC018647.2	0.30728718	1.67E-06
AC087481.3	-0.3373028	1.76E-06
AC090568.2	-0.2666003	1.79E-06
AC092143.3	-0.2334268	1.80E-06
FIRRE	0.42816661	1.86E-06
DKFZP434H168	-0.3805762	1.86E-06
AC020928.1	0.3379413	1.95E-06
Z97986.1	0.27711394	2.01E-06
AC007249.2	-0.1982258	2.03E-06
BACE1-AS	-0.2567029	2.14E-06
ALOX12-AS1	-0.2288941	2.26E-06

Table S2.1 GBM vs LGG

All lncRNAs GBM vs LGG (adj. p-value < 0.05)

ID	LogFC	adj. p
AC104134.1	0.28736009	2.31E-06
NDP-AS1	0.48854164	2.34E-06
DBH-AS1	0.37825552	2.40E-06
AC126474.2	-0.1610146	2.41E-06
AC016597.1	-0.2764413	2.43E-06
AC008429.1	-0.1722655	2.51E-06
AC080112.4	0.32457631	2.51E-06
ZFHX2-AS1	-0.2346773	2.63E-06
NAGPA-AS1	-0.2475394	2.88E-06
AF117829.1	-0.2355423	2.88E-06
FLJ20021	-0.2771347	2.93E-06
AC026362.1	0.20629054	3.04E-06
AC004925.1	-0.5393198	3.09E-06
AL162311.3	-0.21284	3.12E-06
AP001267.1	0.17476102	3.21E-06
AC009090.4	-0.2548789	3.26E-06
AP001468.1	-0.1924045	3.33E-06
AC114730.2	-0.4221913	3.36E-06
LINC01786	-0.2657163	3.37E-06
TH2LCRR	0.17631734	3.37E-06
AC093110.1	-0.3268885	3.46E-06
AL354733.3	0.26377862	3.67E-06
AC103691.1	-0.2760483	3.74E-06
LINC00899	-0.3810154	3.80E-06
AC011495.2	0.23607688	3.82E-06
AC026471.1	-0.2711256	4.26E-06
AL391069.3	0.33468683	4.29E-06
PAX8-AS1	0.96717071	4.41E-06
AC008966.1	-0.3010386	4.43E-06
AC109460.3	0.24840205	4.47E-06
AP002433.1	-0.1749288	4.53E-06
CHL1-AS2	0.53186462	4.54E-06
GS1-124K5.4	0.32756643	4.59E-06
JAKMIP2-AS1	-0.3471572	4.65E-06
AL357153.3	0.18852825	4.79E-06

Table S2.1 GBM vs LGG

All lncRNAs GBM vs LGG (adj. p-value < 0.05)

ID	LogFC	adj. p
ADNP-AS1	0.23963327	5.03E-06
AL592146.2	0.52660659	5.45E-06
L34079.2	0.19064749	5.81E-06
AC114488.2	0.42869675	5.97E-06
AC009283.1	-0.2584383	6.02E-06
AC003102.1	-0.3157505	6.56E-06
AC011466.1	0.21156243	6.78E-06
AC008736.1	0.15631028	6.86E-06
MAN1B1-AS1	-0.3038848	7.00E-06
AC008014.1	-0.2517481	7.32E-06
AC022966.2	0.31915077	8.21E-06
ZNF649-AS1	0.28079307	8.21E-06
AC016747.4	-0.3306102	8.52E-06
WEE2-AS1	0.35487387	9.27E-06
RASAL2-AS1	0.1642445	9.58E-06
AC020978.8	0.25548118	9.59E-06
AC018665.1	-0.3438037	1.00E-05
AC245060.6	-0.3486834	1.02E-05
THAP7-AS1	-0.2443795	1.08E-05
RASSF1-AS1	0.19816034	1.10E-05
LINC00664	0.3055653	1.11E-05
AC010542.2	-0.240536	1.13E-05
AC009133.2	0.34347292	1.13E-05
AP002907.1	0.19377429	1.17E-05
AC008764.2	-0.199899	1.24E-05
AC023632.6	0.2852223	1.24E-05
LINC00920	0.27751059	1.26E-05
AC009034.1	0.23202285	1.28E-05
UBR5-AS1	-0.2231355	1.28E-05
AC006042.1	0.21448747	1.33E-05
AC069224.1	-0.2754858	1.36E-05
CCDC13-AS1	-0.3363507	1.40E-05
AC137630.2	0.20623414	1.41E-05
LINC00662	0.28178398	1.41E-05
SOX2-OT	-0.4897859	1.44E-05

Table S2.1 GBM vs LGG

All lncRNAs GBM vs LGG (adj. p-value < 0.05)

ID	LogFC	adj. p
AL355922.2	0.29453364	1.64E-05
AL031428.1	0.21862717	1.72E-05
AC007938.3	0.21694358	1.72E-05
AC079305.1	0.17633656	1.76E-05
FZD10-AS1	-0.4011954	1.78E-05
AL358472.2	0.2179996	1.81E-05
AC116407.1	0.14648955	1.81E-05
AP001157.1	-0.2919625	1.88E-05
AC120114.3	0.2248473	1.90E-05
CLMAT3	-0.4678195	2.01E-05
AC015912.1	0.26658429	2.02E-05
AC007622.2	0.16970921	2.09E-05
GAS6-AS2	0.28268689	2.13E-05
RBFADN	-0.3045772	2.21E-05
AL136366.1	-0.4907908	2.25E-05
AP000688.2	-0.3528946	2.69E-05
UBOX5-AS1	0.14562423	2.81E-05
ZNF213-AS1	-0.2508188	2.81E-05
AC040162.3	-0.2560522	2.85E-05
AL096870.2	0.20906492	2.97E-05
AL137077.2	-0.2423645	3.00E-05
AC022336.2	-0.4110719	3.01E-05
AC009570.1	-0.1894242	3.05E-05
AC006547.1	0.20386042	3.14E-05
AC010186.3	0.22249573	3.18E-05
ABALON	0.25009367	3.30E-05
AL136304.1	0.14847166	3.35E-05
LINC01338	-0.452703	3.36E-05
ZRANB2-AS1	0.19409084	3.37E-05
CYP1B1-AS1	0.44626677	3.39E-05
AL050331.2	-0.2292913	3.58E-05
AC129492.7	-0.1790527	3.69E-05
TMEM44-AS1	0.31131049	4.17E-05
AC103740.1	-0.3372553	4.33E-05
AC135457.1	0.20183386	4.45E-05

Table S2.1 GBM vs LGG

All lncRNAs GBM vs LGG (adj. p-value < 0.05)

ID	LogFC	adj. p
ANKRD10-IT1	-0.3564791	4.62E-05
ITGB2-AS1	0.34334184	4.65E-05
AC008734.1	0.18409067	4.94E-05
AL355990.1	-0.4541412	5.04E-05
AL022068.1	-0.3390186	5.11E-05
AC021016.2	-0.197021	5.40E-05
AC016738.1	0.40272592	5.41E-05
SOS1-IT1	-0.1735246	5.50E-05
AC006435.2	-0.3311298	5.52E-05
AC007283.1	0.22047693	5.63E-05
AC105020.1	-0.2366959	5.72E-05
AC005730.2	0.22485458	5.99E-05
AC007383.2	-0.2106625	6.03E-05
AL133227.1	0.1680367	6.09E-05
AC005578.1	-0.1580074	6.18E-05
SNHG1	-0.3921181	6.19E-05
AC009133.4	0.29353662	6.27E-05
AC106820.4	-0.3670279	7.33E-05
AL158847.1	0.39836138	7.43E-05
RAET1E-AS1	0.25655796	7.70E-05
LINC01003	0.37163137	8.23E-05
POT1-AS1	0.29399324	8.66E-05
AC090241.2	0.35494543	8.95E-05
RBM5-AS1	-0.3489355	9.17E-05
AC107294.3	-0.2019893	9.45E-05
AC093330.1	-1.2203975	9.63E-05
AC008741.1	-0.1993477	9.72E-05
CCND2-AS1	0.374771	9.84E-05
MYLK-AS1	0.22960644	0.00010169
UGDH-AS1	0.17396124	0.00010347
AC120049.1	0.18224517	0.00011123
AL353763.2	0.26940897	0.00011332
AL450998.3	0.19948516	0.00011416
AC105020.4	0.51326814	0.00011478
AL355472.1	0.20721514	0.00011496

Table S2.1 GBM vs LGG

All lncRNAs GBM vs LGG (adj. p-value < 0.05)

ID	LogFC	adj. p
AC011468.2	0.17006717	0.00012314
ACVR2B-AS1	-0.2226782	0.00012635
AC068385.1	-0.4090182	0.00012923
AC011510.1	0.22462755	0.00012941
AC093668.2	-0.3108257	0.00013158
AP000446.1	0.15716872	0.0001327
AL592528.1	-0.2921563	0.00013285
C10orf25	-0.2667965	0.00013774
AC124283.1	-0.2276037	0.00014174
AL121753.2	-0.2120937	0.00014582
AL137247.1	-0.209891	0.00014636
AC096677.1	0.23919202	0.00014731
AC108062.1	-0.2258251	0.00015094
AL138724.1	0.19727202	0.00015585
AL355490.2	-0.1521027	0.00015677
AC004918.1	0.20034127	0.00015846
AC004528.2	0.27986951	0.00015849
LINC01158	0.51047343	0.00015949
AL138478.1	-0.2520469	0.00016438
AL356095.2	-0.155288	0.00016606
AL354696.2	-0.1590754	0.00017054
AC011270.2	0.59882646	0.00017486
CAHM	-0.3677239	0.0001766
AL359922.2	-0.2640916	0.0001768
AC036176.1	0.23676668	0.0001826
AC007292.1	0.2217196	0.00019166
AL596202.1	-0.3069271	0.00020028
HCG18	-0.2169029	0.00020093
AL033397.2	-0.1927468	0.00021251
AL358472.5	-0.2011518	0.00022331
AC104794.2	0.27503725	0.00023335
AC005332.8	-0.3363234	0.00023335
AL583722.2	0.2396547	0.00025021
AP000229.1	0.44206948	0.0002524
AC092803.2	-0.2515873	0.0002582

Table S2.1 GBM vs LGG

All lncRNAs GBM vs LGG (adj. p-value < 0.05)

ID	LogFC	adj. p
AC137630.3	-0.2226951	0.00026694
ARMCX3-AS1	-0.231256	0.0002891
LINC01238	-0.3101192	0.00028964
AC036108.2	-0.5560547	0.00030187
AC124016.1	0.19299033	0.00030475
GAS5-AS1	0.13373245	0.00030791
LINC00595	0.27704953	0.00031834
AC007038.2	-0.1507522	0.00032614
AC007996.1	0.19536519	0.00032749
AC008537.3	-0.2747819	0.00032847
AL592166.1	0.33012592	0.00033283
HRAT92	0.29979683	0.00033592
AC087362.1	-0.1930347	0.00034749
IPO9-AS1	-0.2680589	0.0003475
AC015917.2	0.18123998	0.00035065
AC093227.1	0.21735266	0.00035194
ASMTL-AS1	-0.226766	0.00035194
AC005013.1	-0.4118292	0.00036574
AC005544.2	-0.605844	0.00037105
AC138028.4	0.366878	0.00037335
AC017100.1	-0.3305171	0.00039733
AL731566.1	0.15591603	0.00042357
AC005520.2	-0.278904	0.00043715
AC115284.1	-0.2476765	0.00043724
AC027309.1	0.35470947	0.0004714
AP005433.1	-0.1746377	0.00047969
ZMIZ1-AS1	0.24855695	0.00048159
PCF11-AS1	-0.2323306	0.00049248
AC008536.1	-0.1710537	0.00049277
AC022973.4	-0.1941772	0.00049694
AP006621.5	-0.4129851	0.00051566
AC087741.1	-0.3529273	0.00051833
AL133375.1	-0.2274321	0.00052032
MORF4L2-AS1	-0.1784246	0.00053677
AC138649.1	-0.3706811	0.00058705

Table S2.1 GBM vs LGG

All lncRNAs GBM vs LGG (adj. p-value < 0.05)

ID	LogFC	adj. p
AC007298.1	0.18074758	0.00059854
AC026271.4	-0.2482435	0.00060236
AC091045.1	0.21227165	0.00060628
ZNF337-AS1	-0.2841052	0.00061015
AC005523.2	-0.1875153	0.00065348
AC115618.3	-0.1779483	0.00066822
AC138028.2	-0.3204961	0.00067083
AC104590.1	-0.2136292	0.00069565
AC008494.3	0.13164664	0.00071544
WASHC5-AS1	0.13983508	0.00071561
POC1B-AS1	-0.1590961	0.00072784
COX10-AS1	0.21179226	0.00074063
AL031772.1	-0.2167804	0.0007587
AP001469.1	-0.236615	0.0007587
AC099522.2	-0.2007615	0.00076634
AL137058.2	-0.2077164	0.00077097
AC137834.2	0.25987195	0.00078588
AC008771.1	0.22578117	0.00078971
AC090114.2	-0.2746431	0.00079309
JAZF1-AS1	0.2092083	0.00080775
LINC01816	-0.255639	0.00082119
AL132639.3	-0.165134	0.00084248
AC008742.1	0.25827639	0.00084839
AC093323.1	-0.1800254	0.00084857
AC112484.2	0.2074464	0.00089815
RUSC1-AS1	0.18312643	0.0009306
LINC00173	-0.2856003	0.0009306
AC110597.3	0.3460734	0.00101053
AC068152.1	-0.195045	0.00101272
LINC00467	0.29826068	0.0010236
SEPT7-AS1	-0.2357365	0.00107317
AL355312.3	-0.1760647	0.00110615
COLCA1	-0.4207661	0.00117929
ADIRF-AS1	-0.4173052	0.00120181
SCAMP1-AS1	0.26339378	0.0012243

Table S2.1 GBM vs LGG

All lncRNAs GBM vs LGG (adj. p-value < 0.05)

ID	LogFC	adj. p
CTBP1-AS2	-0.2088907	0.00130251
MAPKAPK5-AS1	0.20663522	0.00134702
DIO3OS	-0.3135553	0.00135863
AL136418.1	-0.2194152	0.00138422
LPP-AS2	0.24682291	0.00144565
AC131238.1	0.14732261	0.00148368
AL139384.2	0.24162804	0.00148368
AP002026.1	0.22763762	0.00149845
AC106782.2	0.15278379	0.00151851
AC109322.1	0.21317564	0.00153224
AC124242.1	-0.1575159	0.00155676
AC021739.4	-0.2384024	0.00156432
AC091059.1	-0.1416334	0.00158988
AC127496.6	0.18015011	0.00160384
FLJ27354	-0.2311589	0.00160613
AC046168.2	-0.2886093	0.00162994
AL358216.1	-0.4284646	0.001685
SERPINB9P1	0.29843679	0.00169958
LINC00982	-0.4515265	0.00172388
AC005606.1	0.20988994	0.00184494
MAMDC2-AS1	0.22587455	0.00184691
AC084033.3	0.46567747	0.0019394
AC007620.2	0.2934019	0.00199611
Z98752.1	-0.2256457	0.00206277
AC073073.2	0.16909149	0.00220515
AL136322.1	-0.2863748	0.00226718
AC244517.1	-0.3487282	0.00227873
SLCO4A1-AS1	0.344188	0.00228907
AC130343.1	-0.1776083	0.00228996
AC136469.2	-0.2581722	0.00233614
HCG25	-0.1514049	0.00236054
AC006001.2	0.24616993	0.00240202
AC078777.1	-0.1972928	0.00250553
AL391988.1	-0.1349412	0.00273692
AC104699.1	-0.1610323	0.0027512

Table S2.1 GBM vs LGG

All lncRNAs GBM vs LGG (adj. p-value < 0.05)

ID	LogFC	adj. p
AC010809.2	0.24647337	0.00279333
AC021755.2	0.26522428	0.00280809
AC011483.3	-0.6686823	0.00280809
KCNMA1-AS1	-0.2637397	0.0029006
LINC00963	0.23242603	0.00293171
AC005261.4	0.21191692	0.00295668
ZNF790-AS1	0.21009363	0.00310999
AC008105.1	0.31761083	0.00322432
Z97056.1	-0.3932557	0.0032518
AC090204.1	0.37691166	0.00328546
KF459542.1	0.15558824	0.0036351
AC087164.1	0.22216976	0.00390292
AL662907.2	-0.1567317	0.0040472
AP003501.2	0.24969645	0.0040472
HHIP-AS1	0.32596687	0.00409366
OPA1-AS1	-0.1545662	0.00412763
AC025918.1	-0.1433954	0.00415577
IL21R-AS1	0.35969499	0.00429305
SLC26A4-AS1	-0.5568248	0.00436327
AL683813.1	-0.2492932	0.00436826
KANSL1-AS1	0.36120659	0.00440433
SH3RF3-AS1	-0.2013839	0.00440893
ALDH1L1-AS1	0.45618955	0.00465276
AC091564.7	0.31345671	0.00467468
NFYC-AS1	0.17934597	0.00472378
AC004852.2	0.4213872	0.00472378
AC090061.1	0.3092617	0.00475342
PCAT6	-0.2536311	0.00482416
SVIL-AS1	-0.2500823	0.00484667
AC145285.7	0.19213073	0.00484667
NAV2-AS1	-0.2998814	0.00488859
AP001347.1	0.2395955	0.00488859
AC016876.1	-0.2098366	0.00494581
AC244517.11	-0.4668347	0.00507086
SBF2-AS1	0.19573253	0.00514204

Table S2.1 GBM vs LGG

All lncRNAs GBM vs LGG (adj. p-value < 0.05)

ID	LogFC	adj. p
AL080317.3	-0.2918216	0.00527967
AC005921.2	-0.1769169	0.00551848
AC025048.2	-0.1624619	0.00551848
CASK-AS1	-0.2123264	0.00555871
AC006450.2	0.32683002	0.00574973
AL023584.1	-0.2111293	0.00576772
AC091887.1	0.13402265	0.00587459
RFX3-AS1	-0.2004878	0.00604049
AL390208.1	-0.2349387	0.00612738
AC136475.1	-0.3170716	0.00621871
C5orf64	-0.251584	0.00627188
ERVK13-1	-0.3094333	0.00627188
AL590006.1	-0.2228991	0.00643379
AC022509.1	-0.3205001	0.00647965
AC093249.6	-0.194819	0.00649322
CIRBP-AS1	0.16196408	0.00649577
AL358473.1	-0.3732984	0.00652389
AC092809.4	0.16955702	0.00654363
AL928921.2	0.19257408	0.00658119
AL139424.2	-0.2883651	0.00663676
AC020765.2	-0.1838194	0.00666213
AC092070.3	0.23106464	0.00672822
AC012363.1	-0.2113672	0.00676497
AP003119.3	0.29562476	0.00685241
AC024270.3	-0.1633084	0.00685734
AC024075.2	-0.2153504	0.00701513
AC002310.6	-0.1609456	0.00707899
ADORA2A-AS1	-0.136277	0.00707899
AC134407.3	-0.171128	0.00709291
NUTM2A-AS1	-0.2700493	0.00713961
NPPA-AS1	-0.3196099	0.00715222
AC092821.3	0.23503561	0.0071682
AC027097.2	0.10936567	0.00721356
AL021707.3	-0.2737965	0.00724043
AC137767.1	-0.1952591	0.00738351

Table S2.1 GBM vs LGG

All lncRNAs GBM vs LGG (adj. p-value < 0.05)

ID	LogFC	adj. p
MZF1-AS1	0.23299456	0.00759304
AC025257.1	-0.2745378	0.0075993
LINC00630	-0.149648	0.00771191
AC084018.1	-0.2513415	0.00771859
AC009019.1	-0.1180116	0.00804734
AC099668.1	-0.2937763	0.00826168
AC009061.2	0.16518113	0.00833412
AC019205.2	-0.2127112	0.00837805
RAD51-AS1	-0.2251088	0.00853769
AP002383.3	-0.2372796	0.00854448
AL034549.2	0.14825118	0.00861722
PLCG1-AS1	0.20635456	0.00862787
AC007362.1	0.31499417	0.00870147
MATN1-AS1	0.18343155	0.00874787
ZFAS1	0.30342674	0.00877537
AC002467.1	0.15077496	0.00974839
AL359513.1	0.20591353	0.00974839
AC008608.2	0.17473203	0.01010908
AC002310.1	-0.1733343	0.01029922
AC091138.1	-0.3382079	0.01042984
C21orf62-AS1	-0.1534684	0.01074582
AC006333.2	0.23782346	0.0113797
AC005332.7	-0.2894122	0.01168752
AL135925.1	-0.1681084	0.01169558
AC006449.5	-0.196967	0.01197377
SNHG6	-0.2267084	0.01207524
AL354920.1	0.14534939	0.01229139
EGFR-AS1	0.78085932	0.01256555
AC046185.3	0.26052177	0.01329104
WDR7-OT1	-0.1809133	0.01339702
AC004408.1	-0.2470831	0.01376038
AL121928.1	-0.1508119	0.01413584
EZR-AS1	0.3002062	0.01511963
AL008729.1	-0.1849251	0.01541684
DLX6-AS1	0.83557765	0.01548707

Table S2.1 GBM vs LGG

All lncRNAs GBM vs LGG (adj. p-value < 0.05)

ID	LogFC	adj. p
AC006504.5	0.20199268	0.01719465
AL157938.2	-0.2429845	0.01729698
AC090559.1	0.27446714	0.01762714
AL117190.2	0.50097947	0.01826536
AC092119.2	-0.1777544	0.01835972
AL354771.1	-0.2762169	0.01841259
THRIL	-0.2515847	0.01861253
DM1-AS	0.28199639	0.01880423
AF131216.1	-0.1860475	0.02021574
AC005225.5	-0.2129974	0.02022089
VPS9D1-AS1	-0.1955111	0.0210935
WARS2-IT1	0.23379458	0.02237825
AL359317.1	-0.2076356	0.0228897
AC098487.1	0.18568188	0.02358967
AC079328.2	-0.1761145	0.0239064
AL353150.1	0.25655877	0.02451599
AC142472.1	-0.1697835	0.02479699
AC008080.4	0.54340321	0.02489964
MGC32805	-0.2884687	0.02524097
AC007405.3	0.20957813	0.02592232
CR559946.2	-0.1822307	0.02762849
DARS-AS1	-0.1647095	0.028872
AL136038.2	0.1239784	0.02889723
AL590004.4	0.35049727	0.02924465
LINC01480	-0.2799021	0.02945849
AP002748.3	-0.179182	0.02994937
AC007161.3	0.17468058	0.03052809
AC006058.4	-0.378277	0.03068628
AC133785.1	-0.1835752	0.03148069
USP46-AS1	-0.1533963	0.03214399
AC007342.6	-0.1751862	0.03369649
AC020663.1	0.10915295	0.03384431
XIST	-0.9753629	0.03491965
AC025043.1	0.20285112	0.03582455
AP003774.1	0.24196902	0.0361846

Table S2.1 GBM vs LGG

All lncRNAs GBM vs LGG (adj. p-value < 0.05)

ID	LogFC	adj. p
AL021368.4	-0.1596737	0.03670093
AC093535.1	-0.2939483	0.03699529
AC008443.2	-0.1795142	0.03779965
AC009955.3	0.17845921	0.03882331
AC092567.1	-0.1781021	0.04010143
AC009063.2	-0.2923096	0.04066267
SMAD1-AS1	0.25016551	0.04067643
AC009511.1	-0.1483425	0.04081414
AL451164.3	-0.2466413	0.04184111
AC002116.2	-0.2468113	0.04295702
ACBD3-AS1	0.18577423	0.04438089
AC079601.1	-0.3726639	0.04487454
AC135048.2	0.13310201	0.04634141
LINC00969	-0.2697937	0.04650302
AC116667.1	-0.1590187	0.04697274
AC009414.2	-0.2077529	0.04759256
AC099850.1	-0.1307101	0.04768721
SRP14-AS1	-0.243249	0.0476967
AC055860.1	0.15978542	0.04962198

Table S2.2 Recurrent vs Primary
lnc-pri-miRNAs (adj. p-value < 0.05)

ID	LogFC	adj. p
hsa-mir-551b	1.051552615	1.22E-05
hsa-mir-548u	0.510185423	3.00E-05
hsa-mir-30a	-1.41055559	6.50E-05
hsa-mir-3916	0.481828323	0.000270321
hsa-mir-544b	-0.69308154	0.001052387
hsa-mir-1226	-0.74194604	0.001581538
hsa-mir-6834	0.403371295	0.001896629
hsa-mir-3163	0.328393071	0.002624149
hsa-mir-4435-2	1.112248921	0.003885111
hsa-mir-4510	-0.27315200	0.004163764
hsa-mir-548aa-1	0.581984636	0.005005002
hsa-mir-4435-1	0.865036519	0.018452266
hsa-mir-571	0.414756865	0.023366298
hsa-mir-130b	0.455241599	0.027809544
hsa-mir-6861	0.309967974	0.037433277
hsa-mir-1302-11	0.465074182	0.04210908

Experimental Procedures

LGG vs GBM public data, and primary vs recurrent glioma analysis

Aligned reads for glioblastoma (GBM) and low-grad glioma (LGG) patients were obtained from the GDC Data Portal (https://portal.gdc.cancer.gov/). As for the primary vs recurrent glioma samples, tumor specimens from 31 glioma patients were obtained from the Costello lab at UCSF. Each of these patients underwent surgical resection at UCSF for primary grade-II/III glioma and again subsequently for a recurrent glioma. Both primary and (for some patient multiple) recurrent specimens were profiled by RNA-seq, resulting in 122 total datasets.

Expression of coding and non-coding transcripts was performed with featureCounts (Liao et al., 2014) and a gtf files containing the annotations in the Gencode v28 database and the annotation of microRNA primary transcript structures from Chang *et al*., (Chang et al., 2015). For the primary vs recurrent samples, gtf annotation files from Gencode and Cheng *et al*., (Chang et al., 2015) were mapped from GRch38 to hg19 using liftover from the UCSC Genome Browser (https://genome.ucsc.edu/cgi-bin/hgLiftOver). Expression levels in each count matrix were normalized to counts per million (CPM) based on total Gencode counts and log2 transformed (log2 (CPM+1)). As multiple specimens were sequenced from some of the recurrent cases, but not others, expression levels were averaged by case to obtain 62 datasets for analysis (31 primary, 31 recurrent). Only features with an average expression > 2 CPM in any sample were considered for downstream analysis. Differential expression was accessed using pairwise t-tests and adjusted for multiple testing using the Benjamini-Hochberg (Benjamini et al., 2001) method. lnc-pri-miRNA transcripts were defined as transcripts with genomic coordinates overlapping the coordinates of at least one mature miRNA as annotated in miRbase v21 (Kozomara and

Griffiths-Jones, 2014). Protein coding genes were identified via the "gene type" information in the Gencode database. Significant differences in lnc-pri-miRNA and non lnc-pri-miRNA expression between GBM and LGG (or primary and recurrent) were determined using Fisher's exact test. All subsequent data analysis and visualization was carried out in R (v3.4.2.). PCA analysis was performed on all expressed lnc-pri-miRNA. The heatmap was generated for all lnc-pri-miRNA with loadings <-0.2 or >0.2 for PC1 in PCA analysis, clustering was performed using average linkage clustering and 1-person correlation as distance measure.

Motif discovery and promoter analysis

For all lncRNAs differentially expressed in GBM vs LGG, we analyzed genomic regions encompassing the promoter (2kb upstream to 100bp downstream of TSS) of lnc-pri-miRNAs and other lncRNAs using the software HOMER2 for *de novo* motif discovery.

Chapter 3: miRNA-independent function of lnc-pri-miRNA loci

Summary

In a CRISPR interference (CRISPRi)-based screen of 5,689 lncRNA loci expressed in U87 GBM cells (Liu et al., 2017), lnc-pri-miRNAs were found to be significantly enriched for function in cell propagation. We presumed the primary function of the lnc-pri-miRNAs in cell propagation relates to the miRNAs produced. Here, we show that knockdown of essential miRNA processing machinery (*DGCR8* or *DROSHA*) does not change cell propagation in U87 cells. Moreover, we demonstrate that the cell propagation phenotype of CRISPRi targeting of four lnc-pri-miRNAs is still observed, despite knockdown of *DGCR8* or *DROSHA*. In U87 cells, *LOC646329* is a chromatin-enriched lnc-pri-miRNA that produces miR-29a/b1 -- identified as one of the essential lnc-pri-miRNA in the CRISPRi screen. Knockdown of *LOC646329* using both CRISPRi and ASOs resulted in the reduction of *LOC646329* as well as mature miR-29a and miR-29b1 levels. We show that the reduction of *LOC646329* and miR-29a/b1 levels together led to decreased cell propagation due to increased apoptosis and reduced cell proliferation. The requirement for *LOC646329* is cell-type specific, as the reduction of *LOC646329* in HeLa cells and human astrocytes did not reduce cell propagation. The essential function of *LOC646329* in U87 cells is genetically separable from its cognate miRNAs, miR-29a/b1 – where miR-29a/b1 controls aspects of apoptosis, while *LOC646329-miR29Δ* regulates proliferation. The regulation of proliferation is related to the enhancer-like activity of the *LOC646329* locus, where it regulates oncogene expression. Furthermore, we find that lnc-pri-miRNAs are generally enriched for enhancer characteristics, as compared to the broader class of lncRNAs. Finally, functional testing of 9 additional lnc-pri-miRNAs exhibit enhancer-like regulation of local gene

expression, further demonstrating that lnc-pri-miRNA loci can indeed have miRNA-independent function.

Introduction

Emerging evidence indicates that lnc-pri-miRNAs can have important roles in development and disease (Caronia-Brown et al., 2016; Lu et al., 2017; Ng et al., 2013; Profumo et al., 2019; Sun et al., 2018), but it is unclear whether lnc-pri-miRNA function primarily relates to the miRNAs that are produced. Although certain studies provide evidence for lnc-pri-miRNA function that appears miRNA-independent (Ng et al., 2013; Sun et al., 2018), other studies of these same lnc-pri-miRNAs relate function primarily to their cognate miRNAs (Caronia-Brown et al., 2016; Lu et al., 2017).

In a genome-scale CRISPR interference (CRISPRi) screen of lncRNAs, many lnc-pri-miRNA loci regulate cell proliferation (Liu et al., 2017), and we initially presumed that these lnc-pri-miRNAs functioned primarily through miRNA-based mechanisms. In this chapter, we observed in U87 GBM cell knockdown of *DGCR8* or *DROSHA* – key components of miRNA processing – all of the lnc-pri-miRNA screen hit loci still strongly regulated cell proliferation. To more incisively dissect lnc-pri-miRNA function, we studied *LOC646329*, which hosts miR-29a/b1. Using multiple, complementary methods, we found that *LOC646329* can regulate GBM cell growth independent of its cognate miRNAs, and this miRNA-independent activity corresponded to enhancer-like activation of a neighboring oncogene. To explore whether additional lnc-pri-miRNA loci also have evidence of enhancer-like activity, we analyzed genome-wide data from multiple human cell types, finding that lnc-pri-miRNA loci were significantly enriched for key characteristics of transcriptional enhancers, and CRISPRi targeting

demonstrated enhancer-like function of multiple lnc-pri-miRNA loci.

Results

lnc-pri-miRNA loci regulate cell proliferation in cells with Microprocessor knockdown

In a genome-scale screen of lncRNA function (Liu et al., 2017), CRISPRi was used to target a total of 5,689 lncRNA loci expressed in U87 GBM cells. Of the 65 hits, 5 targeted the TSS of 4 different lnc-pri-miRNA loci, representing a ~6.6-fold enrichment of function (P=0.001) over that of other lncRNAs (**Fig. S3.1A, B**). Similarly, lnc-pri-miRNAs were also significantly enriched for function in MDAMB231 cells, MCF7, and induced pluripotent stem cells (iPSCs) (**Fig. S3.1C**). Using internally controlled growth assays ((Liu et al., 2017) and **Methods**), we validated the 4 lnc-pri-miRNA screen hits with individual CRISPRi sgRNAs in U87-dCas9-KBAB cells (**Fig. 3.1A, B, S3.2A, B**).

To test whether the cell proliferation function of these lnc-pri-miRNA loci requires miRNA production, we generated U87 cells with stable CRISPRi-mediated knockdown of either *DGCR8* or *DROSHA* (**Fig. 3.1C**), key Microprocessor enzymes required for miRNA production (**Fig S3.2C**) (Gregory et al., 2004; Wang et al., 2007), and neither *DGCR8* nor *DROSHA* knockdown altered the propagation of U87 cells (**Fig. 3.1D**). Despite knockdown of *DGCR8* or *DROSHA*, the cell proliferation phenotype of CRISPRi targeting of the 4 lnc-pri-miRNAs was still observed, even in cells that exhibited no further reduction in mature miRNA levels as seen with miR-29a (**Fig. 3.1E, S3.2C, D**). These results suggest that lnc-pri-miRNA loci have important function that is independent of normal Microprocessor function.

LOC646329 knockdown increases apoptosis and reduces proliferation of GBM cells

To more directly test whether a lnc-pri-miRNA locus can regulate cell proliferation independent of its cognate miRNA, we focused on one of the lnc-pri-miRNA hits, *LOC646329*. *LOC646329* encodes a spliced lnc-pri-miRNA transcript (Genbank accession number EU154353) with the miR-29a/b1 cluster located between exon 3 and 4 (Chang et al., 2008; Ru et al., 2016). Using long-read single-molecule Oxford Nanopore direct RNA-sequencing and Illumina RNA-sequencing, we confirmed the production of transcripts from the *LOC646329* TSS that span the miR-29a/b1 cluster (**Fig. 3.2A**). Cell fractionation as well as fluorescent *in situ* hybridization (FISH) analysis demonstrated *LOC646329* to be a nuclear-enriched lncRNA (**Fig. S3.3A, B)**. Consistent with *LOC646329* serving as a lnc-pri-miRNA for miR-29a/b1 (Chang et al., 2008; Ru et al., 2016), targeting CRISPRi repressive complexes to the *LOC646329* TSS – which is ~36 kilobases (kb) upstream of the miR-29a/b1 cluster – reduced levels of both miR-29a and miR-29b1 (**Fig. 3.2B, C, S3.3C)**.

CRISPRi-mediated knockdown of *LOC646329* decreased the propagation of U87 GBM cells (**Fig. S3.3D**), increasing apoptosis as determined by immunocytochemistry (ICC) analysis for activated Caspase 3, and decreasing proliferative cells, as measured by expression of Ki67 (**Fig. 3.2D**). In contrast, *LOC646329* knockdown did not decrease the propagation of HeLa cervical cancer cells (**Fig. S3.4A-C**) or normal human astrocytes (**Fig. S3.4D-F**), consistent with most essential lncRNAs having cell type-specific function (Liu et al., 2017).

CRISPRi represses transcription by sterically blocking RNA polymerase and inducing local heterochromatinization (Gilbert et al., 2013; Qi et al., 2013). To decrease *LOC646329* levels with an orthogonal method, targeting the RNA transcript itself, we used antisense oligonucleotides (ASOs) that trigger RNA degradation via a ribonuclease H-based mechanism.

While ASOs targeting the nascent transcript or near the 5' end of RNA can trigger premature transcriptional termination (Lai et al., 2020; Lee and Mendell, 2020), we used ASOs designed to the distal 3' end of *LOC646329*, which is at least 35,771 bp from the TSS (**Fig. S3.3E**). ASO-mediated *LOC646329* knockdown significantly reduced FISH signal (**Fig. S3.3F, G**) and strongly reduced U87 cell propagation as compared to the negative control ASO (**Fig. 3.2E, S3.5A, B),** increasing apoptosis and decreasing proliferation as determined by ICC analysis for the incorporation of 5-ethynyl-2'-deoxyuridine (EdU) and Ki67 expression (**Fig. 3.2F, S3.5C**). Although *LOC646329* ASO-1 and ASO-2 produce a similar phenotype (**Fig. 3.2F, S3.5C)**, nuclear run-on (NRO) experiments to assess nascent transcription suggests ASO-2 can induce premature transcriptional termination (**Fig. S3.5D**), while ASO-1 only modestly reduces (~24%) nascent transcripts observed at the distal 3' end (**Fig. 3.2G**). Chromatin immunoprecipitation (ChIP) analysis of total Pol II as well as RNA Pol II with Serine 5 phosphorylation (S5P) – a posttranslational modification required for robust initiation and elongation (Rahl et al., 2010) – did not reveal a significant difference in Pol II occupancy throughout the gene body (**Fig. 3.2H**), providing further evidence that ASO-1 does not disrupt transcription through the 5' regions of *LOC646329*. Similarly, short hairpin RNA (shRNA)-mediated degradation of the *LOC646329* transcript also decreased cell propagation (**Fig. S3.5E, F**), suggesting an RNA transcript-based role in cell propagation.

Deletion of miR-29a/b1 does not decrease cell growth

Given that *LOC646329* is a lnc-pri-miRNA for miR-29a and miR-29b1, we investigated whether the growth inhibitory effect of *LOC646329* knockdown in GBM cells was due to decreased miR-29a/b1 activity. First, we used a miR-29 sponge construct (**Fig. S3.6A**) to reduce

miR-29a/b1 levels and activity (**Fig. S3.6B**). While U87 cells expressing the miR-29 sponge did not exhibit a growth defect (**Fig. S3.6C, D**), we considered the possibility that the sponge construct did not fully inhibit miR-29 activity. Thus, we next used CRISPR/Cas9 to genetically delete miR-29a/b1 from *LOC646329*. U87 cells expressing the Cas9 nuclease were transfected to transiently express pairs of single guide RNAs (sgRNAs) that flank the miR-29a/b1 cluster (**Fig. 3.3A**). Cells were then clonally isolated, and miR-29a/b1 knockout cells (*LOC646329-miR29Δ*) were confirmed by PCR genotyping and Sanger sequencing (**Fig. S3.7A**). In *LOC646329-miR29Δ* cells, expression of miR-29a/b1 was essentially abolished as assessed by RT-qPCR analysis and microRNA-sequencing (**Fig. 3.3B, S3.7B**), resulting in the de-repression (Fisher's exact test, P=1.9^{-35}) of known miR-29 target genes (**Fig. S3.7C, D, Table S3.1**). These miR-29 target genes were enriched for regulation of extracellular matrix (ECM) organization and unfolded protein response (**Fig. S3.7E**), consistent with miR-29's role in ECM remodeling (Sengupta et al., 2008), and apoptosis (Park et al., 2009; Ru et al., 2016; Xu et al., 2015). miR-29b2/c – miRNA family members that are encoded from a locus on a different chromosome – were not detected in either wild-type or *LOC646329-miR29Δ* U87 cells (**Fig. S3.7B**).

In all three U87 cell clones (clone 15, 18 and 40) with *LOC646329-miR29Δ*, cellular propagation was not decreased as compared to non-deleted controls. Surprisingly, clones 18 and 40 exhibited a faster cell cycle (**Fig. S3.8A, B**), resulting in greater numbers of cells (1.58–1.74 fold increase) over 15 days of culture (**Fig. S3.8C**). Furthermore, the clones did not exhibit an increase in apoptosis, and more Ki67+ cells were observed in clones 18 and 40 (**Fig. 3.3C**). Taken together, these data indicate that the decrease in U87 cell propagation observed with CRISPRi- (**Fig. S3.3D**) or ASO-mediated *LOC646329* knockdown (**Fig. S3.5A**) does not solely relate to decreased miR-29a/b1 levels.

***LOC646329* has cellular function independent of its cognate miRNAs**

Due to the faster cell cycle times and increased *LOC646329-miR29Δ* transcript expression after miR-29 deletion seen in clones 18 and 40, we hypothesized that *LOC646329* overexpression would increase cell proliferation. To test this, we used CRISPR activation (CRISPRa), with dCas9-VPR (Chavez et al., 2015) to activate the *LOC646329* locus. Using CRISPRa, we observed 4-5 fold overexpression of *LOC646329,* followed by a corresponding increase in cell proliferation (**Fig S3.8D, E**). Surprisingly, CRISPRa of *LOC646329* did not increase miR-29a/b1 levels (data not shown), suggesting that the increase in cell proliferation by activating *LOC646329* is independent of miR-29a/b1 levels.

In cells deleted for miR-29a/b1, transcripts from *LOC646329-miR29Δ* gene were detected at increased levels as compared to wild-type *LOC646329* (up to ~33-fold, **Fig. 3.3D**), accumulating as focal "clouds" in the nucleus, as observed by ISH (**Fig. 3.3E**). The increased levels of *LOC646329-miR29Δ* correlated with a 4-fold increase in transcript half-life (**Fig. S3.8F**), and ChIP analysis revealed increased levels of RNA Pol II as well as RNA Pol II S5P at the TSS of *LOC646329-miR29Δ* (**Fig. S3.8G**). Thus, as compared to the wild-type locus*, LOC646329-miR29Δ* produces lncRNA transcripts with increased stability from a TSS with more RNA Pol II activity.

We next investigated whether *LOC646329* is required for cell proliferation independent of its production of miR-29a/b1. Using the same ASOs effective for *LOC646329* depletion, we knocked down the *LOC646329-miR29Δ* transcripts in U87 cells (**Fig. 3.4A, S3.9A**). Interestingly, knockdown of *LOC646329-miR29Δ* did not increase apoptosis (**Fig. 3.4B, S3.9B**), as was observed with ASO-mediated knockdown of *LOC646329* (**Fig. 3.2F, S3.5C**). However,

in all three clones with miR-29a/b1-deletion, knockdown of *LOC646329-miR29Δ* still strongly reduced cell proliferation (**Fig. 3.4B, S3.9B**). U87 cells with *LOC646329-miR29Δ* knockdown resulted in the differential expression of 290 genes (108 upregulated, 182 downregulated) that had significant overlap (256, 88%, **Table S3.1**) with gene expression changes observed with *LOC646329* knockdown (**Fig. S3.9C, Table S3.1**). This set of common differentially expressed genes are enriched for regulation of sodium ion transmembrane transport and DNA repair (**Figure S3.9D**). Thus, the *LOC646329-miR29Δ* transcript – which no longer serves as a precursor of miR-29a/b1 – is required for robust U87 cell proliferation.

To further test whether *LOC646329* regulates cell proliferation independent of its production of its cognate miRNAs, we introduced miR-29a/b1 into U87 cells with or without knockdown of its lnc-pri-miRNA transcript (**Fig. S3.10A-C**). In control U87 cells without *LOC646329* knockdown, transfection of miR-29a/b1 significantly increased apoptosis without adversely affecting EdU-incorporation or Ki67-expression (**Fig. S3.10A, C**), consistent with the pro-apoptotic effect of miR-29 overexpression (Park et al., 2009; Ru et al., 2016; Xu et al., 2015). In cells with *LOC646329* knockdown, the reintroduction of exogenous miR-29a/b1 partially reversed the apoptosis phenotype, but the cell proliferation defect was not changed (**Fig. S3.10B, C**). Thus, the levels of miR-29 activity (in cells with or without *LOC646329* knockdown) can regulate apoptosis without adversely affecting measures of cell proliferation. Transfection of miR-29a/b1 did not reduce levels of *LOC646329* (**Fig S3.10A**), contrary to recent observation that miR-29b1 can target *LOC646329* in colorectal cancer cells (Javanmard et al., 2020). These data further support the concept that *LOC646329* has critical cellular function that is separable from the function that its cognate miRNAs play in apoptosis.

The *LOC646329* locus contains transcriptional enhancer activity

Some lncRNAs can regulate the expression of gene neighbors (Engreitz et al., 2016; Lai et al., 2020; Luo et al., 2016; Melo et al., 2013; Orom et al., 2010; Wang et al., 2011). Within a 1MB genomic window around *LOC646329*, the expression of *MKLN1* and *linc-PINT* was decreased by both ASO- (**Fig. 3.4C, S3.11A, B**) and CRISPRi-mediated knockdown of *LOC646329* (**Fig. S3.11C**). Of note, *MKLN1,* a putative oncogene in human glioma (Nord et al., 2009), was significantly decreased as early as 4 hours post ASO transfection in U87 cells, suggesting direct regulation by *LOC646329* (**Fig. S3.11D**). To ensure dCas9-KRAB did not directly affect *MKLN1* in the CRISPRi knockdown of *LOC646329*, we conducted H3K9me3 ChIP-seq analysis and found H3K9me3 significantly gained only at the *LOC646329* promoter (**Fig S3.12A)**, but not at the *MKLN1* promoter or any other site genome-wide (**Fig S3.12B**). Furthermore, ASO-mediated knockdown of *MKLN1* decreased U87 cell propagation (**Fig. 3.4D, E, S3.11E**). Double knockdown of both *LOC646329* and *MKLN1* (**Fig. S3.13A**) did not result in a significant difference in apoptosis or proliferation as compared to *LOC646329* knockdown alone (**Fig. S3.13B**), suggesting that *LOC646329* is epistatic to *MKLN1*. Although knockdown of *LOC646329* also resulted in a reduction of *MKLN1* levels in both HeLa and normal human astrocytes (**Fig. S3.14A, C**), ASO-mediated knockdown of *MKLN1* in HeLa or normal human astrocytes did not decrease cell propagation as determined by ICC analysis (**Fig. S3.14B, D**).

Analysis of genome-wide chromosome conformation capture (Hi-C) data generated from human fetal brain tissue (Won et al., 2016) revealed increased DNA-DNA interaction frequencies between the *LOC646329* locus and *MKLN1/linc-PINT*, which are ~ 200kb apart, with *MKLN1* and *linc-PINT* having overlapping but divergent promoters. By integrating 7 genome-wide databases, GeneHancer (Fishilevich et al., 2017) yields a map of high confidence

"double-elite" enhancers, one of which is *LOC646329*, shown as an enhancer interacting with the *MKLN1/linc-PINT* promoters (**Fig. 3.4F**). To confirm these interactions between *LOC646329* and *MKLN1*/linc-*PINT*, we performed chromosome conformation capture (3C) followed by quantitative PCR (**Fig 3.4G, S3.15**). ASO-mediated knockdown of *LOC646329* decreased the observed *LOC646329-MKLN1* interaction frequency (**Fig 3.4G, S3.15**).

Given the observation of these enhancer-like DNA interactions, we next investigated whether sequences from the *LOC646329* locus possess enhancer-like activity. In a plasmid-based enhancer-reporter assay, a 1,992 bp fragment from the 5' end of *LOC646329* increased the basal expression of the reporter gene by ~15-fold, while the TSS regions from three other lncRNAs with function in U87 cells (Liu et al., 2017) exhibited little to no enhancer-like activity (**Fig, 3.4H**). This increase in reporter gene expression was not likely due to transcriptional read-through from the *LOC646329* TSS, as the DNA fragment was cloned into the reporter construct in the reverse orientation (**Fig. S3.16A**). Furthermore, ASOs that target the partial *LOC646329* transcript produced by the reporter construct (**Fig. S3.16B, C**) decreased enhancer-reporter activity (**Fig. S3.16D, E**). Thus, *LOC646329* contains sequences with potent enhancer-like activity and exhibited genomic interactions with *MKLN1*, a coding gene required for robust proliferation of U87 GBM cells.

Due to the observations that the transcript may have function, we hypothesized that the *LOC646329* transcript may be interacting with a protein binding partner in order to "loop" the enhancer-like locus to *MKLN-1*/*linc-PINT*. The transcription factor CTCF is a well-known protein attributed to regulating the 3-dimensional structure of chromatin (Phillips and Corces, 2009). Using RNA Immunoprecipitation to pulldown CTCF followed by quantitative PCR (RIP-qPCR), we found that *LOC646329* transcripts physically interact with CTCF (**Fig S3.16F**).

Thus, *LOC646329* transcripts interact with the protein CTCF, its locus contains sequences with potent enhancer-like activity, and its genomic interactions with *MKLN1* – a coding gene required for robust proliferation of U87 GBM cells – is disrupted after ASO-mediated knockdown.

lnc-pri-miRNA loci are enriched for physical interactions with gene promoters and enhancer characteristics

We next explored whether lnc-pri-miRNA loci as a group have evidence of enhancer-like function. By using PSYCHIC (Ron et al., 2017) to analyze Hi-C data from 7 different human cell lines representing all 3 germ layers (Rao et al., 2014) (**Fig. S3.17A**), we found that lnc-pri-miRNA loci had a ~3-fold increase in physical proximity with gene promoters as compared to the broader set of lncRNAs (**Fig. 3.5A**). Analysis of Pol II occupancy at promoter regions did not reveal significant differences at lnc-pri-miRNA loci as compared to other lncRNAs (**Fig. S3.18)**, suggesting that differences in Pol II enrichment do not underlie the increased proximity of lnc-pri-miRNA loci and coding genes. When compared to the broader set of lncRNAs, the lnc-pri-miRNA loci as a subset were 4-fold enriched for GeneHancer's (Fishilevich et al., 2017) highly filtered set of "double-elite" enhancer elements (**Fig. S3.17B, 3.5B**). These bioinformatic analyses indicate that in addition to hosting miRNAs, loci that encode lnc-pri-miRNAs are enriched for regulatory elements that are in close 3D proximity to potential target gene promoters.

lnc-pri-miRNAs can regulate local genes independent of its cognate miRNAs

To investigate whether the physical interaction of lnc-pri-miRNA loci with coding gene promoters predicts enhancer-like function, we individually tested 9 lnc-pri-miRNAs that

contained GeneHancer double-elite elements and had evidence of physical interactions with coding gene promoters in K562 cells (**Fig. S3.19**). We used CRISPRi in K562-dCas9-KRAB cells, targeting the TSS of the lnc-pri-miRNA, and assessed levels of both the lnc-pri-miRNA transcript and the mRNA produced by the gene that interacts with the lnc-pri-miRNA locus, which is >25 kb away (**Fig. 3.5C**). Of the 5 lnc-pri-miRNA that had effective knockdown with CRISPRi, all 5 also exhibited a corresponding decrease of mRNA from the interacting protein-coding gene (**Fig. 3.5C**). With ChIP, we confirmed H3K9me3 enrichment all 5 lnc-pri-miRNA promoters after lnc-pri-miRNA CRISPRi targeting; H3K9me3 was also increased at 2 out of the 5 interacting protein-coding gene promoters (**Fig S3.20**), which could be an indirect consequence of decreased lnc-pri-miRNA enhancer activity. Next, we used oligonucleotide miRNA inhibitors to investigate whether a reduction in activity of the cognate miRNA caused the decrease in expression of the interacting coding gene. While miRNA inhibitors to miR-6076 (produced by *LINC1588*) caused de-repression of a known miR-6076 target gene (*RPL37*), levels of *ARF6* was not decreased (**Fig. 3.5D**), indicating that a decrease in miR-6076 activity did not indirectly downregulate *ARF6* expression. Similarly, inhibitors to miR-22 and miR-3157, the cognate miRNAs of lnc-pri-miRNA *MIR22HG* and *ENTPD1*-AS1, respectively, did not decrease expression of their coding gene interacting partners (**Fig. 3.5D**). Thus, Hi-C/Genehancer analysis predicts enhancer-like function of lnc-pri-miRNAs, and this activity can be independent of the function of their cognate miRNAs, as observed with *LOC646329* (**Fig. S3.21**).

Discussion

In previous studies, the relationship between lnc-pri-miRNAs and their cognate miRNA(s) has been enigmatic. For example, the lnc-pri-miRNA *MIR100HG* produces miR-100

and miR-125b, and these miRNAs drive cetuximab resistance in colorectal cancer cells (Lu et al., 2017), with *MIR100HG* appearing to function solely as a host for its cognate miRNAs. However, a miRNA-independent role for *MIR100HG* has also been described, as *MIR100HG* knockdown in osteosarcoma cells line affects the cell cycle without an apparent change in levels of miR-100 or miR-125b (Sun et al., 2018). Similarly, knockdown of the lnc-pri-miRNA *RMST* inhibits neurogenesis in human cell culture studies without causing an observable change in levels of its cognate miRNA, miR-135a (Ng et al., 2013). However, other studies demonstrate roles for *miR-135a* in neurogenesis *in vivo* (Caronia-Brown et al., 2016; Pons-Espinal et al., 2019). *PVT1* is another prime example of a lnc-pri-miRNA for which different studies have focused on either miRNA-dependent or miRNA-independent functions (Cho et al., 2018; Papagregoriou et al., 2012; Tseng et al., 2014; Yan et al., 2017). Such apparent differences in lnc-pri-miRNA function may relate in part to cell type and experimental context.

In a CRISPRi screen for essential function (Liu et al., 2017), lnc-pri-miRNAs were enriched as hits in multiple cell lines, including U87 GBM (**Fig. S3.1A**), iPSC, and two breast cancer cell lines, MCF7 and MDA-MB-231 (**Fig. S3.1C**). Neither *DGCR8* nor *DROSHA* knockdown alone affected the propagation of U87 cells (**Fig. 3.1D**). All four lnc-pri-miRNA loci CRISPRi screen hits still regulated U87 cell proliferation when *DGCR8* or *DROSHA* were knocked down, even in cells that exhibited no further reduction in mature miRNA levels, suggesting that these lncRNA loci regulate cell biology via miRNA-independent mechanisms. It is important to consider that while CRISPRi knockdown of lnc-pri-miRNAs in Microprocessor deficient cells exhibited a cell propagation phenotype, it remains possible that residual miRNA levels could influence cell proliferation. lnc-pri-miRNA loci comprised of 8% of the screen hits in U87 cells, while MCF7 and MDA-MB-231 cells had an even greater proportion of lnc-pri-

miRNA hits (11% and 17%, respectively). Future studies to further explore miRNA-independent function of lnc-pri-miRNA loci in other cells could challenge current assumptions about lnc-pri-miRNAs solely functioning as host genes to miRNAs.

For *LOC646329*, with the miR-29a/b1 cluster being located within an intron ~ 36kb downstream from the TSS, we were able to genetically delete the cluster without apparent detrimental effects to transcription from this locus or its enhancer-like activity. Our Nanopore long read single-molecule RNA-seq data confirmed a previously annotated transcript of *LOC646329* that hosts miR-29a/b1 – in addition to several other potential isoforms produced at this locus. It could be possible that there are other functional *LOC646329* isoforms produced. Moreover, there remains a possibility that there are isoforms that do not host miR-29a/b1 due to differential splicing, for example. This is seen from the lnc-pri-miRNA *MIR100HG,* which contains miR-100, let7-a2, and miR-125-b1 embedded within its last intron. Depletion of the *MIR100HG* transcript via antisense oligonucleotides (ASOs) in U2OS cells reduced lnc-pri-miRNA levels, but not its cognate miRNAs (Sun et al., 2018), suggesting differential inclusion of miRNAs during lnc-pri-miRNA production. Interestingly, the miRNAs embedded can have opposing roles in the regulation of proliferation. For example, let7 miRNA is a known tumor suppressor (Roush and Slack, 2008), while miR-100 and miR-125b1 act as pro-proliferative oncogenic miRNAs (Deng et al., 2014; Kim et al., 2012). This may further suggest differential usage of isoforms, where a cell can "pick and choose" which miRNAs the lnc-pri-miRNA will produce.

While LOC646329 did indeed produce miR-29a/b1 – which regulated cellular apoptosis – the function of this lnc-pri-miRNA in U87 cell proliferation was miRNA-independent. Thus, in addition to producing miRNAs, lnc-pri-miRNAs can have genetically separable and potent

biological function. Of note, without the combination of multiple approaches to dissect miR-29a/b1 from *LOC646329*, the biological effects of *LOC646329* knockdown (and also miR-29a/b1-deletion) might have been attributed solely to the loss of these miRNAs and not the enhancer-like function of this locus.

The *LOC646329* locus is in close 3D proximity to the locus containing *MKLN1* and *linc-PINT*, which is ~ 200kb away. While NRO experiments demonstrated that knockdown of *LOC646329* by ASO-2 can disrupt transcription through the locus, ASO-1 only caused a modest reduction of nascent transcripts at the distal 3' end. Although ASO-1 did not disrupt transcription through the 5' end where we observed *LOC646329* enhancer-like activity, it remains possible that this regulatory activity is transcription-dependent, rather than being mediated solely by the RNA transcript itself. ASO-mediated knockdown reduced the interaction frequency between the *LOC646329* promoter and *MKLN1*, suggesting a transcript or transcription-dependent role in maintaining the observed looping interaction. *MKLN1* is a putative oncogene amplified in human glioma (Nord et al., 2009) and known to regulate cell adhesion, cytoskeletal dynamics, and cell proliferation (Delto et al., 2015; Francis et al., 2013; Lampert et al., 2018). Interestingly, *MKLN1* levels are not significantly changed in miR-29Δ cells that exhibit increased *LOC646329* expression. *linc-PINT* has also been described to have roles in cancer cell proliferation and invasion (Duan et al., 2019; Marin-Bejar et al., 2017). Whether the observed regulatory interactions between *LOC646329* and *MKLN1/linc-PINT* are derived from a disease state such as GBM (Flavahan et al., 2016), and how *linc-PINT* may contribute to GBM pathogenesis remains to be further investigated. While a variant of *LOC646329* may sponge miR-29b1 in HCT116 colorectal cancer cells (Javanmard et al., 2020), we did not find evidence for this lnc-pri-miRNA being a miR-29 target in U87 GBM cells (**Fig.**

S3.6B, S3.10A). Furthermore, while we have highlighted the enhancer-like activity of *LOC646329*, mechanisms that involve binding with specific RNA-binding proteins have been described for other lnc-pri-miRNAs (Ng et al., 2013; Sun et al., 2018). ShRNA knockdown of *LOC646329* reduced cell proliferation (**Fig. S3.5E, F**), and ASO-mediated knockdown of *LOC646329* transcripts in our enhancer-reporter assay reduced reporter expression, suggesting that the transcript may play a role in its enhancer activity. Our RIP data suggests the *LOC646329* transcript is able to interact with the genome organizing factor CTCF. It is possible that the 3D looping interactions (and therefore enhancer-like activity) we observe are dependent on this *LOC646329*-CTCF interaction. The *LOC646329* locus contains several binding sites which are bound by CTCF. Although CTCF has direct DNA-binding capabilities, it remains possible that CTCF binding to DNA may be affected by changes to *LOC646329* transcript levels. Nonetheless, it remains possible that lnc-pri-miRNAs including *LOC646329* can have multiple miRNA-independent functions.

As compared to the broader population of lncRNAs, lnc-pri-miRNAs were enriched for enhancer-like characteristics. For any particular lnc-pri-miRNA, the degree to which miRNA production and enhancer-like activity contributes to the cellular phenotype being studied will likely require detailed molecular-genetic studies of individual loci. For instance, the "essential" function of *LOC646329* in GBM cell proliferation was genetically separable from its production of miR-29a/b1. In K562 cells, Hi-C evidence of 3D "looping" interactions was predictive of enhancer-like activity between lnc-pri-miRNA loci and coding genes, despite these lnc-pri-miRNAs not being scored as hits in screens of cell proliferation. Whether cellular phenotypes are observed with perturbation of lnc-pri-miRNA enhancer-like function may depend upon the assay employed and its sensitivity.

Other lncRNA loci have been previously shown to harbor enhancer-like activity (Engreitz et al., 2016; Lai et al., 2013; Li et al., 2013; Melo et al., 2013; Orom et al., 2010; Wang et al., 2011). *LOC646329* is distinct example of a lncRNA locus that can function as both a transcriptional enhancer and genetic precursor of miRNAs. Besides *LOC646329*, there is a separate locus (*MIR29B2CHG)* that contains the miR-29b2/c cluster. Interestingly, although we found that *MIR29B2CHG* is extremely lowly expressed in U87 cells – and miR-29c are not detected by small RNA-seq – the *MIR29B2CHG* locus contains high confidence enhancers. Whether these enhancers are active, and what roles they may play remains to be further investigated. This relationship between enhancer-like lncRNA activity and cognate miRNA production, along with the genome-wide enrichment of enhancer-like characteristics within lnc-pri-miRNA loci, suggests a model of genome evolution wherein some miRNAs become embedded into lncRNA loci with enhancer-like activity. That is, while intragenic miRNAs embedded within protein-coding genes may have co-evolved function with their "host" genes (Franca et al., 2017), some intergenic miRNAs (*e.g.,* miR-29a/b1) embedded within lncRNA loci may have co-evolved function with the host enhancer-like activity.

Intriguingly, *LOC646329* seems to have been recently evolved, as it is a primate-specific lncRNA. While miR-29 is highly conserved and expressed in mouse, there is currently no lnc-pri-miRNA annotated in mouse that has the same genomic structure – where miR-29 resides within the intron – as in human *LOC646329*. However, miR-29 function is highly conserved and can regulate animal behavior in both mouse and zebrafish (Bitetti et al., 2018). Of note, zebrafish and humans have diverged more than 450 million years ago (Kumar and Hedges, 1998). Through single-cell sequencing of the developing human neocortex, *LOC646329* is found to be highly enriched and specifically expressed in radial glia, the "stem cell" population

of the developing brain (Liu et al., 2016). Not surprisingly, miR-29 is also a brain-enriched miRNA. One very obvious difference between the mouse (or zebrafish) and human brain is the physical size. Due to *LOC646329* expression in radial glia and GBM cells, one might postulate that this lnc-pri-miRNA is normally important for cell growth and proliferation of the brain. While our studies focus on *LOC646329* essential function in GBM cells, this locus may also be important for normal brain development.

Essential lncRNA function is highly cell type-specific (Liu et al., 2017), and it is unclear how such exquisite functional specificity is achieved. lncRNA expression alone does not predict function. For instance, human astrocytes express *LOC6436329,* but knockdown of this lnc-pri-miRNA did not reduce cell growth (**Fig. S3.4D-F**). Similarly, HeLa cells also express *LOC646329*, and miR-29 regulates apoptosis in this cell line (Park et al., 2009). However, *LOC646329* knockdown did not inhibit HeLa cell growth (**Fig. S3.4A-C**). Moreover, while a variant of *LOC646329* may sponge miR-29b1 in HCT116 colorectal cancer cells (Javanmard et al., 2020), we did not find evidence for this lnc-pri-miRNA being a miR-29 target in U87 GBM cells (**Fig. S3.6B, S3.10A**). For lncRNAs with multiple biological functions such as *LOC646329*, we speculate that each distinct molecular mechanism may play a greater or lesser biological role depending on cell type and/or disease state. For instance, it is possible that in GBM, the enhancer-like activity of *LOC646329* becomes the dominant function that promotes cell proliferation. Potential differences in the "utilization" of such distinct mechanisms could underlie the apparent cell type-specificity of lncRNA function.

In GBM cells, miR-29a/b1 deletion greatly increased levels of *LOC646329* (which was related to longer transcript half-life and an increase in Pol II localization (**Fig. S3.8F, G**). For lncRNA loci that function as enhancers, both the lncRNA transcript and local transcription

appear to underlie their enhancer-like activity (Kopp and Mendell, 2018). Interestingly, genetic deletion of miRNAs hosted within lnc-pri-miRNA is not unusual in cancer (Chang et al., 2007; Johnson et al., 2005; Yanaihara et al., 2006). In particular, loss of miR-29 occurs in chronic lymphocytic leukemia (CLL), acute myeloid leukemia (AML), and lung cancer (Calin et al., 2005; Fabbri et al., 2007; Pekarsky et al., 2006). Aberrant enhancer activity has been noted to be a driver of oncogenesis (Akhtar-Zaidi et al., 2012; Herranz et al., 2014; Loven et al., 2013; Pomerantz et al., 2015). Thus, we raise the possibility that in cancer, genetic loss of miRNAs hosted within lnc-pri-miRNAs may result in aberrant enhancer-like activity, contributing to the gene expression that drives tumor cell growth.

Overall, our studies identify key functional characteristics that distinguish lnc-pri-miRNAs from the broader population of lncRNAs. In addition to being enriched for function in cell proliferation, genome-wide analyses provided evidence of enhancer-like function within lnc-pri-miRNA loci. The study of individual lnc-pri-miRNAs including *LOC646329* highlighted a previously unappreciated function of lnc-pri-miRNA genes, demonstrating that enhancer-like activity can co-exist with their miRNA production. More generally, we hope that our results lay groundwork for the continued efforts at functional classification of the vast diversity of lncRNAs produced by the noncoding genome.

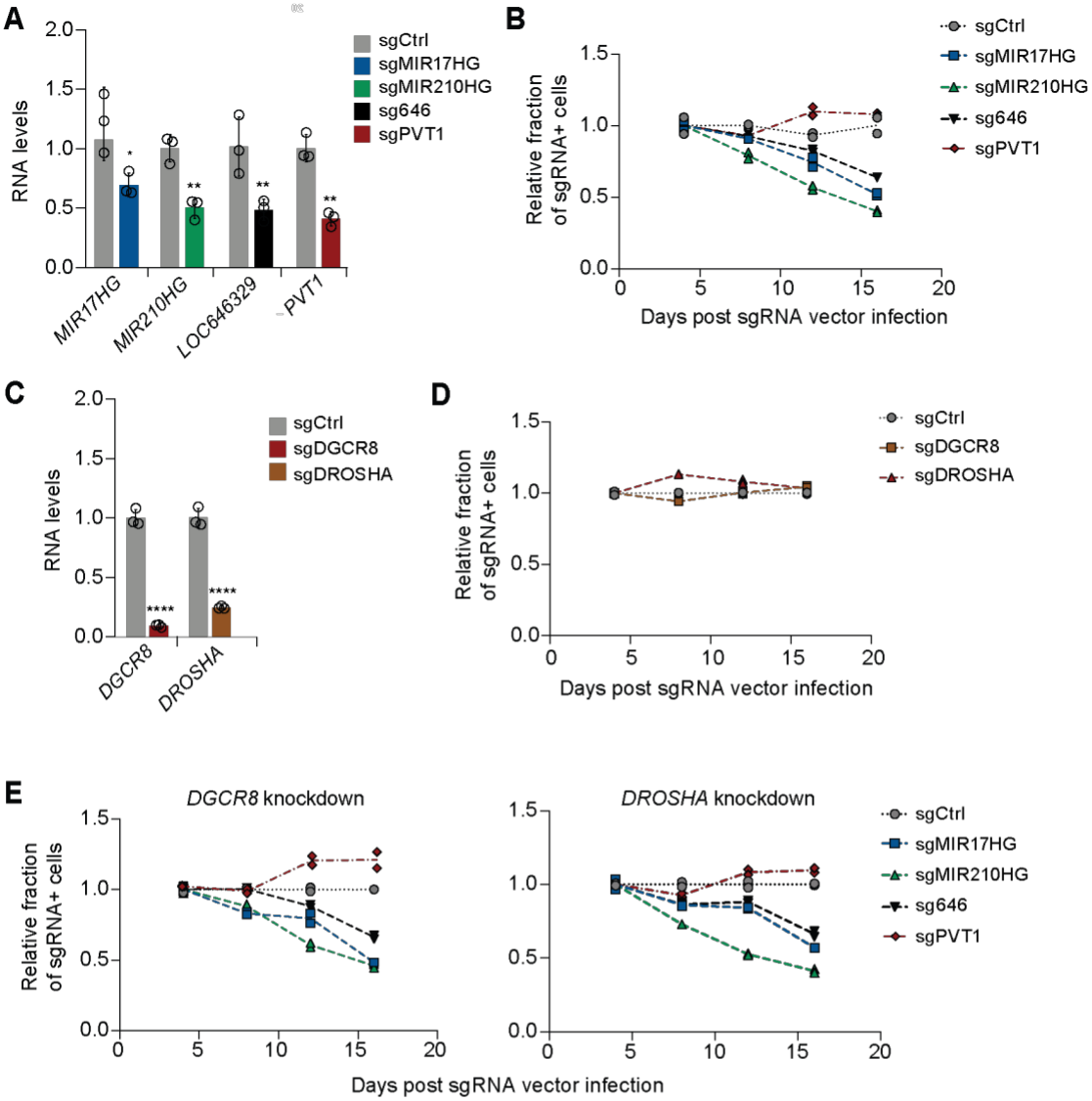

Fig 3.1 lnc-pri-miRNA loci can regulate cell proliferation in cells with Microprocessor knockdown.

(A) RT-qPCR quantification of CRISPRi knockdown in U87 dCas9-KRAB cells. * *P*-value < 0.05, ** *P*-value < 0.01; unpaired two sample t-test. (B) Internally controlled growth assays performed with sgRNAs targeting lnc-pri-miRNA loci in U87 dCas9-KRAB cells. sgRNA-expressing cells were quantified by flow cytometry and represented as the fraction observed at 4 days after sgRNA vector infection. Each sgRNA vector infection was performed in biological duplicates, as shown by individual points on the graph. (C) RT-qPCR quantification of CRISPRi-mediated knockdown of *DGCR8* and *DROSHA*. **** *P*-value < 0.0001; unpaired two sample t-test. (D) Internally controlled growth assays of U87 cells with *DGCR8* or *DROSHA* knockdown. Each sgRNA vector infection was performed in biological duplicates, as shown by individual points on the graph. (E) Internally controlled growth assays performed with sgRNAs targeting lnc-pri-miRNA loci in U87 dCas9-KRAB cells with *DGCR8* or *DROSHA* knockdown. Each sgRNA vector infection was performed in biological duplicates, as shown by individual points on the graph.

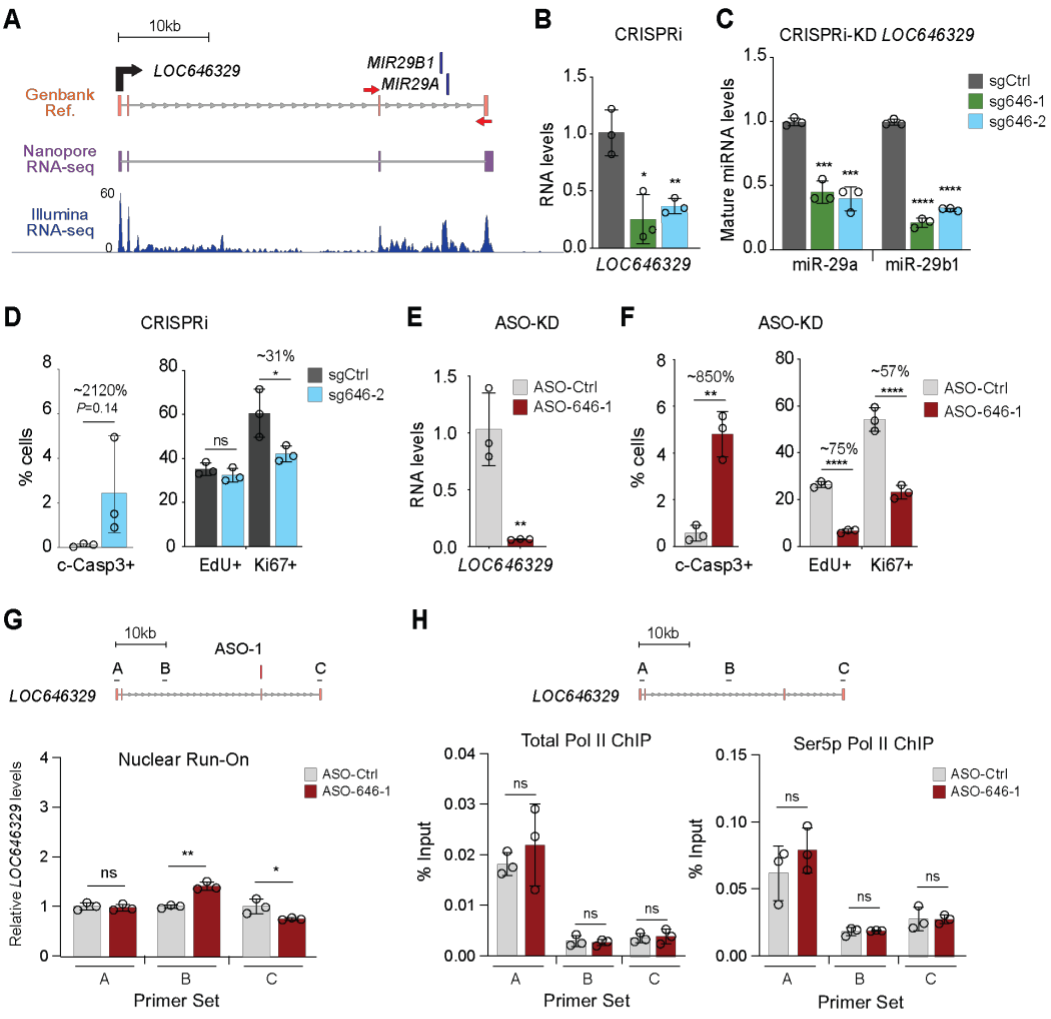

Fig 3.2 *LOC646329* produces miR-29a/b1 and is required for U87 cell propagation.

(A) Genbank reference (EU154353) of *LOC646329* aligned with long-read, single molecule Oxford Nanopore direct RNA-seq reads (purple) and Illumina RNA-seq reads (blue) in U87 cells. Red arrows indicate exon3-4 junction spanning qPCR primers. (B) RT-qPCR quantification of *LOC646329* in U87-dCas9-KRAB cells upon CRISPRi with two independent sgRNAs targeting the TSS of *LOC646329,* relative to control Gal4 sgRNA. * *P-value* < 0.05, ** *P-value* < 0.01; unpaired two sample t-test. (C) RT-qPCR quantification of mature miR-29a and miR-29b after CRISPRi-mediated knockdown of *LOC646329* (n = 3 biological replicates per condition). Gal4 sgRNA is used as control. *** *P-value* < 0.001, **** *P-value* < 0.0001; unpaired two sample t-test. (D) Quantification of ICC of U87-dCas9-KRAB cells one week post CRISPRi-mediated *LOC646329* knockdown (n = 3 biological replicates per condition). ns = not significant, * *P-value* < 0.05; unpaired two sample t-test. (E) RT-qPCR quantification of *LOC646329* 48 hours post ASO transfection. ** *P-value* < 0.01; unpaired two sample t-test. (F) Quantification of ICC of U87 cells 48 hours post ASO-mediated *LOC646329* knockdown (n = 3 biological replicates per condition). * *P-value* < 0.05, ** *P-value* < 0.01, **** *P-value* < 0.0001; unpaired two sample t-test. (G) RT-qPCR quantification of *LOC646329* nascent transcript levels in Nuclear run-on experiments in U87 cells with and without *LOC646329* ASO-mediated knockdown. Primer sets and locations are indicated by the schematic above. * *P-value* < 0.05, ** *P-value* < 0.01, ns = not significant; unpaired two sample t-test. (H) ChIP analysis with antibodies to Total RNA Pol II (left) and RNA Pol II Ser5p (right) using qPCR primers indicated in the schematic above.

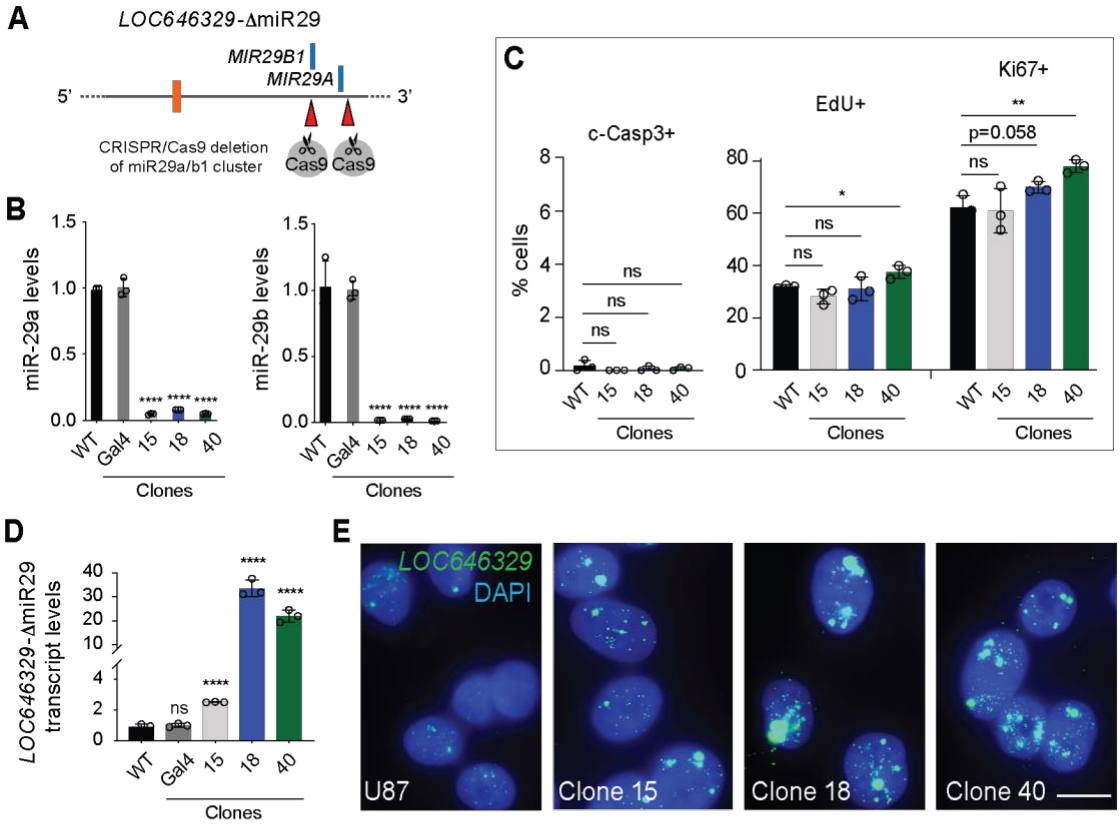

Fig 3.3 Deletion of miR-29a/b1 does not decrease cell growth.

(A) Schematic of genetic removal of miR-29a/b1 using CRISPR-Cas9. (B) RT-qPCR quantification of mature miR-29a and miR-29b levels in CRISPR-edited clones and controls (n = 3 biological replicates per condition). **** *P-value* < 0.0001; unpaired two sample t-test. (C) Quantification of ICC in wildtype and CRISPR-edited clones (n = 3 biological replicates per condition). ns = not significant, * *P-value* < 0.05, ** *P-value* < 0.01; unpaired two sample t-test. (D) RT-qPCR of *LOC646329* in CRISPR-edited clones and controls (n = 3 biological replicates per condition). ns = not significant, **** *P-value* < 0.0001; unpaired two sample t-test. (E) FISH of *LOC646329* (green) in U87 cells, Clone 15, Clone 18, and Clone 40. Nuclei are counterstained in DAPI (blue). Scale bars = 8μM.

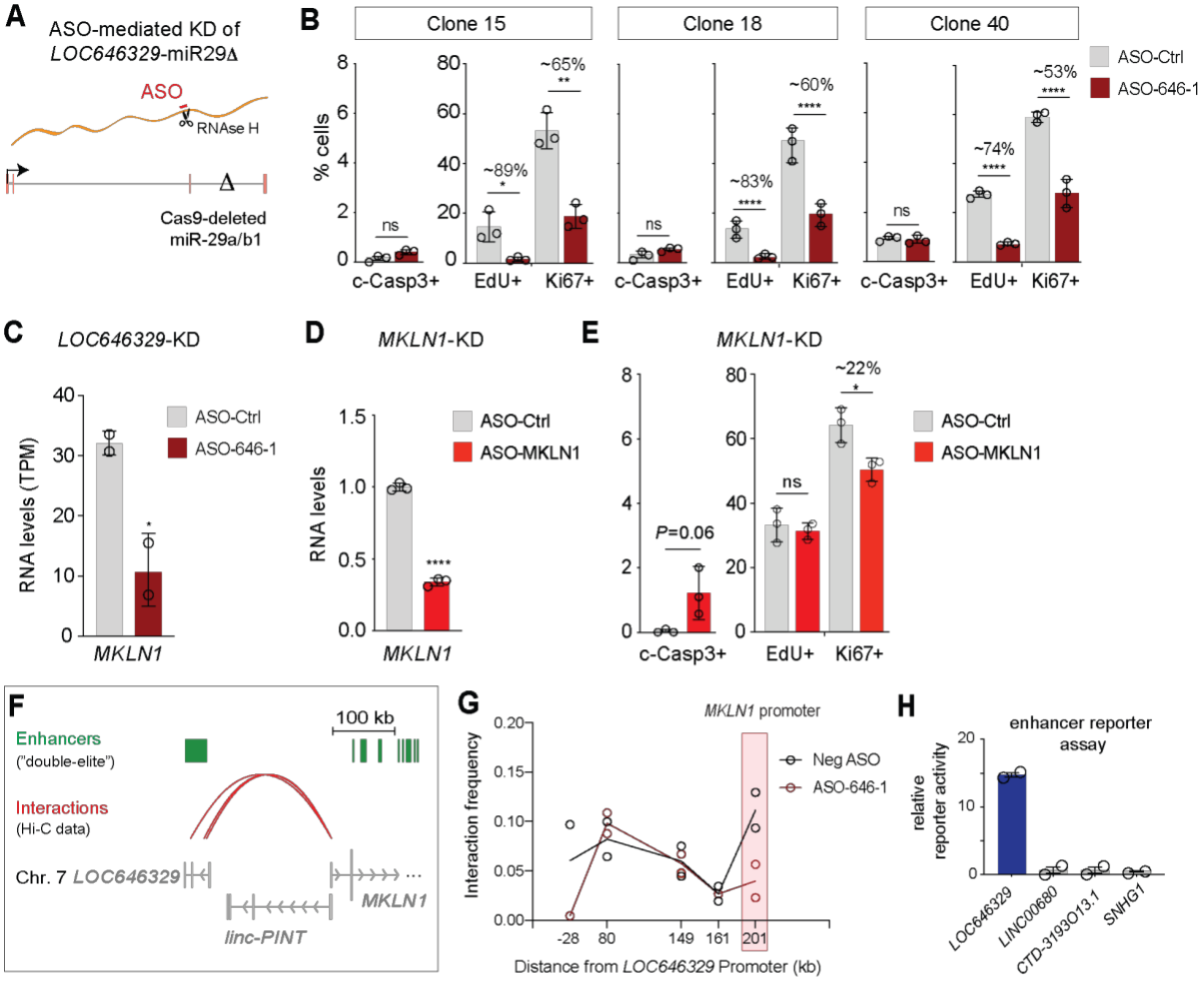

Fig 3.4 *LOC646329* regulates cell proliferation independent of miR29a/b1 and exhibits enhancer-like activity.

(A) Schematic of ASO degradation (targeting exon 3) of U87 *LOC646329*-miR29Δ. (B) ICC quantification of U87 *LOC646329*-miR29Δ cells 48 hours post ASO-mediated *LOC646329* knockdown. ns = not significant, * *P-value* < 0.05, ** *P*-value < 0.01, *** *P*-value < 0.001, **** *P*-value < 0.0001; two sample unpaired t-test. (C) Quantification of *MKLN1* normalized read counts in TPM (transcript per million) from RNA-seq 24 hours after ASO-mediated *LOC646329* knockdown. * indicates significant difference as determined by the likelihood ratio test. (D) Quantification of *MKLN1* levels 48 hours after transfection of ASOs. (E) Quantification of ICC of U87 cells 48 hours post ASO-mediated *MKLN1* knockdown. ns = not significant, * *P*-value < 0.05; unpaired two sample t-test. (F) Analysis of GeneHancer high confidence enhancers and physical interactions between *LOC646329* and *MKLN1/linc-PINT.* (G) 3C-qPCR analysis in U87 cells with *LOC646329* promoter as bait. Red highlighted region indicates the *MKLN1* promoter region. Data represented by negative control ASO treated U87 cells are shown in black, while data represented by ASO-1-mediated *LOC646329* knockdown are shown in red. Each region is analyzed in duplicate, with each dot representing an individual replicate. (H) Enhancer reporter activity of the promoter region of four functional lncRNAs, listed on the x-axis.

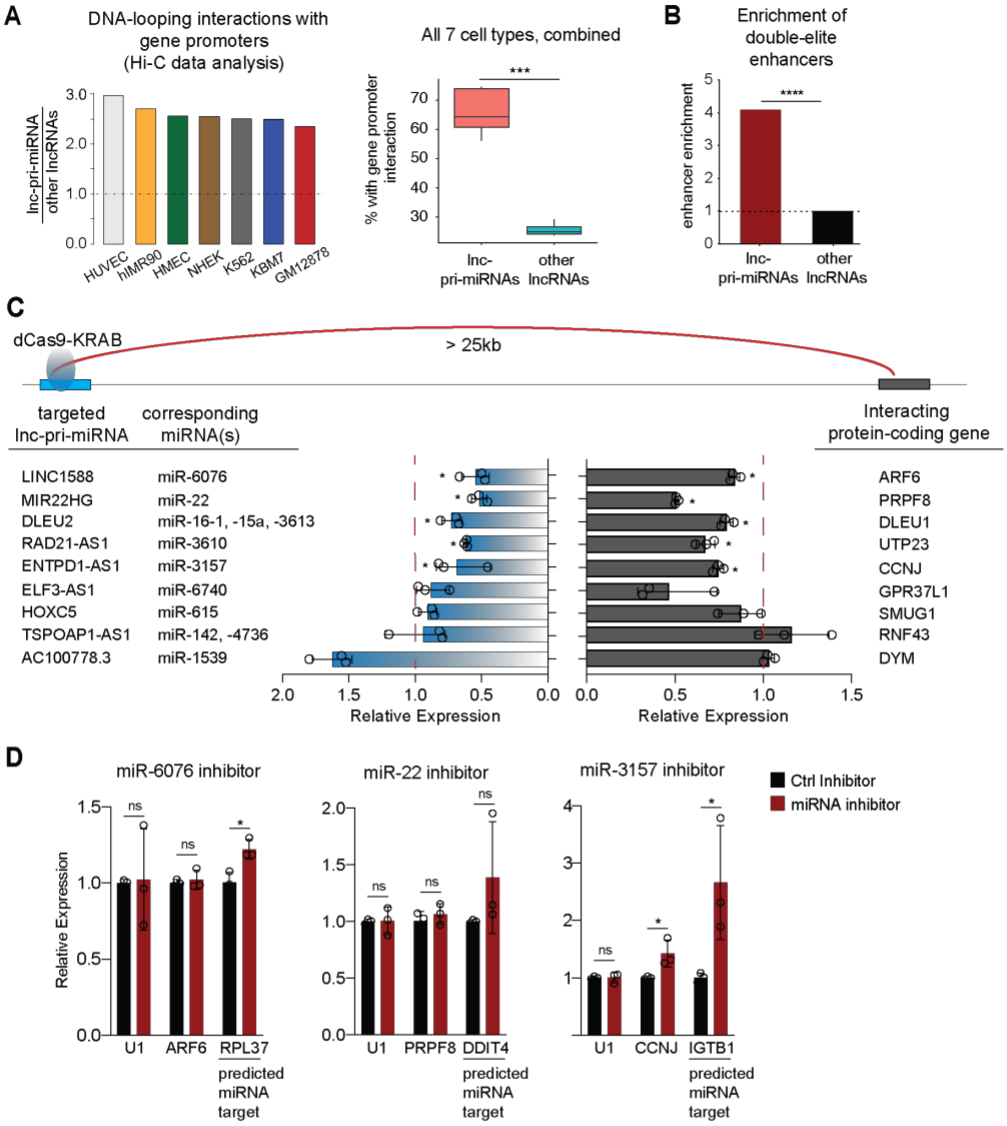

Fig 3.5 lnc-pri-miRNA are enriched for enhancer-like characteristics.

(A) Enrichment score ratios from genome-wide DNA-looping interaction (Hi-C) analysis across seven different cell lines, shown individually (left). Box plot (right) shows the percentage of lnc-pri-miRNAs (or other lncRNAs) that interact with gene promoters in Hi-C data analysis. Horizontal line represents the median, the whiskers represent the interquartile range. *** *P-value* < 0.001; Wilcoxon rank-sum test. (B) Enrichment of double-elite enhancer elements in lnc-pri-miRNA loci, relative to other lncRNAs. **** *P*-value < 0.0001; Fisher's exact test. (C) RT-qPCR quantification of lnc-pri-miRNA levels (blue bars, left) and its interacting protein-coding gene (>25kb away determined by Hi-C, gray bars, right) 30 hours post sgRNA transfection (n = 3 biological replicates per condition). Data shown are normalized to Gal4 sgRNA and U1 controls. * *P-value* <0.05; unpaired two-sample t-test. (D) RT-qPCR quantification of K562-dCas9-KRAB cells 48 hours after transfection with miRNA inhibitors (n = 3 biological replicates per condition). Data shown are normalized to the control inhibitor and U1. ns = not significant, * *P-value* < 0.05; unpaired two-sample t-test.

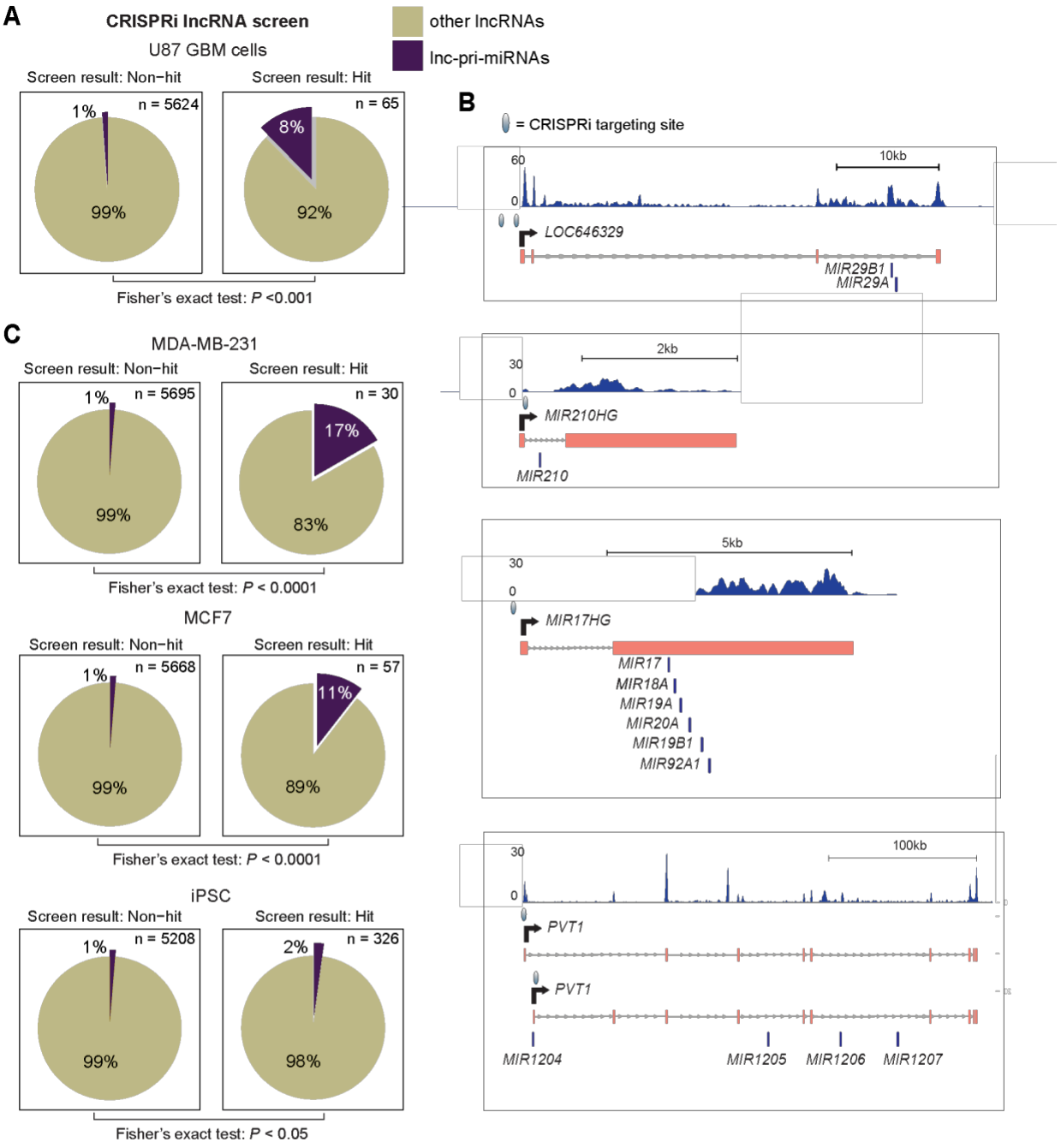

Fig S3.1 lnc-pri-miRNA loci are enriched for function in cell proliferation.

(A) Pie charts showing the proportion of lnc-pri-miRNA loci (purple) that are non-hits (left chart) versus hits (right chart) in a genome-scale CRISPRi-based cell growth screen of U87 cells. (B) Genomic structure of the five lnc-pri-miRNA hits -- *LOC646329*, *MIR210HG*, *MIR17HG*, and two isoforms of *PVT1* (different TSS's) -- in the U87 GBM cell CRISPRi screen. Illumina RNA-seq reads are shown in dark blue, and the sgRNA CRISPRi targeting sites are indicated by the light blue ovals. (C) Pie charts showing the proportion of lnc-pri-miRNA loci (purple) that are non-hits (left charts) versus hits (right charts) in a genome-scale CRISPRi-based screen for essential function in MDA-MB-231 (top), MCF7 (middle), and iPSCs (bottom). *P*-values (Fisher's exact test) are shown below each panel.

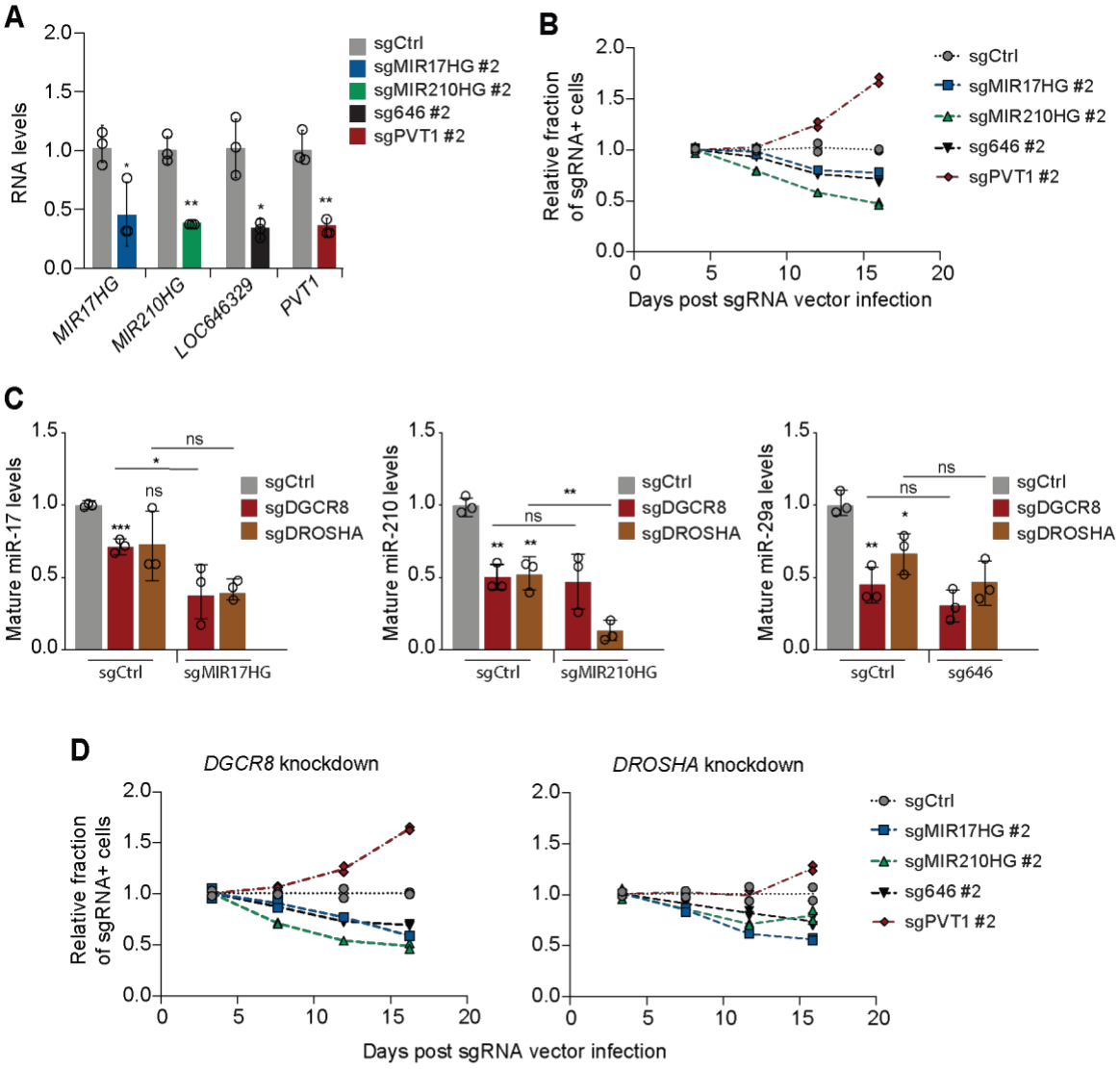

Fig S3.2 lnc-pri-miRNA knockdown analyses in cells with and without Microprocessor knockdown.

(A) RT-qPCR quantification of CRISPRi knockdown in U87 dCas9-KRAB cells. * *P*-value < 0.05, ** *P*-value < 0.01; unpaired two sample t-test. (B) Internally controlled growth assays performed with sgRNAs targeting lnc-pri-miRNA loci in U87 dCas9-KRAB cells. sgRNA-expressing cells were quantified by flow cytometry and represented as the fraction observed at 4 days after sgRNA vector infection. Each sgRNA vector infection was performed in biological duplicates, as shown by individual points on the graph. (C) RT-qPCR quantification of miR-17 (left), miR-210 (middle), or miR-29a (right) after knockdown of Microprocessor enzymes or knockdown of Microprocessor and lnc-pri-miRNA knockdown. * *P*-value < 0.05, ** *P*-value < 0.01, ns = not significant; unpaired two sample t-test. (D) Internally controlled growth assays of U87 cells with *DGCR8* or *DROSHA* knockdown. Each sgRNA vector infection was performed in biological duplicates, as shown by individual points on the graph.

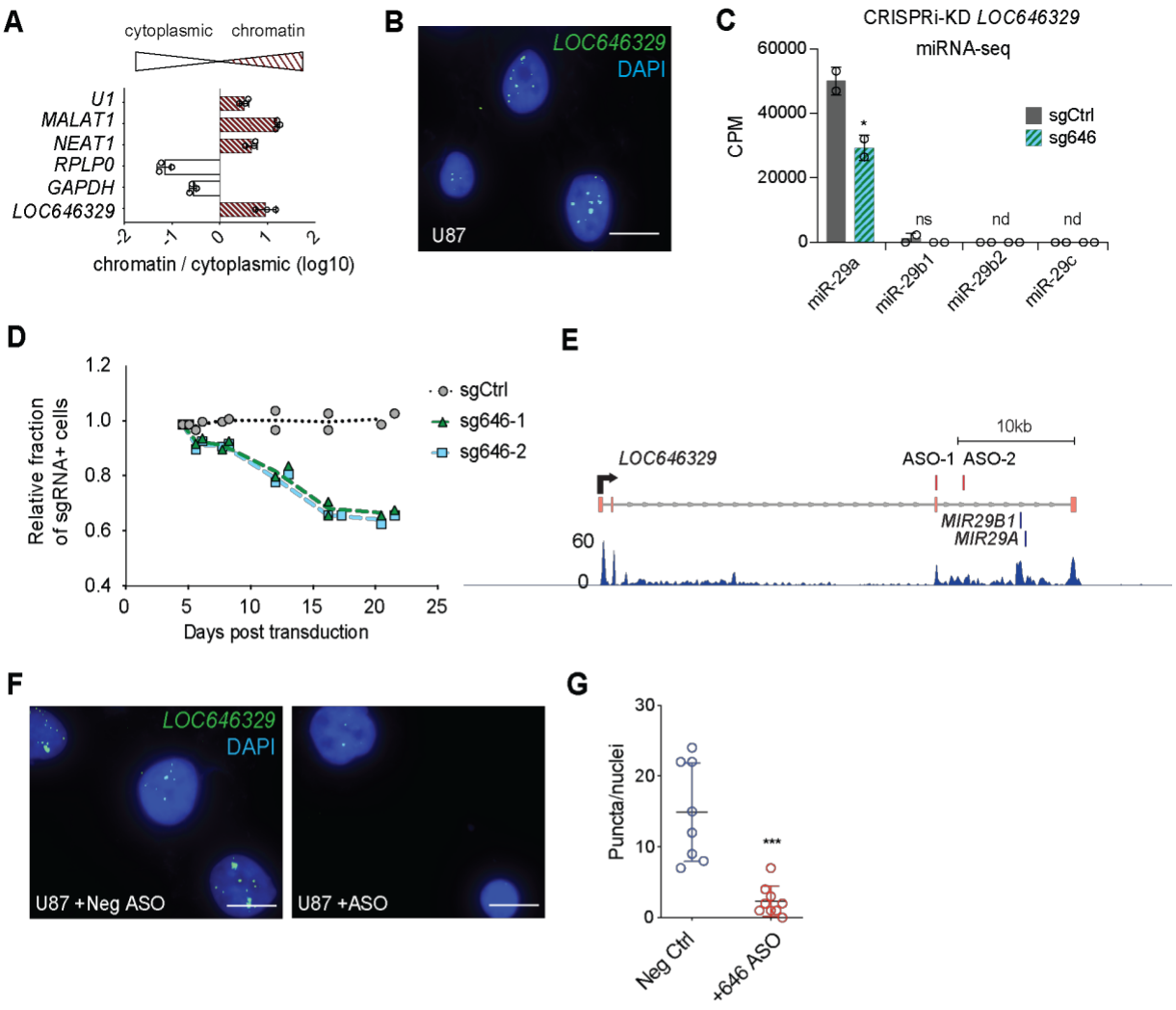

Fig S3.3 Analysis of cellular localization of *LOC646329* transcript, production of miR-29a/b1, and cell growth after *LOC646329* KD.

(A) Cellular fractionation and RT-qPCR analysis of transcripts in U87 cells (n = 3 biological replicates). (B) RNA FISH image of *LOC646329* (green) in U87 cells. Nuceli are counterstained with DAPI (blue). Scale bar = 9μM. (C) Small RNA-seq quantification of miR-29a, miR-29b1, miR-29b2, and miR-29c in counts per million (CPM) after CRISPRi-mediated knockdown of *LOC646329* (n = 2 biological replicates per condition). * indicates statistical significance; likelihood ratio test. ns = not significant. nd = not detected. (D) Internally controlled growth assays measured by flow cytometry of sgRNA expressing cells after *LOC646329* CRISPRi knockdown. sgRNA-expressing cells were quantified by flow cytometry and represented as the fraction observed at 4 days after sgRNA vector infection (n=2 biological replicates, shown as individual points on the graph). (E) Schematic indicating the location of ASOs (red vertical bars) targeting *LOC646329*. Genbank reference (EU154353) of *LOC646329* is aligned with Illumina RNA-seq reads (blue) from U87 cells. (F) RNA FISH image of *LOC646329* (green) in U87 cells 24 hours after negative control ASO (left) or *LOC646329* ASO (right). Nuceli are counterstained with DAPI (blue). Scale bar = 9μM. (G) Quantification of RNA FISH image in negative control or *LOC646329* knockdown cells. *** *P-value* < 0.001; unpaired two sample t-test.

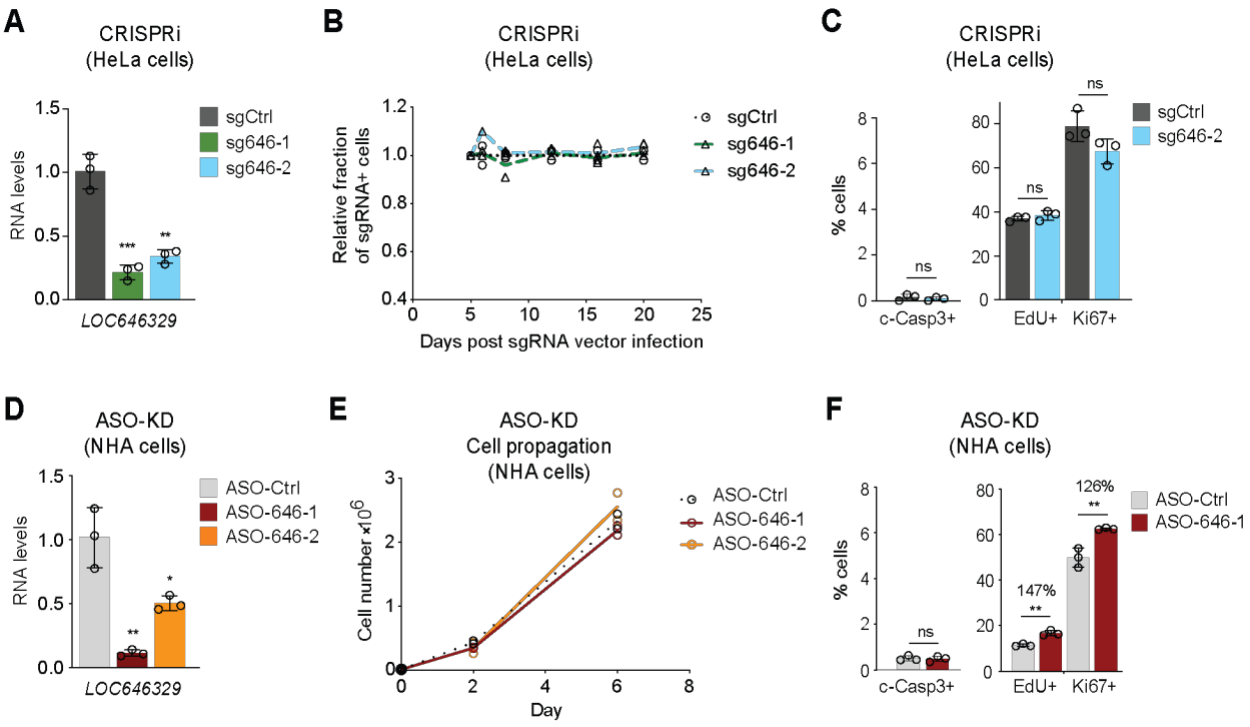

Fig S3.4 Knockdown of *LOC646329* does not decrease growth of HeLa or normal human astrocytes.

(A) RT-qPCR quantification of *LOC646329* in HeLa cells upon CRISPRi-mediated knockdown with two independent sgRNAs targeting *LOC646329,* relative to control Gal4 sgRNA (n = 3 biological replicates per condition). ** *P-value* < 0.01, *** *P-value* < 0.001; unpaired two sample t-test. (B) Internally controlled growth assays performed with sgRNAs targeting *LOC646329* in U87 dCas9-KRAB cells. sgRNA-expressing cells were quantified by flow cytometry and represented as the fraction observed at 5 days after sgRNA vector infection. Each sgRNA vector infection was performed in biological duplicates, as shown by individual points on the graph. (C) Quantification of ICC of HeLa-dCas9-KRAB cells one week post CRISPRi-mediated *LOC646329* knockdown (n = 3 biological replicates per condition). ns = not significant; unpaired two sample t-test. (D) RT-qPCR quantification of *LOC646329* in NHA cells 48 hours post ASO transfection (n = 3 biological replicates per condition). * *P-value* < 0.05, ** *P-value* < 0.01; unpaired two sample t-test. (E) Quantification of NHA cell numbers over time in culture. ASO transfected at day 2. (F) Quantification of ICC of NHA cells 48 hours post ASO-mediated *LOC646329* knockdown (n = 3 biological replicates per condition). ns = not significant, * *P-value* < 0.05, ** *P-value* < 0.01, *** *P-value* < 0.001, **** *P-value* < 0.0001; unpaired two sample t-test.

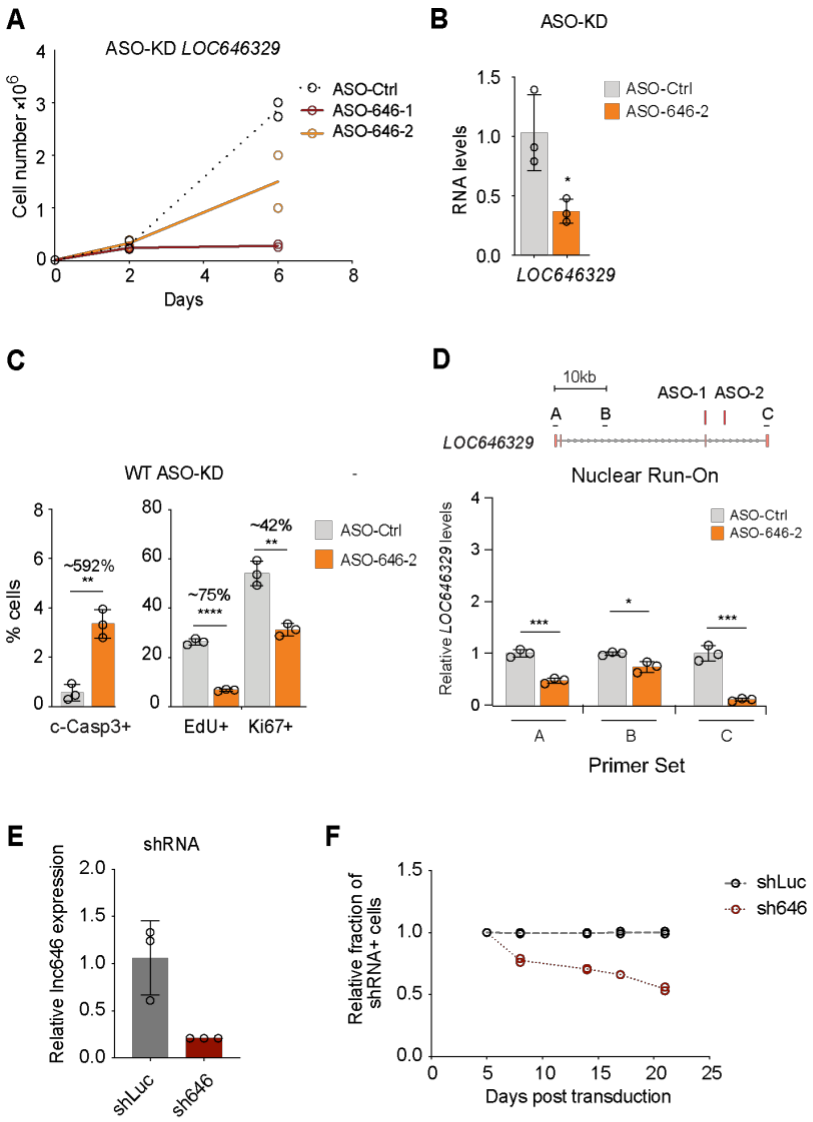

Fig S3.5 Analysis of cell growth and transcriptional termination after *LOC646329* KD.

(A) Quantification of cell numbers over time in culture. ASO transfected at day 2 (n = 2 biological replicates per condition). (B) RT-qPCR quantification of *LOC646329* 48 hours post ASO transfection. * *P-value* < 0.05; unpaired two sample t-test. (C) Quantification of ICC of U87 cells 48 hours post ASO-mediated *LOC646329* (ASO #2) knockdown (n = 3 biological replicates per condition). ** *P-value* < 0.01, **** *P-value* < 0.0001; unpaired two sample t-test. (D) RT-qPCR quantification of *LOC646329* nascent transcript levels in nuclear run-on experiments in U87 cells with and without *LOC646329* ASO-mediated knockdown. Primer sets and locations are indicated by the schematic above. * *P-value* < 0.05, ** *P-value* < 0.01, *** *P-value* < 0.001, ns = not significant; unpaired two sample t-test. (E) RT-qPCR quantification of *LOC646329* 48 hours post shRNA transfection, relative to shRNA to luciferase as control. * *P-value* < 0.05; unpaired two sample t-test. (F) Internally controlled growth assays measured by flow cytometry of shRNA-expressing cells. shRNA-expressing cells were quantified by flow cytometry and represented as the fraction observed at 5 days after shRNA vector infection (n = 2 biological replicates, shown as individual points on the graph).

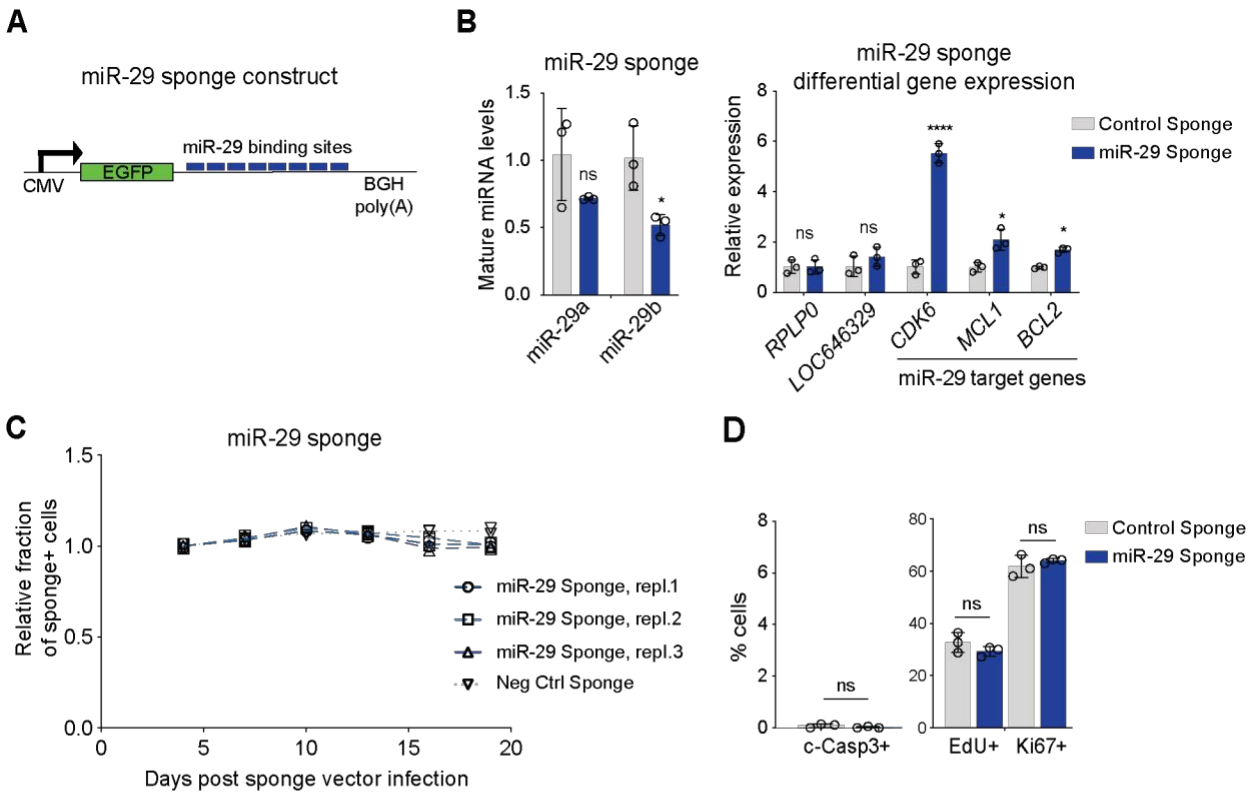

Fig S3.6 Inhibition of miR-29 activity with lentiviral miR-29 sponge construct.

(A) Schematic of miR-29 lentiviral sponge construct. (B) RT-qPCR analysis of mature miR-29a, miR-29b levels (left) and miR-29 target genes levels (right) after transduction of miR-29 sponge (n = 3 biological replicates per condition). ns = not significant, * *P*-value < 0.05, **** *P*-value < 0.0001; unpaired two sample t-test. (C) Internally controlled growth assays measured by flow cytometry of sponge expressing cells after miR-29 sponge infection. Sponge-expressing cells were quantified by flow cytometry and represented as the fraction observed at 4 days after miR-29 sponge vector infection (n=3 biological replicates). (D) Quantification of ICC of U87 cells treated with miR-29 lentiviral sponge one week post transduction (n = 3 biological replicates per condition). ns = not significant, * *P-value* < 0.05; unpaired two sample t-test.

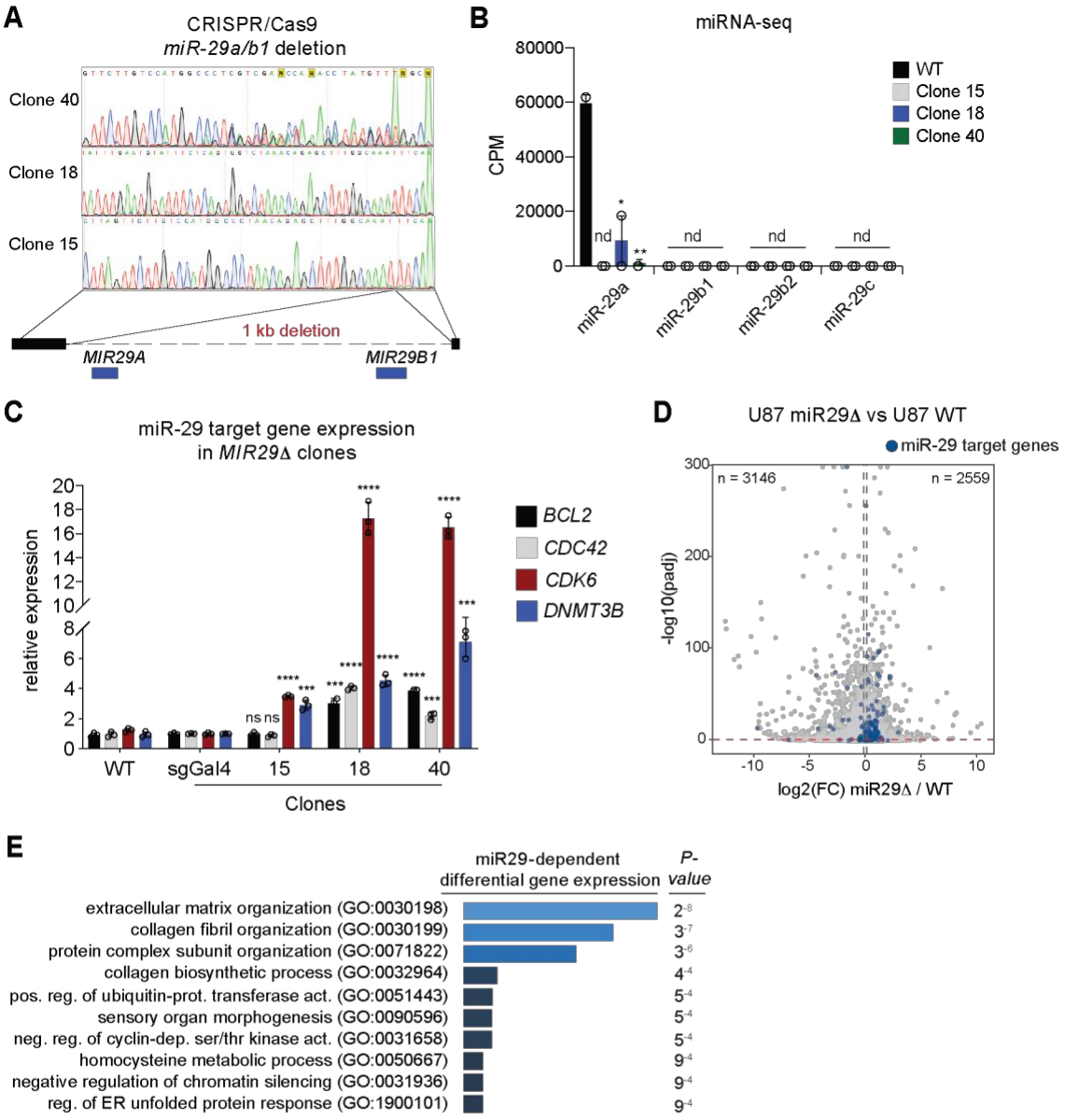

Fig S3.7 Characterization of U87 *LOC646329-miR29*Δ cells.

(A) Sanger sequencing of *LOC646329*-miR29Δ cells showing genetic deletion of the miR-29a/b1 cluster. (B) Small RNA-seq quantification of miR-29a, miR-29b1, miR-29b2, and miR-29c in WT, Clones 15, 18, and 40 (n = 2 biological replicates per condition). ns = not significant, nd = not detected, * *P-value* < 0.05, ** *P-value* < 0.01; unpaired two sample t-test. (C) RT-qPCR quantification of known miR-29 target genes, showing de-repression of targets (n = 3 biological replicates per condition). ns = not significant, *** *P-value* < 0.001, **** *P-value* < 0.0001; unpaired two sample t-test. (D) Volcano plot of differential gene expression in U87 miR29Δ vs U87 WT cells. Each gray dot represents a single gene, with blue dots representing predicted miR-29 target genes. (E) Gene ontology analysis of miR-29 target genes de-repressed in U87 miR29Δ vs U87 WT cells, with *P-value* indicated on the right.

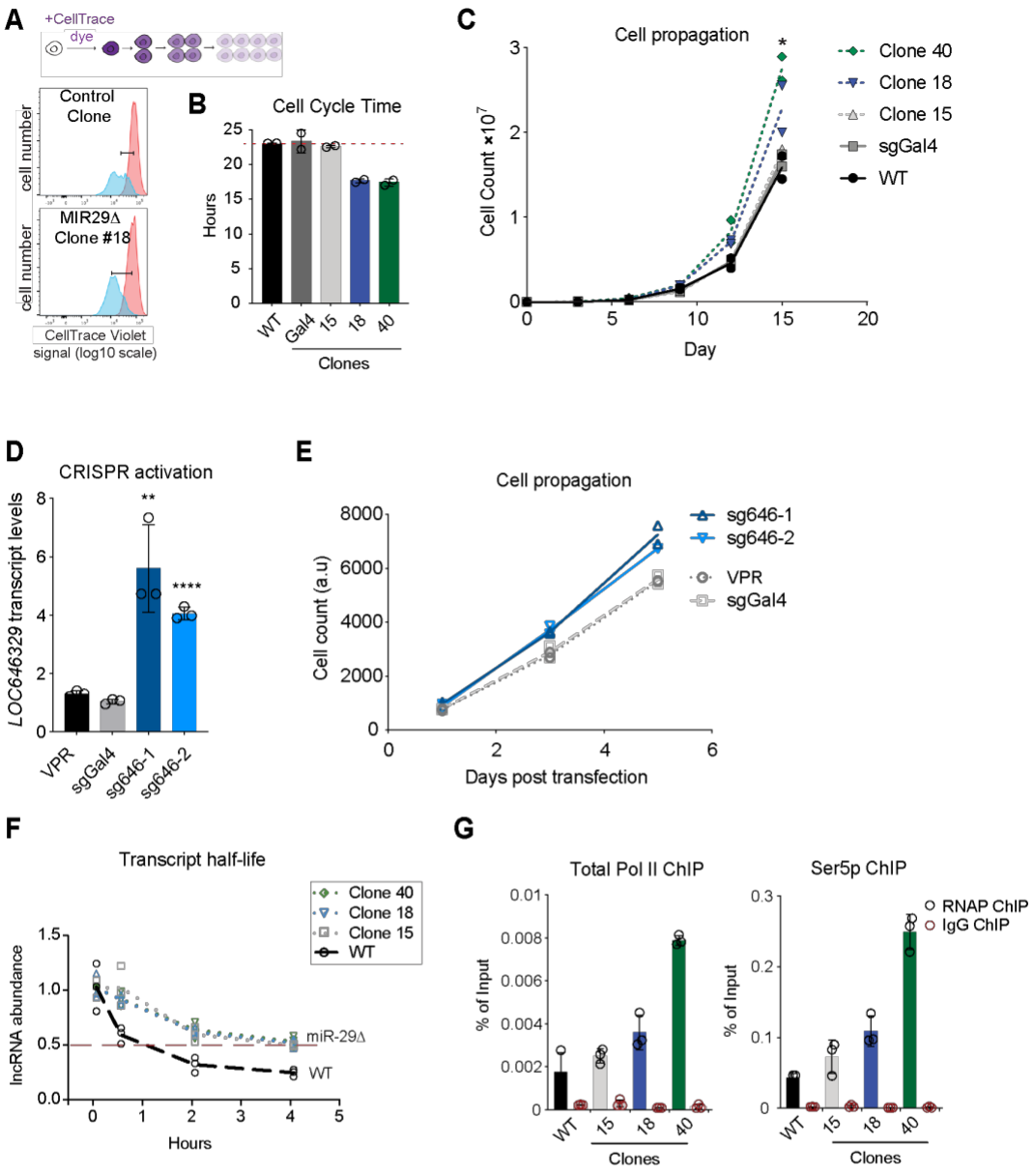

Fig S3.8 Analysis of proliferation of *LOC646329-miR29Δ* cells, lncRNA transcript half-life, and Pol II localization at the *LOC646329* TSS.

(A) Schematic of CellTrace Violet assay, followed by examples of CellTrace Violet flow cytometry data. (B) Quantification of cell cycle time in CRISPR-edited clones and controls using CellTrace data (n = 2 biological replicates per condition). (C) Quantification of cell numbers over time in culture. * *P-value* < 0.05; unpaired two sample t-test (n = 2 biological replicates per condition). (D) RT-qPCR quantification of LOC646329 in U87-dCas9-VPR cells upon CRISPRa with two independent sgRNAs targeting the TSS of LOC646329, relative to control VPR only. ** *P-value* < 0.01, **** *P-value* < 0.0001; unpaired two sample t-test. (E) Quantification of cell numbers using CellTiter assay. (F) Transcript half-life analysis via RT-qPCR quantification of *LOC646329* transcripts after treatment with the transcriptional inhibitor actinomycin. (G) ChIP analysis with antibodies to RNA Pol II (left) and RNA Pol II Ser5p (right) using qPCR primers to the *LOC646329* TSS (n = 3 biological replicates per condition).

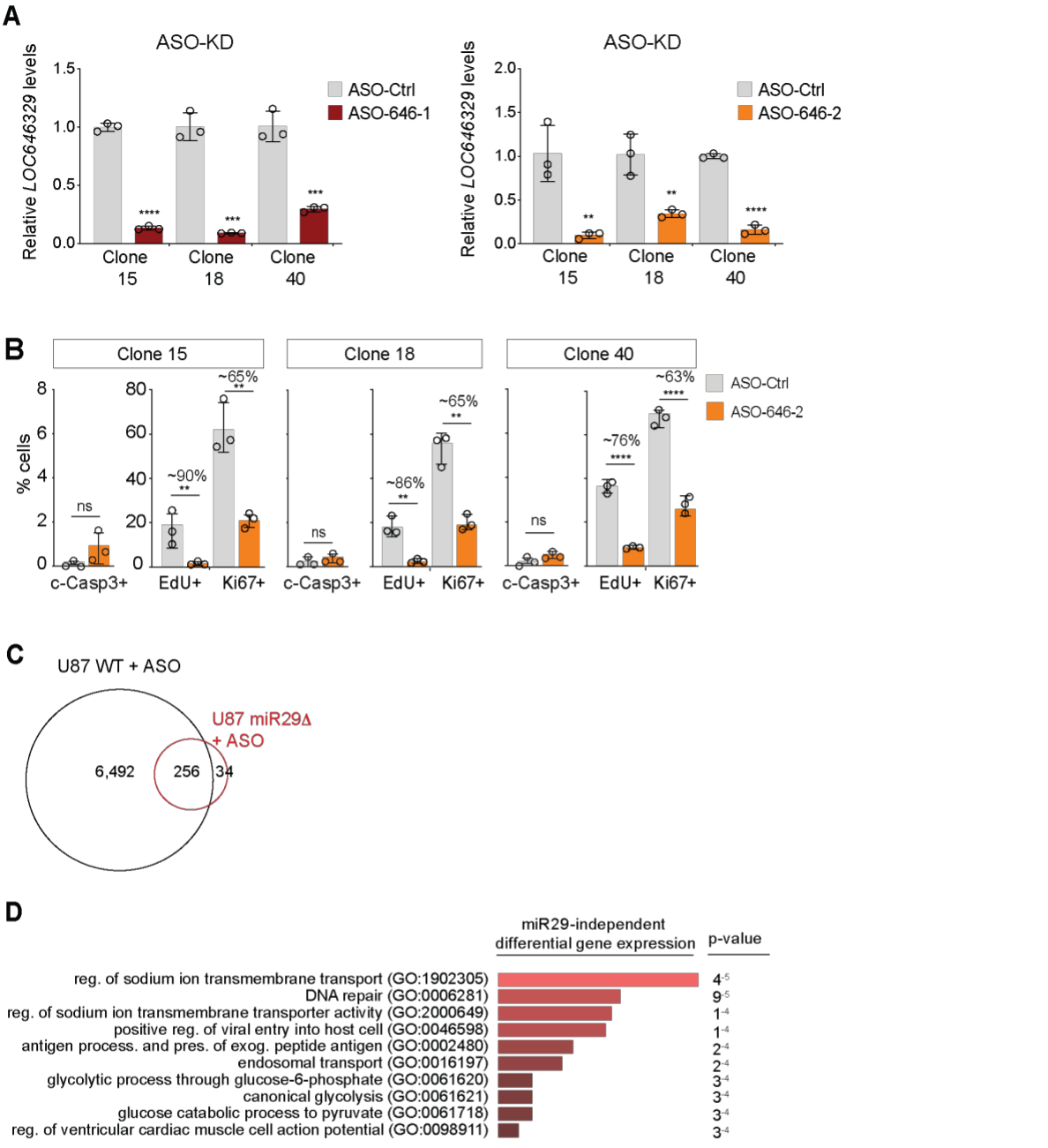

Fig S3.9 ICC and transcriptomic analysis of *LOC646329-miR29*Δ transcript knockdown.

(A) RT-qPCR of U87 *LOC646329*-miR29Δ clones 48 hours post ASO-mediated *LOC646329* knock-down. Knockdown with ASO-1 shown on the left panel, while knockdown with ASO-2 is shown on the right panel. ** *P-value* < 0.01, *** *P-value* < 0.001, **** *P-value* < 0.0001; unpaired two sample t-test. (B) ICC quantification of U87 *LOC646329*-miR29Δ cells 48 hours post ASO-mediated *LOC646329* knockdown. ns = not significant, ** *P*-value < 0.01, **** *P*-value < 0.0001; two sample unpaired t-test. (C) Venn diagram showing the overlap of differentially expressed genes in U87 cells (black circle, 6,748 total genes, 3,094 upregulated, 3,654 downregulated) and U87 *LOC646329*-miR29Δ clones (red circle) upon *LOC646329* ASO-mediated knockdown. (D) Gene ontology of the common set of 256 genes differentially expressed in both U87 cells and *LOC646329*-miR29Δ clones after *LOC646329*

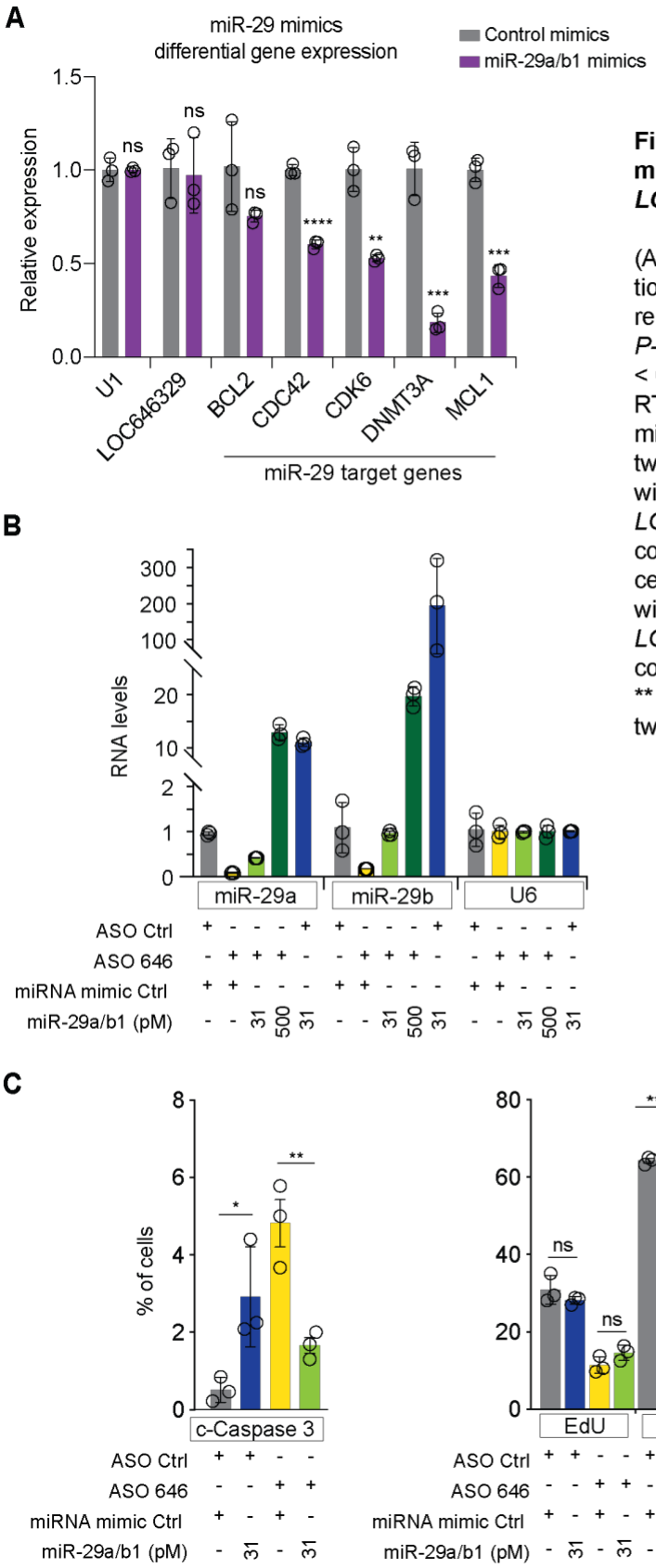

Fig S3.10 Transfection of miR-29a/b1 mimics in U87 cells with or without *LOC646329* knockdown.

(A) RT-qPCR analysis 48 hours post transfection of miR-29a/b1 mimics (n = 3 biological replicates per condition). ns = not significant, ** *P-value* < 0.01, *** *P-value* < 0.001, **** *P-value* < 0.0001; unpaired two sample t-test. (B) RT-qPCR quantification of mature miR-29a, miR-29b, and control U6 RNA after addition of two different amounts of miR-29a/b1 mimics, with or without ASO-mediated knockdown of *LOC646329* (n = 3 biological replicates per condition). (C) Quantification of ICC in U87 cells treated with miR-29a/b1 mimics with or without ASO-mediated knockdown of *LOC646329* (n = 3 biological replicates per condition). ns = not significant, * *P*-value < 0.05, ** *P*-value < 0.01, *** *P*-value < 0.001; unpaired two sample t-test.

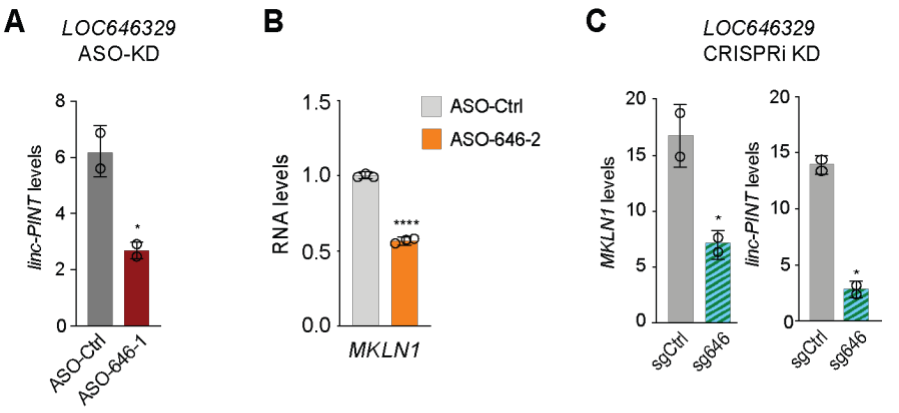
A
LOC646329
ASO-KD
linc-PINT levels
ASO-Ctrl
ASO-646-1
B
RNA levels
ASO-Ctrl
ASO-646-2
MKLN1
C
LOC646329
CRISPRi KD
MKLN1 levels
linc-PINT levels
sgCtrl
sg646

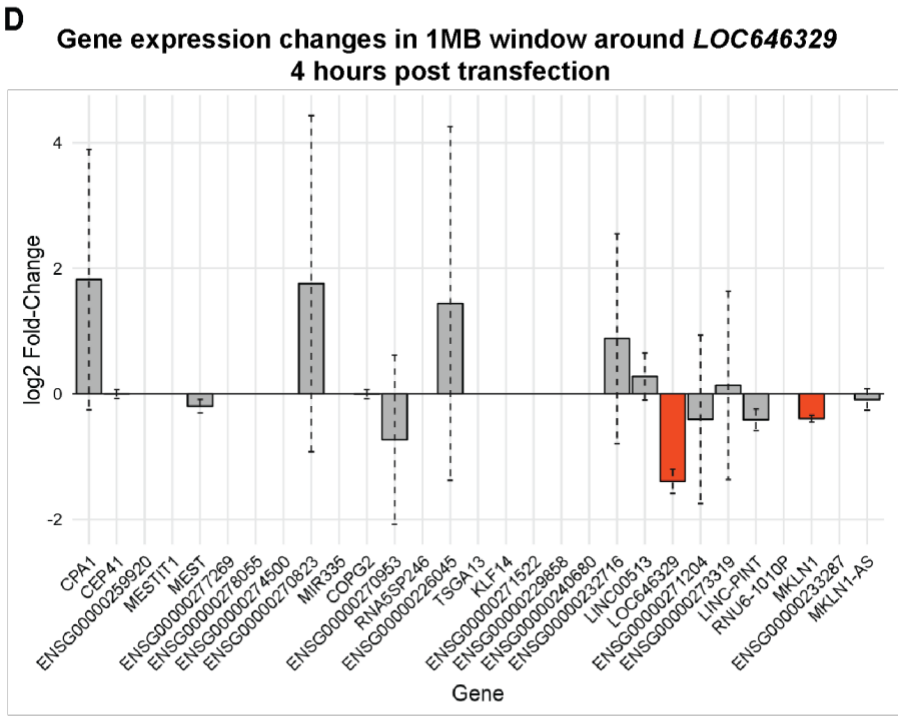
D
Gene expression changes in 1MB window around LOC646329
4 hours post transfection
log2 Fold-Change
Gene

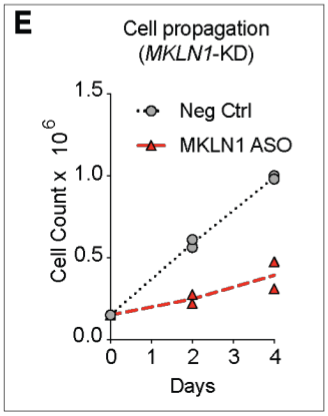
E
Cell propagation
(MKLN1-KD)
Neg Ctrl
MKLN1 ASO
Cell Count x 10^6
Days

Fig S3.11 Analysis of *MKLN1* and *linc-PINT* expression after *LOC646329* knockdown, and cell proliferation effect of *MKLN-1* knockdown.

(A) Quantification of *linc-PINT* normalized read counts in TPM (transcript per million) from RNA-seq 24 hours after ASO-mediated *LOC646329* knockdown (n = 2 biological replicates per condition). * indicates significant difference as determined by the likelihood ratio test. (B) RT-qPCR quantification of *MKLN1* 48 hours post ASO-646-2 transfection. **** *P-value* < 0.0001; unpaired two sample t-test.(C) Quantification of *MKLN1* (left) and *linc-PINT* (right) normalized read counts in TPM from RNA-seq after CRISPRi-mediated *LOC646329* knockdown (n = 2 biological replicates per condition). * indicates significant difference as determined by the likelihood ratio test. (D) Local gene expression (+/- 500kb of *LOC646329* promoter) changes 4 hours after ASO-mediated *LOC646329* knockdown. Statistically significant genes (*LOC646329, MKLN1*) are highlighted in orange (adj. *P*-value < 0.05). (E) Quantification of cell numbers over time in culture after ASO-mediated knockdown of *MKLN-1*.

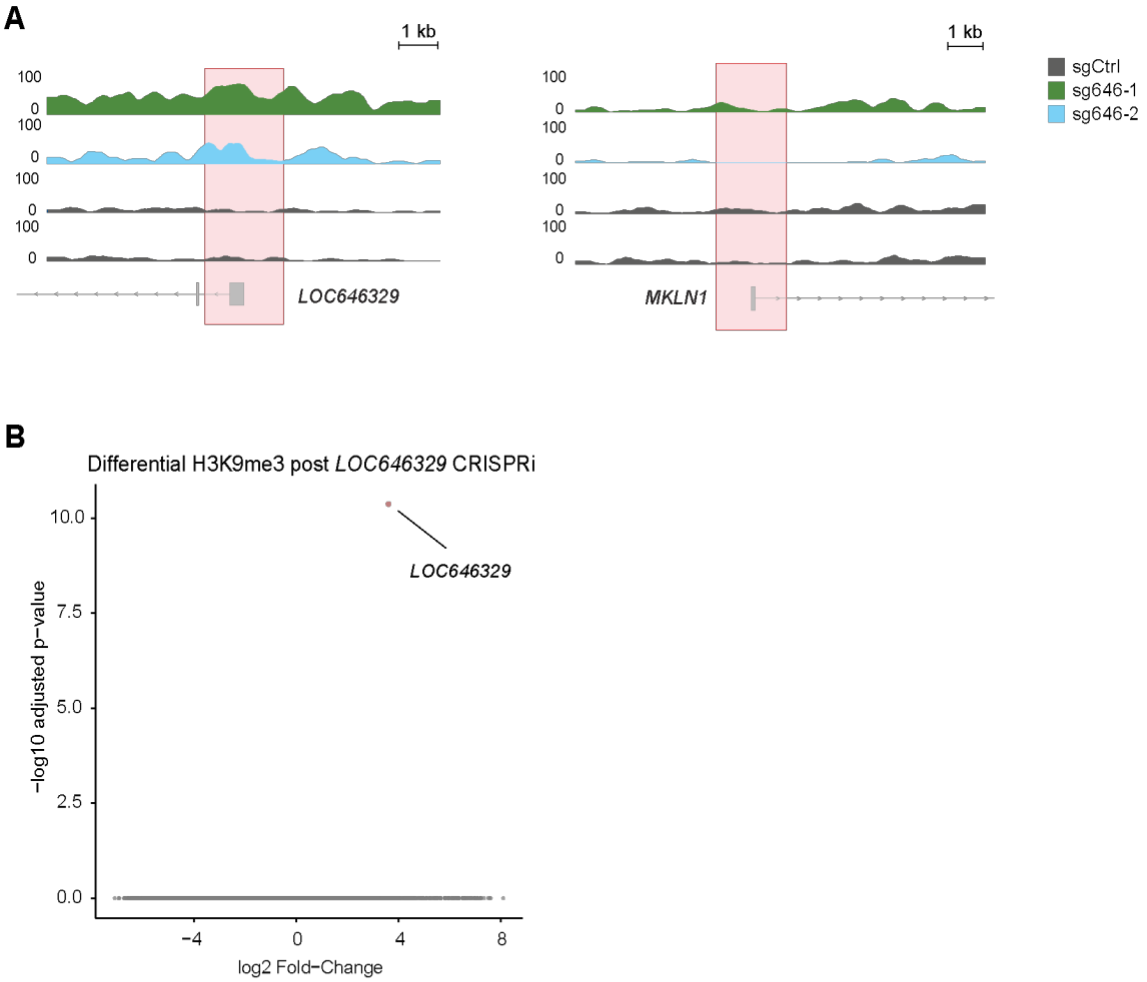

Fig S3.12 H3K9me3 ChIP-seq analysis after CRISPRi knockdown of *LOC646329*.

(A) H3K9me3 ChIP-seq read aligned with either *LOC646329* or *MKLN1* promoter. Grey tracks are derived from cells treated with control sgRNA to Gal4, while green and blue tracks are derived from cells treated with two independent sgRNAs to *LOC646329*. The red shaded box highlights the promoter regions. (B) Volcano plot of genome-wide differential H3K9me3 enrichment of gene promoters in U87-dCas9-KRAB *LOC646329* CRISPRi cells compared to sgCtrl CRISPRi cells. Each gray dot represents a single gene, with the red dot representing the significant locus, *LOC646329*.

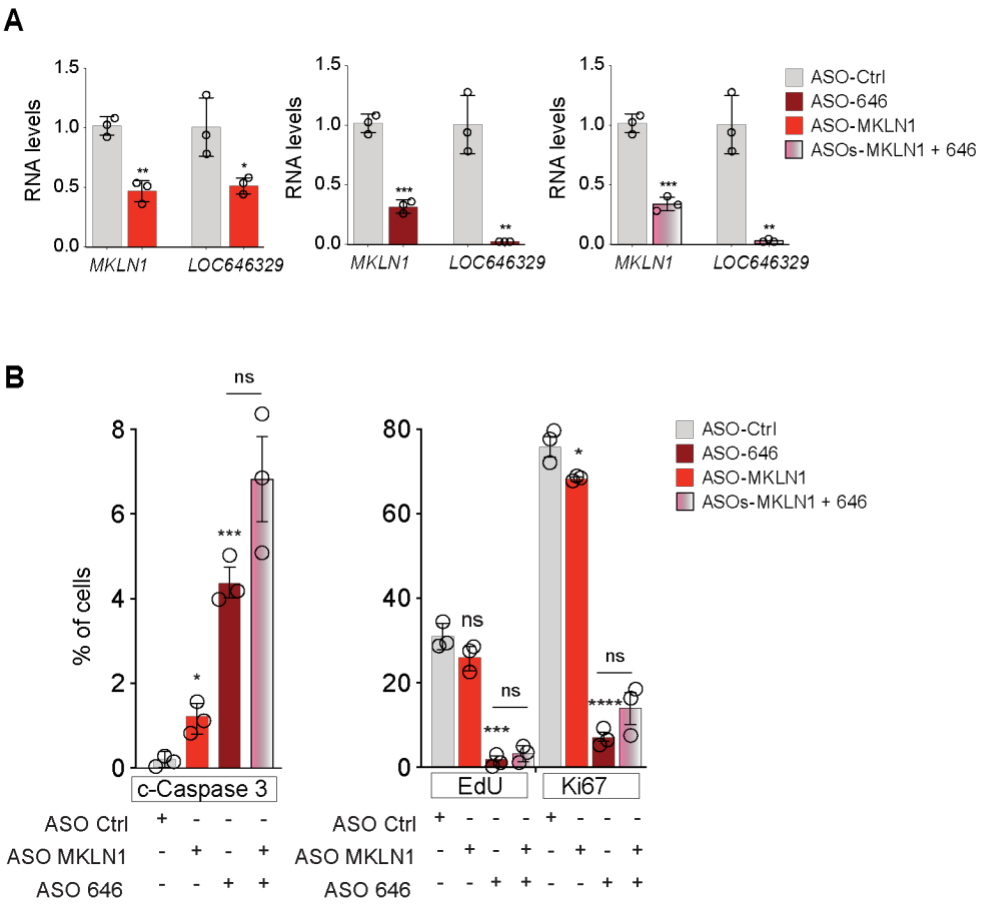

Fig S3.13 Analysis of *MKLN1* and *LOC646329* double knockdown in U87 cells.

(A) RT-qPCR quantification of *MKLN1* or *LOC646329* levels in U87 cells 48 hours post ASO-mediated knockdown with either negative control, *MKLN1* alone, *LOC646329* alone, or *MKLN1* and *LOC646329* double knockdown. (n = 3 biological replicates per condition). * *P-value* < 0.05, ** *P-value* < 0.01, *** *P-value* < 0.001; unpaired two sample t-test. (B) Quantification of ICC of U87 cells 48 hours post ASO-mediated knockdown with either negative control, *MKLN1* alone, *LOC646329* alone, or *MKLN1* and *LOC646329* double knockdown. (n = 3 biological replicates per condition). * *P-value* < 0.05, *** *P-value* < 0.001, **** *P-value* < 0.0001, ns = not significant; unpaired two sample t-test.

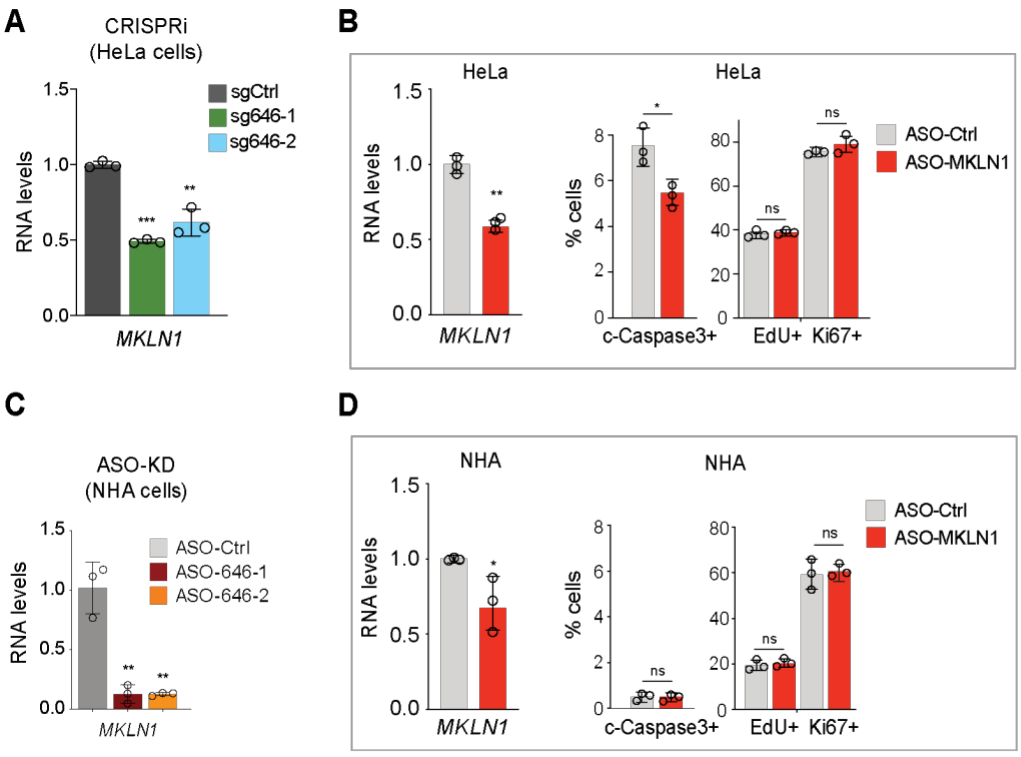

Fig S3.14 Analysis of *MKLN1* after *LOC646329* knockdown, and knockdown of *MKLN1* followed by ICC analysis in HeLa or normal human astrocytes.

(A) RT-qPCR quantification of *MKLN1* in HeLa cells upon CRISPRi-mediated knockdown with two independent sgRNAs targeting *LOC646329,* relative to control Gal4 sgRNA (n = 3 biological replicates per condition). ** *P-value* < 0.01, *** *P-value* < 0.001; unpaired two sample t-test. (B) RT-qPCR quantificaiton of *MKLN1* in HeLa cells 48 hours post ASO-mediated *MKLN1* knockdown (left panel). Quantification of ICC of HeLa cells 48 hours post ASO-mediated *MKLN1* knockdown (right panel) (n = 3 biological replicates per condition). * *P-value* < 0.05, ** *P-value* < 0.01, ns = not significant; unpaired two sample t-test. (C) RT-qPCR quantification of *MKLN1* in NHA cells 48 hours post ASO-mediated *LOC646329* knockdown (n = 3 biological replicates per condition). ** *P-value* < 0.01; unpaired two sample t-test. (D) RT-qPCR quantificaiton of *MKLN1* in HeLa cells 48 hours post ASO-mediated *MKLN1* knockdown (left panel). Quantification of ICC of NHA cells 48 hours post ASO-mediated *MKLN1* knockdown (n = 3 biological replicates per condition). * *P-value* < 0.05, ns = not significant; unpaired two sample t-test.

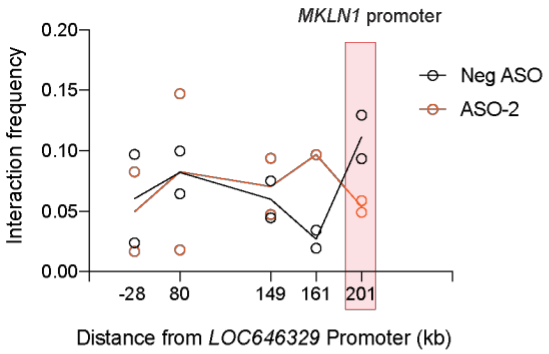

Fig S3.15 Chromosome conformation capture analysis with *LOC646329* promoter as bait.

3C-qPCR analysis in U87 cells with *LOC646329* promoter as bait. Red highlighted region indicates the *MKLN1* promoter region. Data represented by negative control ASO treated U87 cells are shown in black, while data represented by ASO-2-mediated *LOC646329* knockdown are shown in orange. Each region is analyzed in duplicate, with each dot representing an individual replicate.

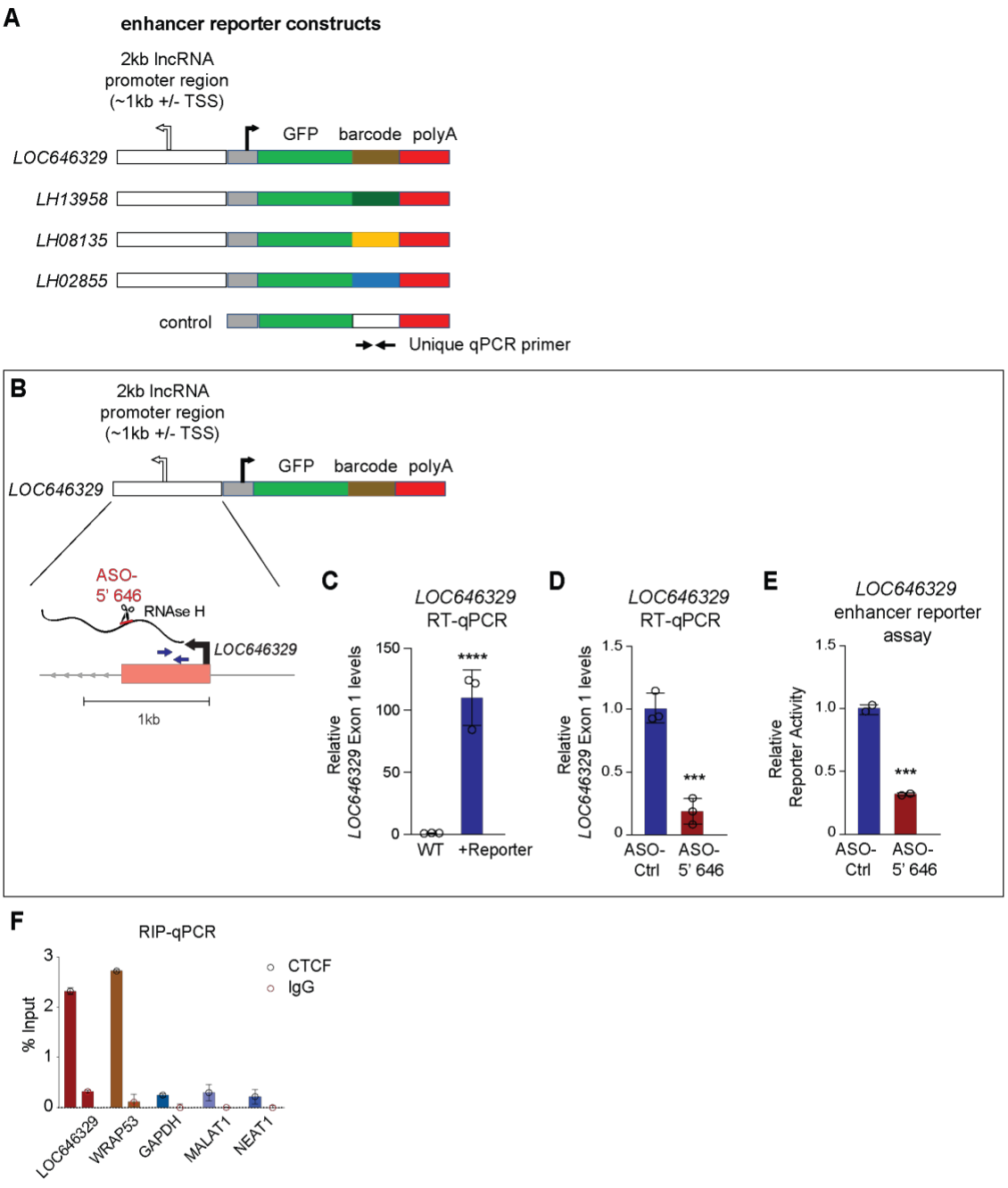

Fig S3.16 Analysis of enhancer-like function of *LOC646329* and RIP analysis.

(A) Schematic of enhancer-reporter constructs. *LOC646329* is cloned in the "negative" orientation. (B) Schematic detailing the 1,992 bp fragment cloned into the reporter construct and RNA transcript produced, showing the 5' ASO target site on Exon 1 (red), and Exon 1 specific primers (blue arrows). (C) RT-qPCR quantification of *LOC646329* Exon 1 in U87 cells +/- *LOC646329* enhancer reporter construct (n = 3 biological replicates per condition). **** *P*-value < 0.0001; two sample unpaired t-test. (D) RT-qPCR quantification of *LOC646329* Exon 1, 48 hours post 5' ASO transfection (n = 3 biological replicates per condition). *** *P*-value < 0.001; two sample unpaired. (E) Enhancer reporter activity of the promoter region of *LOC646329* with or without transfection of the 5' ASO (n = 2 biological replicates per condition). *** *P*-value < 0.001; two sample unpaired t-test. (F) RIP analysis with antibodies to CTCF or IgG using qPCR primers for *LOC646329*.

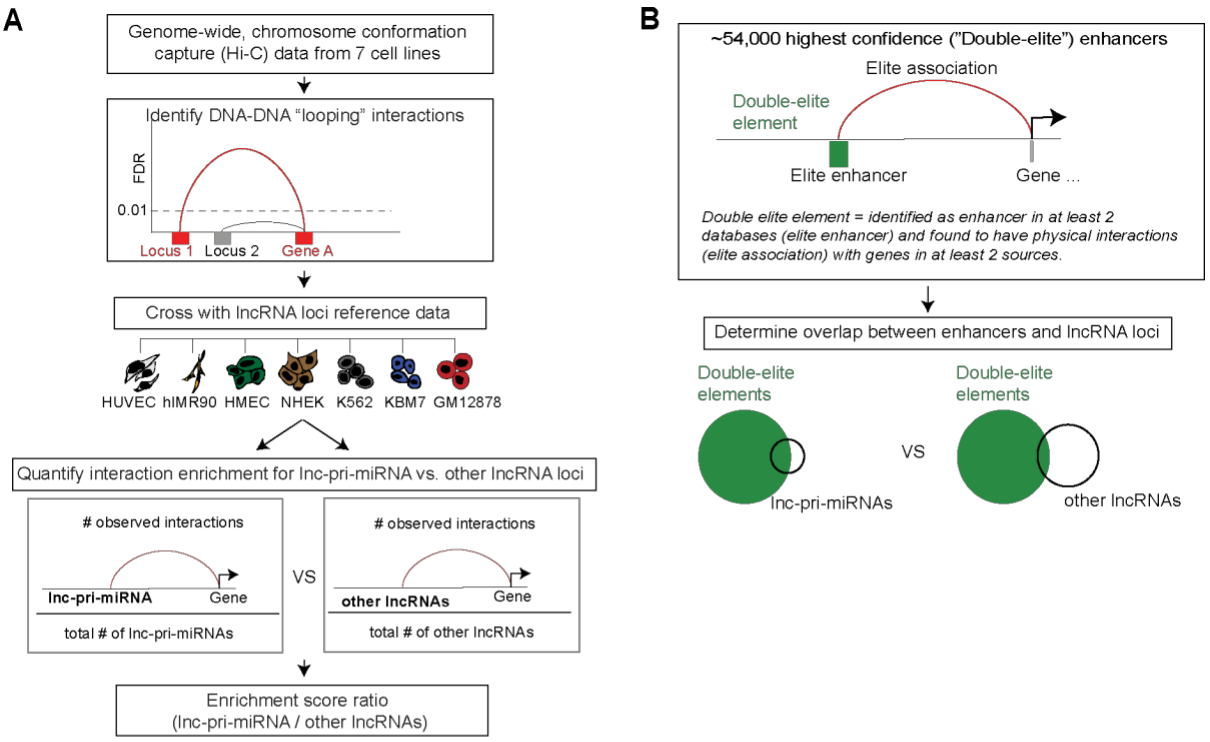

Fig S3.17 Genome-wide DNA-looping interaction and enhancer enrichment analysis.

(A) Schematic illustrating Hi-C data data analysis, evaluating enrichment of DNA-DNA interactions between lnc-pri-miRNA (or other lncRNA) loci and the promoters of other genes. The proportion of lnc-pri-miRNA (or other lncRNA) loci that interact with gene promoters was determined ("interaction enrichment"), which was used to calculate an "enrichment score ratio" (lnc-pri-miRNAs / other lncRNAs). (B) Schematic illustrating the analysis of "Double-elite" enhancer elements and the loci of lnc-pri-miRNAs vs. other lncRNAs. The Venn diagrams illustrate the overlap between double-elite elements and lnc-pri-miRNA loci (left) and other lncRNA loci (right).

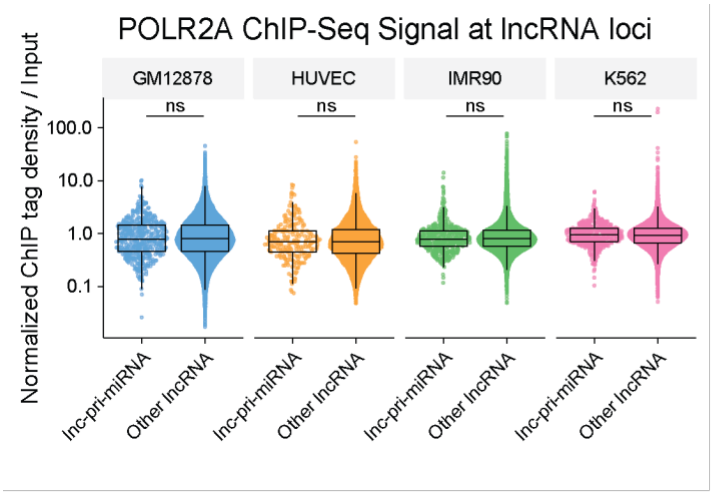

Figure S3.18 RNA Polymerase II ChIP analysis

Pol II ChIP-seq analysis shown in log scale at promoter regions (2kb upstream to 200bp downstream of TSS) of lnc-pri-miRNA genes, or other lncRNAs in four different cell lines (GM12878, HUVEC, IMR90, and K562). Reads were normalized to total mapped reads for the entire sample, and ChIP-seq reads were calculated as a ratio of ChIP reads to input reads at each promoter. The Wilcoxon rank sum test was used to determine statistical significance.

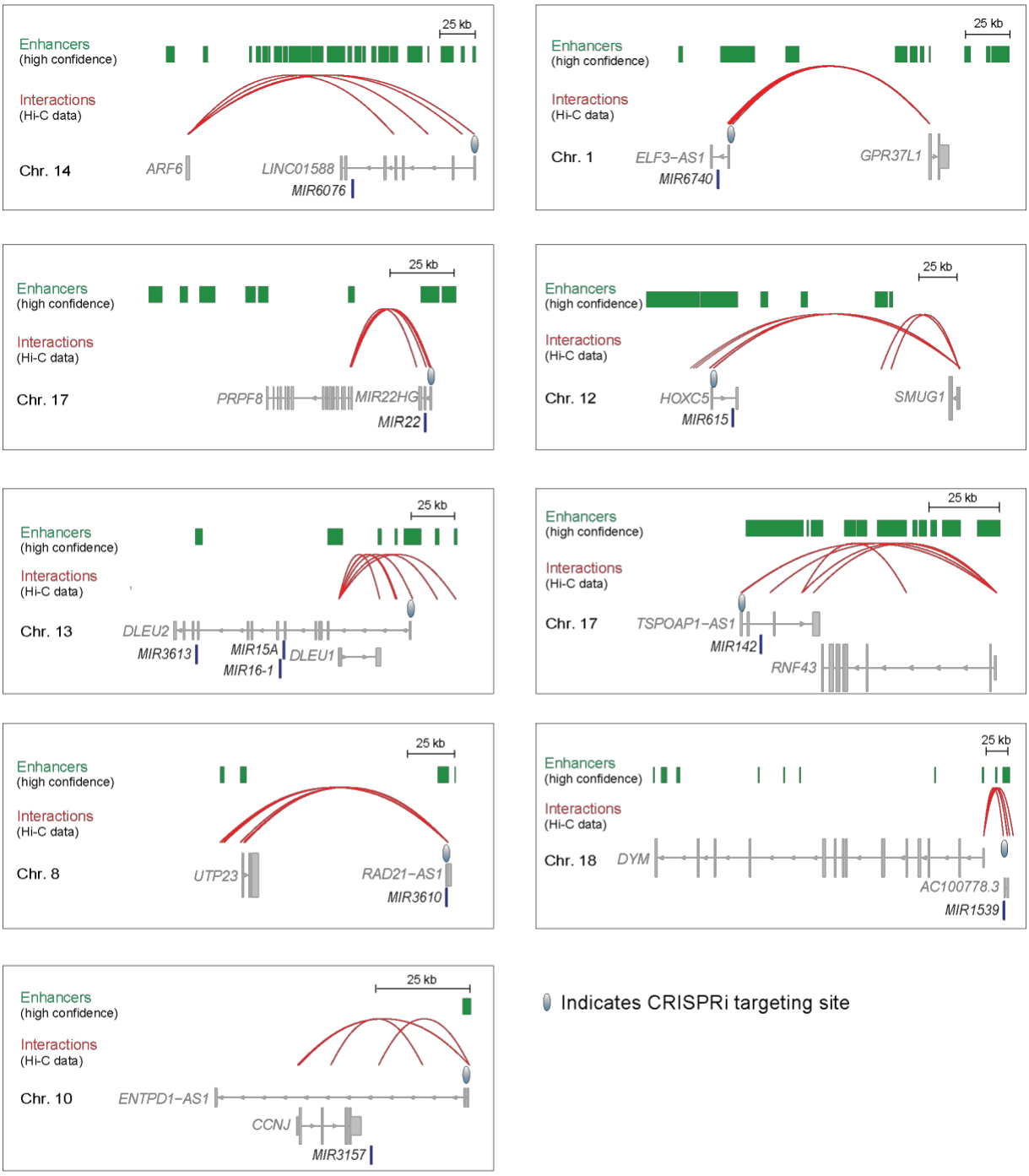

Fig S3.19 Genomic characteristics of 9 lnc-pri-miRNA loci tested in K562 cells.

Schematic of lnc-pri-miRNAs identified with GeneHancer "high confidence" double-elite enhancers (green), along with physical 3D "looping" (red) proximity to protein-coding gene promoters. CRISPRi targeting site indicated by the light blue oval. miRNAs residing within lnc-pri-miRNA loci are indicated by a blue bar.

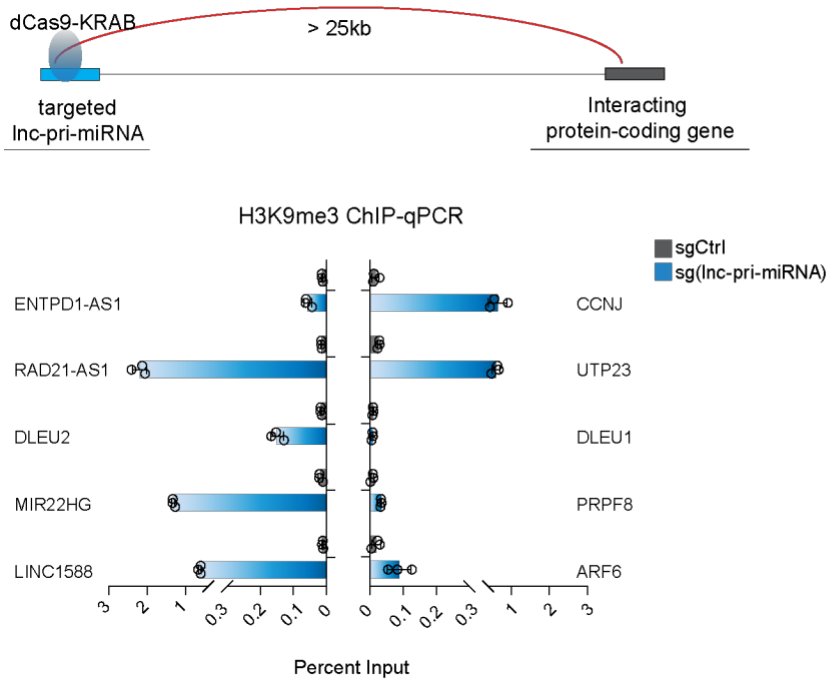

Fig S3.20 H3K9me3 ChIP analysis in K562-dCas9-KRAB cells post lnc-pri-miRNA CRISPRi

ChIP analysis with antibodies to H3K9me3 in lnc-pri-miRNA CRISPRi K562-dCas9-KRAB cells and sgCtrl CRISPRi cells using qPCR primers to either the lnc-pri-miRNA promoter, or the interacting protein-coding gene promoter.

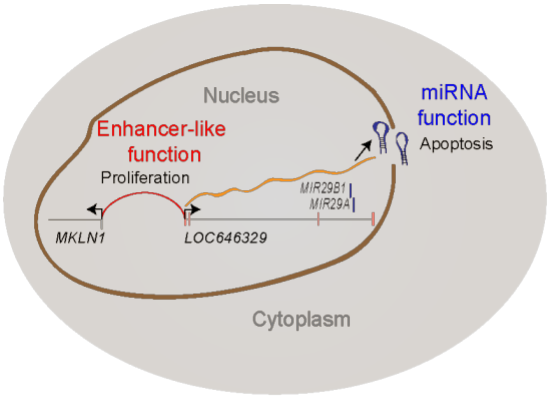

Fig S3.21 Model of dual function of lnc-pri-miRNA loci.

Schematic showing dual function of lnc-pri-miRNA loci, using *LOC646329* as an example. The enhancer-like activity of *LOC646329* is near the TSS, which is more than 35kb upstream of the cognate miRNAs, miR-29a/b1. *LOC646329* interacts with and exhibits enhancer-like activity for *MKLN1,* which is required for GBM cell proliferation. The *LOC646329* transcript (orange) produces miR-29a/b1 (blue), which regulates apoptosis, but is not required for the proliferation of GBM cells.

Table S3.1:

gene_name	gene_id	padj	direction
VHL	ENSG00000134086	1.73E-77	down
SETX	ENSG00000107290	9.25E-58	down
TENM4	ENSG00000149256	9.02E-56	down
TMEM38B	ENSG00000095209	2.94E-52	down
WDR12	ENSG00000138442	4.45E-51	down
ZFYVE9	ENSG00000157077	1.69E-50	down
LINC01411	ENSG00000249306	3.23E-50	down
TSSC1	ENSG00000032389	1.40E-46	down
ASCC3	ENSG00000112249	6.95E-45	down
DIP2C	ENSG00000151240	7.91E-45	down
YIPF4	ENSG00000119820	1.64E-44	down
HK1	ENSG00000156515	2.12E-43	down
UPRT	ENSG00000094841	3.83E-43	down
CCNH	ENSG00000134480	2.60E-42	down
RB1	ENSG00000139687	3.14E-41	down
WWC2	ENSG00000151718	3.40E-41	down
ANKMY2	ENSG00000106524	4.32E-41	down
SLC39A11	ENSG00000133195	1.15E-40	down
DLG1	ENSG00000075711	2.35E-39	down
GOLGA3	ENSG00000090615	1.01E-38	down
KIAA1217	ENSG00000120549	3.43E-38	down
MRRF	ENSG00000148187	9.31E-38	down
PRUNE2	ENSG00000106772	1.99E-37	down
DIS3L2	ENSG00000144535	4.03E-37	down
POLA1	ENSG00000101868	6.80E-37	down
PTPRG	ENSG00000144724	8.43E-37	down
LARS	ENSG00000133706	1.18E-36	down
DKK1	ENSG00000107984	1.33E-36	up
FNDC3B	ENSG00000075420	5.42E-35	down
AFF3	ENSG00000144218	1.62E-34	down
CEP128	ENSG00000100629	1.89E-34	down
AP2A1	ENSG00000196961	1.95E-34	down
CSMD2	ENSG00000121904	2.63E-34	down
CDC14B	ENSG00000081377	2.63E-34	down
HLCS	ENSG00000159267	7.52E-34	down
RAD51B	ENSG00000182185	1.98E-33	down
ANTXR1	ENSG00000169604	6.29E-33	down

Table S3.1:

gene_name	gene_id	padj	direction
PLCB1	ENSG00000182621	5.34E-32	down
MND1	ENSG00000121211	5.78E-32	down
PI4KA	ENSG00000241973	7.69E-31	down
DHX32	ENSG00000089876	1.14E-30	down
GFPT2	ENSG00000131459	2.40E-30	down
FHOD1	ENSG00000135723	3.02E-30	down
STK33	ENSG00000130413	5.86E-30	down
PPIP5K1	ENSG00000168781	6.22E-30	down
RALGAPA1	ENSG00000174373	7.06E-30	down
DMXL1	ENSG00000172869	3.09E-29	down
NBEA	ENSG00000172915	6.36E-29	down
CPA4	ENSG00000128510	8.88E-29	up
MAP2K4	ENSG00000065559	1.18E-28	down
WDFY3	ENSG00000163625	2.62E-28	down
UTRN	ENSG00000152818	5.19E-28	down
MICALL1	ENSG00000100139	9.52E-28	down
CACNA2D1	ENSG00000153956	9.55E-28	down
EPB41L2	ENSG00000079819	2.04E-27	down
APBB2	ENSG00000163697	2.04E-27	down
ZGRF1	ENSG00000138658	2.36E-27	down
HERC1	ENSG00000103657	2.36E-27	down
POLE	ENSG00000177084	3.97E-27	down
KIAA0556	ENSG00000047578	1.01E-26	down
TRAPPC9	ENSG00000167632	1.60E-26	down
PAPPA2	ENSG00000116183	2.03E-26	down
CLCN3	ENSG00000109572	3.43E-25	down
EVC	ENSG00000072840	4.86E-25	down
TRPC4AP	ENSG00000100991	1.38E-24	down
SPG11	ENSG00000104133	1.61E-24	down
GTF2H2C	ENSG00000183474	2.57E-24	down
GALNT13	ENSG00000144278	1.55E-23	down
ACSF2	ENSG00000167107	1.88E-23	down
OTOGL	ENSG00000165899	2.07E-23	down
GOLIM4	ENSG00000173905	2.49E-23	down
RRAD	ENSG00000166592	2.51E-23	up
GHR	ENSG00000112964	3.00E-23	down
MUT	ENSG00000146085	5.17E-23	down

Table S3.1:

gene_name	gene_id	p.adj	direction
EXOC4	ENSG00000131558	6.69E-23	down
PTPRK	ENSG00000152894	7.18E-23	down
LRRC28	ENSG00000168904	7.57E-23	down
HIPK2	ENSG00000064393	1.01E-22	down
ARRDC4	ENSG00000140450	1.39E-22	up
BCAS3	ENSG00000141376	2.06E-22	down
OTUD5	ENSG00000068308	3.12E-22	down
DNAH11	ENSG00000105877	3.23E-22	down
CPS1	ENSG00000021826	3.31E-22	down
FDXR	ENSG00000161513	3.72E-22	up
RALGAPA2	ENSG00000188559	4.16E-22	down
PHACTR2	ENSG00000112419	7.85E-22	down
GPRC5A	ENSG00000013588	9.90E-22	up
GALNT10	ENSG00000164574	1.33E-21	down
SMC1A	ENSG00000072501	2.41E-21	down
KRT34	ENSG00000131737	2.97E-21	up
PALMD	ENSG00000099260	3.11E-21	down
PEAK1	ENSG00000173517	3.90E-21	down
CDKAL1	ENSG00000145996	6.67E-21	down
RIC1	ENSG00000107036	9.64E-21	down
MKNK2	ENSG00000099875	1.29E-20	up
ANAPC1	ENSG00000153107	1.61E-20	down
PCBP3	ENSG00000183570	2.15E-20	down
SRBD1	ENSG00000068784	3.01E-20	down
PTPRD	ENSG00000153707	3.08E-20	down
ITFG1	ENSG00000129636	3.64E-20	down
ATP11C	ENSG00000101974	4.44E-20	down
KIF16B	ENSG00000089177	7.03E-20	down
GPHN	ENSG00000171723	7.52E-20	down
FAR1	ENSG00000197601	1.01E-19	down
PTPRM	ENSG00000173482	1.20E-19	down
WDR7	ENSG00000091157	3.45E-19	down
NEDD4L	ENSG00000049759	4.49E-19	down
SMYD3	ENSG00000185420	4.71E-19	down
PTPN4	ENSG00000088179	4.76E-19	down
DNM1	ENSG00000106976	2.19E-18	down
LEPR	ENSG00000116678	2.94E-18	down

Table S3.1:

gene_name	gene_id	p.adj	direction
ZC3H13	ENSG00000123200	3.21E-18	down
VWA8	ENSG00000102763	7.41E-18	down

Experimental Procedures

Data and Code Availability

The raw and processed imaging datasets generated during this study are available on Mendeley Data (http://dx.doi.org/10.17632/c443rtpbyk.1). The raw and processed sequencing datasets generated during this study are available on GEO (GSE137048).

Tissue culture

We maintained male U87-MG (ATCC Cat#HTB-14), fetal HEK293T cells (ATCC Cat#CRL-3216), female HeLa-dCas9-KRAB, NHA (Sonoda et al., 2001) of unknown sex (as no information reported on Clonetics website), and any U87-derived cells (e.g. miR-29Δ clones) in DMEM (Thermo Fisher Scientific), 10% heat-inactivated FBS (VWR), and 1% antibiotic/antimyocotic (Thermo Fisher Scientific). K562-dCas9-KRAB cells were maintained in RPMI media with 25mM HEPES, L-Glutamine (GIBCO), 10% FBS (VWR), and 1% antibiotic/antimycotic (Thermo Fisher Scientific). All cells were grown at 37°C and 5% CO_2 atmosphere. The U87-dCas9-KRAB and HeLa-dCas9-KRAB lines were authenticated by BFP expression, and effective CRISPRi knockdown. Each of the miR-29Δ cell lines (Clones 15, 18, and 40) were authenticated by PCR genotyping, Sanger sequencing, qPCR, and RNA-sequencing.

Lentivirus production

We plated 400,000 293T cells in a 6-well plate the day prior to transfecting with 1.35µg of packaging vector pCMV-dR8.91 (Stewart et al., 2003), 165ng packaging vector pMD2-G

(Addgene plasmid #12259), and 1.5µg of lentiviral plasmid. At 48 hours post transfection, we harvested viral supernatants and filtered them through a 0.45µM syringe filter prior to use.

Spinfection

We plated 300,000 cells in a 6-well plate the day prior to transduction. We removed all media prior to transduction, and added 1ml of harvested viral medium containing 8µg/mL (final concentration) of polybrene prior to spinning at 2,000g for 30 minutes in a centrifuge at room temperature. After spinfection, all viral media is removed, and replaced with fresh media. In 2 days, cells were 20-30% infected. Puromycin selection can begin (1µg /mL) for 4 days, with a 2 day recovery. Otherwise, cells can be analyzed by flow cytometry to assess infection efficiency.

Chromatin Immunoprecipitation

Cells were fixed using a final concentration of 1% formaldehyde added straight to the culture plates, shaking at room temperature for 10 minutes. After fixing, cells were quenched with 125mM (final concentration) Glycine, shaking at room temperature for 5 minutes to stop formaldehyde fixation. Cells were then washed 2X using ice-cold PBS. Cells were scraped off of the plate using a cell lifter and pelleted for 4 minutes at 2,000 rpm at 4°C. Pellet was then thawed and resuspended in Cell Lysis Buffer (5 mM PIPES pH 8, 86 mM KCl, freshly added 1% IGEPAL) with protease inhibitors (Pierce Halt Protease Inhibitor Cocktail). Cells were then homogenized using a type B glass dounce homogenizer, pelleted, and resuspended in Nuclei Lysis Buffer (50 mM Tris-HCl pH 8, 10 mM EDTA, 1% SDS). Chromatin was incubated on ice for 30 min and then flash frozen in liquid nitrogen. Next, chromatin was thawed and sonicated in

Diagenode TPX tubes using the Diagenode Bioruptor to 150–500 bps as determined by gel electrophoresis. Debris was pelleted and discarded, and an aliquot was removed for Input DNA sequencing from the sonicated chromatin within the supernatant. Sonicated chromatin was then diluted 5-fold in IP Dilution Buffer (50 mM Tris-HCl pH 7.4, 150 mM NaCl, 1% IGEPAL, 0.25% deoxycholic acid, 1 mM EDTA pH 8) with protease inhibitors and pre-cleared with Life Technologies Protein G Dynabeads for 2 hrs at 4°C. 1 µg of antibody was added per million cells, and samples were incubated overnight at 4°C. Antibody-bound chromatin was then collected using Life Technolgoies Protein G Dynabeads and washed twice using IP Dilution Buffer, twice with IP Wash Buffer 2 (100 mM Tris-HCl pH 9, 500 mM LiCl, 1% IGEPAL, 1% deoxycholic acid), and once with IP Wash Buffer 3 (100 mM Tris-HCl pH 9, 500 mM LiCl, 150 mM NaCl, 1% IGEPAL, 1% deoxycholic acid), and once with IP Wash Buffer 3 (100 mM Tris-HCl pH 9, 500 mM LiCl, 150 mM NaCl, 1% IGEPAL, 1% deoxycholic acid). Precipitated chromatin was then eluted for 30 minutes at 65°C with Elution Buffer (1% SDS, 50 mM $NaHCO_3$). ChIP and Input DNA crosslinks were reversed by adding 5 M NaCl and heating at 65°C overnight. The following day, 10 mg/ml RNAse A was added to precipitated chromatin, and chromatin was incubated for 30 minutes at 37°C. DNA was then recovered using Agencourt AMPure XP Beads and quantified using Life Technologies Qubit Fluorometer.

Genome-wide Pol II ChIP-seq Analysis

Raw POLR2A ChIP-Seq datasets from K562, HUVEC, IMR90, and GM12878 were downloaded from ENCODE and aligned to the human genome (GRCh38 release 95) using hisat2 (v2.1.0). Reads mapping to promoters (defined as 2000 bp upstream to 200 bp downstream of transcriptional start site) of lnc-pri-miRNAs and all other lncRNAs were

determined using featureCounts (subread 2.0.1). ChiP-Seq signal at each promoter was determined by calculating the ratio of ChIP reads to input reads at each promoter. All reads were normalized to the total mapped reads for the entire sample. The Wilcoxon rank sum test was used to determine statistical significance between lnc-pri-miRNA and non-lnc-pri-miRNA lncRNAs.

CRISPRi Chromatin Silencing ChIP-seq Analysis

Reads were aligned to the hg19 genome using hisat2. Differential H3K9me3 enrichment of gene promoters was performed according to Liu *et al*., (Liu et al., 2017) by using featureCounts to quantify mapped reads in a 2kb window around the TSS and DESeq2 for differential enrichment testing.

Chromatin Isolation By Biochemical Fractionation

Chromatin isolation protocol was performed according to Wysocka J et al (Wysocka et al., 2001). We harvested 1 x 10^7 cells by using a cell scraped and spun at 1,000 rpm for 2 minutes prior to discarding the supernatant. Cell pellets were washed 2X with PBS, spinning for 2 minutes at 1,000 rpm in between washes. Cells were then resuspended in 200µl of Buffer A (10mM HEPES, pH 7.9, 10mM KCl, 1.5mM $MgCl_2$, 0.34M Sucrose, 10% Glycerol, 1mM DTT, Protector RNAse Inhibitor (Sigma), and Protease Inhibitor (Pierce Halt). After resuspension, Triton X-100 was added to a final concentration of 0.1%. Cells were then incubated on ice for 8 minutes. The mixture was then centrifuged at 1,300g in 4^{o}C for 5 minutes to separate the supernatant (S1, cytosolic) fraction from the pellet (P1, nuclei) fraction. The supernatant (S1) was further centrifuged at high speed (20,000g) in 4^{o}C for 5

minutes; collect the supernatant for the final cytosolic (S2) fraction. Wash P1 once with Buffer A and lyse with 100µl of Buffer B (3mM EDTA, 0.2M EGTA, 1mM DTT, protease inhibitor (Pierce Halt) for 30 minutes. Centrifuge at 1,700g 4^{o}C for 5 minutes; separate supernatant from the pellet (chromatin, P3). The pellet (P3) and S2 can be directly lysed in 1ml of Trizol for RNA extraction.

RNA Extraction

Cells (either on a plate) or a cell pellet are lysed and harvested using Trizol (e.g. 300µl in a single well of a 6-well plate). After harvesting with Trizol, the mixture is prepared and RNA is extracted using the Zymo Direct-zol RNA extraction kit and protocols. RNA concentration is quantified using the Nanodrop.

Small RNA Library Preparation for Sequencing

Extracted RNA was prepared following the SMARTer smRNA-Seq Kit (Takara Bio, Catalog #635029) protocol and sequenced with the HiSeq 4000.

Internally Controlled Cell Competition Assay

Lentiviral sgRNA infection was performed at <30% infection efficiency. Treated cells were assessed using flow cytometry 4 days post transduction and sgRNA expressing cells (either GFP or BFP-tagged) were followed for a period of 2-3 weeks. A non-targeting, sgRNA control was designed to target Gal4. For the *DROSHA* or *DGCR8* double knockdown experiments, stable U87 CRISPRi cells were selected under puromycin for 4-5 days prior to a 2 day recovery to select for stable CRISPRi knockdown of *DROSHA, DGCR8,* or Gal4 (GFP+

vectors) cells. Either Gal4, *DROSHA*, or *DGCR8* CRISPRi knockdown cells were infected with lentiviral sgRNAs targeting control Gal4, or a lnc-pri-miRNA (BFP+ vectors). Double knockdown cells were assessed using flow cytometry of cells expressing dual fluorescent tags (BFP+, GFP+ cells).

CellTrace Proliferation Assay

5mM CellTrace Violet was prepared by adding 20µl of DMSO. 500K cells were plated in a well of a 6-well plate the day prior. 24hrs after plating cells, dilute the stock (5mM) CellTrace solution in pre-warmed (37^{o}C) PBS for a final 5µM solution. The culture media was removed from the cells, and replaced with the working solution containing the CellTrace dye, making sure to note complete coverage of the entire well. Cells were incubated at 37^{o}C, protected from light, for 20 minutes. The working solution is then removed, and washed twice with pre-warmed media, before replacing the entire well with fresh complete media. The following day, cells were analyzed by flow cytometry to assess uptake and quantification the dye at Timepoint 0. Cells were then followed up to 5 days. With each cell division, fluorescence is reduced in half, thus allowing us to back-calculate and quantify division time.

Antisense oligonucleotide and microRNA mimic transfections

Locked Nucleic Acid (LNA) antisense oligonucleotides were designed and purchased from Exiqon. miR-29 mimics were purchased from Dharmacon (C-300521-05-0005 and C-300504-07-0005). These were transfected into cells using Thermo Fisher Scientific Lipofectamine® RNAiMAX Reagent under manufacturer's guidelines. A final working concentration of 50nM was determined effective by titration and used for final experiments.

Immunocytochemistry

Immunostaining was performed using Thermo Fisher Scientific's Click-iT® EdU Imaging Kit. Cells were pulsed for 1 hour using a final concentration of 10μM EdU provided by the kit prior to following manufacturer's directions. Cells were blocked for at least 1 hour using blocking buffer (50% PBS, 10% normal goat serum, 1% BSA, 0.3% TX-100, 0.3M Glycine final concentrations), prior to incubating with primary antibodies for 2 hours in the dark, and secondary antibodies for 30 minutes in the dark. Slides were mounted and dried overnight prior to imaging.

Generation of miR-29 clones using CRISPR-Cas9 mediated cleavage

U87 cells constitutively expressing Cas9 using the pLentiCas9-T2A-BFP construct (Pulido-Quetglas et al., 2017) were exposed to transient transfection of single guide RNAs (sgRNAs) cloned into the pU6-sgRNA EF1Alpha-puro-T2A-BFP construct (Gilbert et al., 2013) for 24 hours, followed by a 2 day selection period using 1μg/ml puromycin. The selected cells were then sparsely plated so single colonies were allowed to form. Each colony was individually and manually picked and plated within a well of a 96-well plate to allow for clonal expansion. *LOC646329-miR29Δ* cells were then confirmed by PCR genotyping, RT-qPCR of mature miR-29a/b1, and de-repression of validated miR-29 target genes.

sgRNA sequences used:

AGGAAGCTGGTTTCATATGGTGG

CCTAGAGTATACCTTTGATATGG

CRISPR-Inhibition

For CRISPRi, cells stably expressing dCas9-KRAB (Addgene plasmid #46911) were transduced with sgRNA for 2 days prior to a 4 day puromycin selection and RT-qPCR for confirmation of knockdown. CRISPRi cells were also followed by flow cytometry without selection to track BFP expression in cell competition assays.

sgRNAs used are shown below.

sgLOC646329-1:

GGACTCAAGACGACCAACAC

sgLOC646329-2:

GCACGTGGCTGCCATCTCAG

sgLINC01588:

GCACACTAGACGCCAGATGC

sgMIR22HG:

GTGGGGGTTGCTGCACGAGG

sgDLEU2:

GGCTCCCCGCCCCATCGCCG

sgRAD21-AS1:

GACCCTGGGCTGCGGAGGGA

sgENTPD1-AS1:

CCGGATATATTGAATCGCCG

sgELF3-AS1:

GGGGTACAGGTGGGTCTCAG

sgHOXC5:

GACCCATCCTTACAAGACAG

sgTSPOAP1:

GGACCAGCTTGGAGTTGTGT

sgAC100778.3:

GAAGCCTCGCCGCGCCCCTT

RNA Fluorescence In Situ Hybridization

FISH probes were designed and purchased from Advanced Cell Diagnostics (ACD). Cells were plated in Thermo Fisher Scientific Lab-tek 16-well chamber slides prior to sample preparation using modifications to ACD's Fixed Frozen Tissue Using RNAscope® Fluorescent Assay.

Modifications: Skipped Part 1, Preparation of Tissue Sections. Probes were warmed to 40°C for 10 minutes prior to cooling to room temperature and usage. Submerging samples in target retrieval solution was skipped. Protease III treatment was performed by diluting 1:15 and incubating cells in solution for 10 minutes at room temperature prior to washing off in distilled water and proceeding with the RNAscope® Fluorescent Multiplex Kit User Manual Part 2 (Doc. No. 320293) available at http://www.acdbio.com/technical-support/user-manuals.

RNA Half Life Assessment

Transcription was inhibited by adding 5μg/ml of Actinomycin D to U87 cells, and RNA was harvested at 0, 0.5, 2, and 4 hrs after treatment before performing RT-qPCR using GAPDH for normalization.

Hi-C data analysis

The raw mapping Hi-C data for seven cell lines were obtained from GEO (GSE63525) (Rao et al., 2014). The promoter-promoter/enhancer interactions were identified from Hi-C data using PSYCHIC (Ron et al., 2017) with 25Kb resolution window size. The output of PSYCHIC (at a threshold of FDR < 1e-2) was intersected with the Gencode transcripts (including lncRNAs and coding genes) before we count for the calculation of the ratio for lnc-pri-miRNAs/non lnc-pri-miRNA lncRNAs. The intersections between interactions (at FDR < 1e-2) and lnc-pri-miRNAs/non lnc-pri-miRNA lncRNAs were performed by using bedtools2-2.26.0. Statistical analysis was performed using the Mann-Whitney test.

GeneHancer analysis

GeneHancer list of "double elite" enhancers (Fishilevich et al., 2017) was intersected with Gencode v28 database and the annotation of microRNA primary transcript structures from Chang *et al*., (Chang et al., 2015). Enhancer enrichment ratio was calculated using the proportion of lnc-pri-miRNAs overlapping "double elite" enhancers, relative to the proportion of other lncRNAs (non lnc-pri-miRNAs) overlapping "double elite" enhancers. Statistical significance was determined by Fisher's exact test.

LGG vs GBM public data, and primary vs recurrent glioma analysis

Aligned reads for glioblastoma (GBM) and low-grad glioma (LGG) patients were obtained from the GDC Data Portal (https://portal.gdc.cancer.gov/). As for the primary vs recurrent glioma samples, tumor specimens from 31 glioma patients were obtained from the Costello lab

at UCSF. Each of these patients underwent surgical resection at UCSF for primary grade-II/III glioma and again subsequently for a recurrent glioma. Both primary and (for some patient multiple) recurrent specimens were profiled by RNA-seq, resulting in 122 total datasets.

Expression of coding and non-coding transcripts was performed with featureCounts (Liao et al., 2014) and a gtf files containing the annotations in the Gencode v28 database and the annotation of microRNA primary transcript structures from Chang *et al.*, (Chang et al., 2015). For the primary vs recurrent samples, gtf annotation files from Gencode and Cheng *et al.*, (Chang et al., 2015) were mapped from GRch38 to hg19 using liftover from the UCSC Genome Browser (https://genome.ucsc.edu/cgi-bin/hgLiftOver). Expression levels in each count matrix were normalized to counts per million (CPM) based on total Gencode counts and log2 transformed (log2 (CPM+1)). As multiple specimens were sequenced from some of the recurrent cases, but not others, expression levels were averaged by case to obtain 62 datasets for analysis (31 primary, 31 recurrent).

Only features with an average expression > 2 CPM in any sample were considered for downstream analysis. Differential expression was accessed using pairwise t-tests and adjusted for multiple testing using the Benjamini-Hochberg (Benjamini et al., 2001) method. lnc-pri-miRNA transcripts were defined as transcripts with genomic coordinates overlapping the coordinates of at least one mature miRNA as annotated in miRbase v21 (Kozomara and Griffiths-Jones, 2014). Protein coding genes were identified via the "gene type" information in the Gencode database. Significant differences in lnc-pri-miRNA and non lnc-pri-miRNA expression between GBM and LGG (or primary and recurrent) were determined using Fisher's exact test. All subsequent data analysis and visualization was carried out in R (v3.4.2.). PCA analysis was performed on all expressed lnc-pri-miRNA. The heatmap was

generated for all lnc-pri-miRNA with loadings <-0.2 or >0.2 for PC1 in PCA analysis, clustering was performed using average linkage clustering and 1-person correlation as distance measure.

Generation of mammalian DNA-tag reporter vectors

To increase the throughput testing enhancer activity of lncRNA promoters, we modified the barcoded reporter system that was published previously (Nam et al., 2010). The GFP-tag sequence was PCR amplified from each of the 13 DNA-tag vector (Nam et al., 2010) using primers F: ATGAGCAAGGGCGAGGAACT, R: CCATGGTGCTGCGCAGATC. The resulting PCR products were individually cloned into a modified pGL4.23 vector (Promega) that already contained a mammalian SCP1 promoter (Juven-Gershon et al., 2006). The promoter regions of lncRNA (1kb upstream and 1 kb downstream from TSS) were PCR amplified and cloned into the multiple cloning sites upstream of the SP1 promoter. An empty vector without any lncRNA DNA sequence was used as the negative control. Enhancer activity assay 65 plasmids were generated each containing a promoter region of the 65 tested lncRNAs using method described above. These 65 plasmids were transfected into U87 cells in 7 separate batches, in which plasmids with different tags were mixed at equal molar ratio. The negative control vector was co-transfected in each batch. For ASO knockdown experiments, ASO and enhancer-reporter constructs were co-transfected into the same cells. Cells were collected 48 hours after transfection. DNA and RNA were extracted using AllPrep DNA/RNA micro kit (Qiagen) following the manufacture's protocol. qPCR experiments were performed on both DNA and cDNA templates using primers specific to each tag-DNA (Nam et al., 2010). To calculate the enhancer activity, the relative expression level of each tag compared

to the negative control (result from cDNA) was normalized to the amount of transfected DNA (Nam et al., 2010).

RNA-Sequencing and Gene Expression Analysis

RNA-Sequencing libraries were prepared using the Illumina TruSeq Stranded mRNA Kit and sequenced on an Illumina HiSeq 4000 in paired-end mode for 100 cycles with a minimum of 50 million reads per replicate. Read quality assessment, quality trimming, and adapter removal were performed using fastp before aligning to the human reference genome (GRCh38 release 84) with the hisat2 (2.1.0) spliced aligner. Gene expression was quantified using featureCounts (1.5.0) and differentially expressed genes were analyzed using DESeq2 (1.22) in R (3.5) using the likelihood ratio test at a false discovery rate of 0.05. Gene ontology analysis was performed using Enrichr - top 50 genes sorted by "log2 fold change" are used as the input list. For genes related to *LOC646329-miR29Δ* knockdown, the top 50 genes sorted by "log2 fold change" are considered if the genes were also statistically and significantly changed in the "wildtype" *LOC646329* knockdown condition. Predicted target genes of miR-29 were obtained using miRTarBase (Chou et al., 2018) and TargetScan (Agarwal et al., 2015). Small RNA-seq data was aligned using STAR (Dobin et al., 2013)

RNA isolation, Nanopore sequencing, and base calling

Total RNA was isolated from U87 human glioblastoma cells using TRI Reagent Solution (ThermoFisher), followed by bead-based poly(A) selection. Approximately 750 ng of poly(A) RNA was used for dT adapter ligation, followed by reverse transcription, and additional ligation of motor adapter prior to loading onto the Oxford Nanopore Technologies (ONT) PromethION

for sequencing. The ionic current trace for each poly(A) RNA strand is base called using the ONT Albacore algorithm.

Reduction of miRNA activity using mirVana miRNA inhibitors

5nmol lyophilized inhibitors to miR-6076, miR-22, miR-15a, miR-16-1, miR-3613, miR-3157 were ordered from Life Technologies (Catalog #4464084 with assay IDs MH26155, MH10203, MH10235, MH12371, MH19501, MH16540 respectively), and negative control inhibitor Catalog #4464076. Inhibitor stocks were diluted in nuclease-free water and 30pmol of each inhibitor was transfected following the RNAiMAX protocol. Cells were harvested 24 hours post transfection for RT-qPCR analysis.

Nuclear Run-On

Nuclear run-on was performed as described in Mendell *et al.,* (Lee and Mendell, 2020) with minor modifications. 5 million cells were harvested with Trypsin/EDTA, washed with cold PBS, and centrifuged at 4C for 5 minutes. The PBS was aspirated and cell pellet resuspended in 500µl cold lysis buffer (10mM HEPES pH 7.4, 10mM KCl, 1.5mM $MgCl_2$, 0.34M sucrose, 0.1% (v/v) TX-100, 1mM DTT) and incubated on ice for 20 minutes. Samples were centrifuged at 1300g for 5 minutes at 4C and washed once in 1ml of cold lysis buffer. The nuclei were then resuspended in 100µl of cold nuclear storage buffer (50mM Tris-HCl pH 8, 0.1mM EDTA, 5mM $MgCl_2$, 40% (v/v) glycerol) and incubated on ice. Transcription reaction for each sample was prepared with: 50µl of 2x transcription buffer (20mM Tris-HCl pH 8, 5mM $MgCl_2$, 300mM KCl, 4mM DTT), 4µl SUPERase In RNase Inhibitor (20U/µl, Invitrogen), 1µl 100mM BrUTP (Sigma-Aldrich), 2µl 100mM ATP (Roche), 2µl 100mM GTP (Roche), 2µl 100mM CTP (Roche), 1µl

100mM UTP (Roche), mixed well and combined with nuclei in storage buffer. This reaction (total volume of 100µl) was mixed by pipetting and incubated at 37C for 30 minutes. After 30 minutes, 600µl Trizol LS (Thermo) was added and incubated at room temperature for 5 minutes. RNA was then isolated using the Zymo mini RNA isolation columns, following manufacturer instructions with the DNase step. After RNA isolation, bromouridylated RNA was immunoprecipitated: For each sample, 30µl protein G Dynabeads (Invitrogen) was pre-washed in PBST (0.1% (v/v) Tween-20 in PBS) and combined with 2 mg of anti-BrdU monoclonal antibody (Santa Cruz Biotechnology). After incubation on a rotating platform for 10 min at room temperature, the beads were washed twice in PBSTR (PBST supplemented with 8 U/µl SUPERase In) and resuspended in 100µl PBSTR. 2µg of bromouridylated RNA was denatured at 65C for 5 min, mixed with the anti-BrdU conjugated beads, and rotated at room temperature for 30 minutes. Immunocomplexes were magnetically separated and washed three times with PBSTR. To harvest the RNA, 500µl of TRIzol (Ambion) was added to the beads, mixed by pipetting, and incubated for 5 min at room temperature. 100µl of chloroform was added, vortexed for 10s, and incubated for 10 min at room temperature. The samples were then centrifuged at 15,000 rpm for 10 min at 4C. The aqueous phase was collected and transferred to a new tube. RNA was precipitated by adding 250µl of isopropanol and 20µl of GlycoBlue (15 mg/ml, Invitrogen). cDNA was synthesized using the Transcriptor cDNA synthesis kit with random hexamer primers (Roche). Real-time PCR amplification was performed using Fast SYBR Green master mix (Life Technologies). Relative quantification of each target, normalized to an endogenous control (*RPLP0*), was performed using the DDCt method.

Chromosome Conformation Capture (3C-qPCR)

In-nucleus 3C was performed as described in Stadhouders *et al*., and Nagano *et al*., (Nagano et al., 2015; Stadhouders et al., 2013) with minor modifications. Cells were fixed by adding 37% formaldehyde to a final concentration of 1% and incubating for 10 min at room temperature while tumbling, followed by addition of glycine to a final concentration of 0.125M to quench. Samples were then centrifuged at 300g for 8 min at 4°C, and supernatant was removed. Samples were washed with cold PBS and resuspended in 5 mL ice-cold lysis buffer (10 mM Tris-HCl (pH 8.0), 10 mM NaCl, 0.2% NP-40, 1× complete protease inhibitor (Roche), followed by 10 min incubation on ice. Samples were centrifuged at 300g for 5 min at 4°C and resuspended in 500 uL 1.2x NEB Buffer 2.1 (B7202S). 20% SDS was added to a final concentration of 0.3%, and samples were incubated for 1 hr at 37°C while shaking at 900 rpm on a thermomixer. 20% Triton X-100 was added to a final concentration of 2%, followed by incubation for 1 hr at 37°C while shaking at 900 rpm on a thermomixer. 500U of EcoRI (NEB R0101L) was added to each sample and incubated 20 hr at 37°C while shaking at 900 rpm on a thermomixer. For in-nucleus ligation: 7ml of ligation mix (820 µl of 10× T4 DNA ligase reaction buffer [NEB], 41 µl of 20 mg/ml bovine serum albumin [NEB B9000S] and rest water) and 10000U of T4 DNA Ligase (NEB M0202M) was added per sample. Ligation was performed for 4-6 hrs at 16°C. De-crosslinking was performed by adding 300 ug proteinase K (Thermo) and incubating for 16 hr at 65°C. 300 ug RNase (Thermo) was added and incubated for 30 min at 37°C. Samples were purified by phenol:chloroform extraction. Pellets were air dried and resuspended in 150 uL 10 mM Tris-HCl (pH 7.5). Digestion efficiency was checked using primer pairs amplifying across EcoRI site using undigested and digested not ligated aliquots as in Hagege *et al*., (Hagege et al., 2007). Bacterial artificial chromosome (BAC) clones (RP11-10I12 and RP11-815G13) were ordered

from BACPAC Resources and used as control templates to cover the genomic region under study. BAC DNA was digested using 700 units of EcoRI (NEB) at 37 °C overnight. After DNA purification, digested DNA fragments were ligated using T4 DNA ligase (NEB) at 16 °C overnight. DNA was purified by phenol-chloroform and ethanol extraction.

All primers were designed to be within 25–100 bp from the nearest restriction enzyme digestion site using the 3C primer design software, 3PD. Quantitative real-time PCR was performed using SYBR Green chemistry on Roche Light Cycler480. The linear range of amplification for templates were determined by serial dilution using titration primers in Naumova *et al*.,(Naumova et al., 2012). To quantify specific chromatin interactions, normalized relative amount of 3C product was calculated using the following formula: $2^{-\Delta\Delta Ct} = 2^{((Ct\ 3Cinteraction - Ct\ 3Ccontrol)-(Ct\ BACinteraction - Ct\ BACcontrol)}$. where $Ct^{3Cinteraction}$ and $Ct^{BACinteraction}$ quantify PCR products at the test locus in the 3C and BAC template, respectively, and $Ct3^{Ccontrol}$ and $Ct^{BACcontrol}$ quantify PCR product at internal control locus in the 3C and BAC template, respectively.

Quantification and statistical analysis

For quantification of immunostaining, RT-qPCR, cell count, unpaired t tests were used to determine the statistical significance. Mean values +/- standard deviation are shown, unless otherwise stated. In each of the figure legends, n represents the number of biological or technical replicates as stated. Statistical analyses for RNA sequencing data, a likelihood ratio test (LRT) was used. Enrichment of function statistical analyses comparing lnc-pri-miRNA and “other” lncRNAs were performed using the Fisher’s exact test. Enhancer enrichment analyses comparing lnc-pri-miRNA and “other” lncRNAs were performed using the Fisher’s exact test.

Hi-C data analyses were performed using the Mann-Whitney test. The statistical details of experiments can also be found in the figure legends and corresponding results.

References

1. Agarwal, V., Bell, G.W., Nam, J.W., and Bartel, D.P. (2015). Predicting effective microRNA target sites in mammalian mRNAs. Elife *4*.
2. Akhtar-Zaidi, B., Cowper-Sal-lari, R., Corradin, O., Saiakhova, A., Bartels, C.F., Balasubramanian, D., Myeroff, L., Lutterbaugh, J., Jarrar, A., Kalady, M.F.*, et al.* (2012). Epigenomic enhancer profiling defines a signature of colon cancer. Science *336*, 736-739.
3. Benjamini, Y., Drai, D., Elmer, G., Kafkafi, N., and Golani, I. (2001). Controlling the false discovery rate in behavior genetics research. Behav Brain Res *125*, 279-284.
4. Bitetti, A., Mallory, A.C., Golini, E., Carrieri, C., Carreno Gutierrez, H., Perlas, E., Perez-Rico, Y.A., Tocchini-Valentini, G.P., Enright, A.J., Norton, W.H.J.*, et al.* (2018). MicroRNA degradation by a conserved target RNA regulates animal behavior. Nat Struct Mol Biol *25*, 244-251.
5. Calin, G.A., Ferracin, M., Cimmino, A., Di Leva, G., Shimizu, M., Wojcik, S.E., Iorio, M.V., Visone, R., Sever, N.I., Fabbri, M.*, et al.* (2005). A MicroRNA signature associated with prognosis and progression in chronic lymphocytic leukemia. N Engl J Med *353*, 1793-1801.
6. Canzio, D., Nwakeze, C.L., Horta, A., Rajkumar, S.M., Coffey, E.L., Duffy, E.E., Duffie, R., Monahan, K., O'Keeffe, S., Simon, M.D.*, et al.* (2019). Antisense lncRNA Transcription Mediates DNA Demethylation to Drive Stochastic Protocadherin alpha Promoter Choice. Cell *177*, 639-653 e615.
7. Caronia-Brown, G., Anderegg, A., and Awatramani, R. (2016). Expression and functional analysis of the Wnt/beta-catenin induced mir-135a-2 locus in embryonic forebrain development. Neural Dev *11*, 9.
8. Cassidy, S.B., Schwartz, S., Miller, J.L., and Driscoll, D.J. (2012). Prader-Willi syndrome. Genet Med *14*, 10-26.

9. Ceccarelli, M., Barthel, F.P., Malta, T.M., Sabedot, T.S., Salama, S.R., Murray, B.A., Morozova, O., Newton, Y., Radenbaugh, A., Pagnotta, S.M.*, et al.* (2016). Molecular Profiling Reveals Biologically Discrete Subsets and Pathways of Progression in Diffuse Glioma. Cell *164*, 550-563.
10. Chang, T.C., Pertea, M., Lee, S., Salzberg, S.L., and Mendell, J.T. (2015). Genome-wide annotation of microRNA primary transcript structures reveals novel regulatory mechanisms. Genome Res *25*, 1401-1409.
11. Chang, T.C., Wentzel, E.A., Kent, O.A., Ramachandran, K., Mullendore, M., Lee, K.H., Feldmann, G., Yamakuchi, M., Ferlito, M., Lowenstein, C.J.*, et al.* (2007). Transactivation of miR-34a by p53 broadly influences gene expression and promotes apoptosis. Mol Cell *26*, 745-752.
12. Chang, T.C., Yu, D., Lee, Y.S., Wentzel, E.A., Arking, D.E., West, K.M., Dang, C.V., Thomas-Tikhonenko, A., and Mendell, J.T. (2008). Widespread microRNA repression by Myc contributes to tumorigenesis. Nat Genet *40*, 43-50.
13. Chavez, A., Scheiman, J., Vora, S., Pruitt, B.W., Tuttle, M., E, P.R.I., Lin, S., Kiani, S., Guzman, C.D., Wiegand, D.J.*, et al.* (2015). Highly efficient Cas9-mediated transcriptional programming. Nat Methods *12*, 326-328.
14. Cho, S.W., Xu, J., Sun, R., Mumbach, M.R., Carter, A.C., Chen, Y.G., Yost, K.E., Kim, J., He, J., Nevins, S.A.*, et al.* (2018). Promoter of lncRNA Gene PVT1 Is a Tumor-Suppressor DNA Boundary Element. Cell *173*, 1398-1412 e1322.
15. Chou, C.H., Shrestha, S., Yang, C.D., Chang, N.W., Lin, Y.L., Liao, K.W., Huang, W.C., Sun, T.H., Tu, S.J., Lee, W.H.*, et al.* (2018). miRTarBase update 2018: a resource for experimentally validated microRNA-target interactions. Nucleic Acids Res *46*, D296-D302.
16. Danan, M., Schwartz, S., Edelheit, S., and Sorek, R. (2012). Transcriptome-wide discovery of circular RNAs in Archaea. Nucleic Acids Res *40*, 3131-3142.

17. Delto, C.F., Heisler, F.F., Kuper, J., Sander, B., Kneussel, M., and Schindelin, H. (2015). The LisH motif of muskelin is crucial for oligomerization and governs intracellular localization. Structure *23*, 364-373.

18. Deng, L., Shang, L., Bai, S., Chen, J., He, X., Martin-Trevino, R., Chen, S., Li, X.Y., Meng, X., Yu, B.*, et al.* (2014). MicroRNA100 inhibits self-renewal of breast cancer stem-like cells and breast tumor development. Cancer Res *74*, 6648-6660.

19. Djebali, S., Davis, C.A., Merkel, A., Dobin, A., Lassmann, T., Mortazavi, A., Tanzer, A., Lagarde, J., Lin, W., Schlesinger, F.*, et al.* (2012). Landscape of transcription in human cells. Nature *489*, 101-108.

20. Dobin, A., Davis, C.A., Schlesinger, F., Drenkow, J., Zaleski, C., Jha, S., Batut, P., Chaisson, M., and Gingeras, T.R. (2013). STAR: ultrafast universal RNA-seq aligner. Bioinformatics *29*, 15-21.

21. Du, W.W., Yang, W., Liu, E., Yang, Z., Dhaliwal, P., and Yang, B.B. (2016). Foxo3 circular RNA retards cell cycle progression via forming ternary complexes with p21 and CDK2. Nucleic Acids Res *44*, 2846-2858.

22. Duan, J., Ma, X., Shi, J., Xuan, Y., Wang, H., Li, P., Zhang, Y., Fan, Y., Gong, H., Ma, X.*, et al.* (2019). Long noncoding RNA LINC-PINT promotes proliferation through EZH2 and predicts poor prognosis in clear cell renal cell carcinoma. Onco Targets Ther *12*, 4729-4740.

23. Engreitz, J.M., Haines, J.E., Perez, E.M., Munson, G., Chen, J., Kane, M., McDonel, P.E., Guttman, M., and Lander, E.S. (2016). Local regulation of gene expression by lncRNA promoters, transcription and splicing. Nature *539*, 452-455.

24. Fabbri, M., Garzon, R., Cimmino, A., Liu, Z., Zanesi, N., Callegari, E., Liu, S., Alder, H., Costinean, S., Fernandez-Cymering, C.*, et al.* (2007). MicroRNA-29 family reverts aberrant methylation in lung cancer by targeting DNA methyltransferases 3A and 3B. Proc Natl Acad Sci U S A *104*, 15805-15810.

25. Fishilevich, S., Nudel, R., Rappaport, N., Hadar, R., Plaschkes, I., Iny Stein, T., Rosen, N., Kohn, A., Twik, M., Safran, M.*, et al.* (2017). GeneHancer: genome-wide integration of enhancers and target genes in GeneCards. Database (Oxford) *2017*.

26. Flavahan, W.A., Drier, Y., Liau, B.B., Gillespie, S.M., Venteicher, A.S., Stemmer-Rachamimov, A.O., Suva, M.L., and Bernstein, B.E. (2016). Insulator dysfunction and oncogene activation in IDH mutant gliomas. Nature *529*, 110-114.

27. Franca, G.S., Hinske, L.C., Galante, P.A., and Vibranovski, M.D. (2017). Unveiling the Impact of the Genomic Architecture on the Evolution of Vertebrate microRNAs. Front Genet *8*, 34.

28. Francis, O., Han, F., and Adams, J.C. (2013). Molecular phylogeny of a RING E3 ubiquitin ligase, conserved in eukaryotic cells and dominated by homologous components, the muskelin/RanBPM/CTLH complex. PLoS One *8*, e75217.

29. Gilbert, L.A., Larson, M.H., Morsut, L., Liu, Z., Brar, G.A., Torres, S.E., Stern-Ginossar, N., Brandman, O., Whitehead, E.H., Doudna, J.A.*, et al.* (2013). CRISPR-mediated modular RNA-guided regulation of transcription in eukaryotes. Cell *154*, 442-451.

30. Gregory, R.I., Yan, K.P., Amuthan, G., Chendrimada, T., Doratotaj, B., Cooch, N., and Shiekhattar, R. (2004). The Microprocessor complex mediates the genesis of microRNAs. Nature *432*, 235-240.

31. Groff, A.F., Sanchez-Gomez, D.B., Soruco, M.M.L., Gerhardinger, C., Barutcu, A.R., Li, E., Elcavage, L., Plana, O., Sanchez, L.V., Lee, J.C.*, et al.* (2016). In Vivo Characterization of Linc-p21 Reveals Functional cis-Regulatory DNA Elements. Cell Rep *16*, 2178-2186.

32. Hagege, H., Klous, P., Braem, C., Splinter, E., Dekker, J., Cathala, G., de Laat, W., and Forne, T. (2007). Quantitative analysis of chromosome conformation capture assays (3C-qPCR). Nat Protoc *2*, 1722-1733.

33. Herranz, D., Ambesi-Impiombato, A., Palomero, T., Schnell, S.A., Belver, L., Wendorff, A.A., Xu, L., Castillo-Martin, M., Llobet-Navas, D., Cordon-Cardo, C.*, et al.* (2014). A NOTCH1-

driven MYC enhancer promotes T cell development, transformation and acute lymphoblastic leukemia. Nat Med *20*, 1130-1137.

34. Javanmard, A.R., Dokanehiifard, S., Bohlooli, M., and Soltani, B.M. (2020). LOC646329 long non-coding RNA sponges miR-29b-1 and regulates TGFbeta signaling in colorectal cancer. J Cancer Res Clin Oncol *146*, 1205-1215.
35. Johnson, S.M., Grosshans, H., Shingara, J., Byrom, M., Jarvis, R., Cheng, A., Labourier, E., Reinert, K.L., Brown, D., and Slack, F.J. (2005). RAS is regulated by the let-7 microRNA family. Cell *120*, 635-647.
36. Juven-Gershon, T., Cheng, S., and Kadonaga, J.T. (2006). Rational design of a super core promoter that enhances gene expression. Nat Methods *3*, 917-922.
37. Kim, S.W., Ramasamy, K., Bouamar, H., Lin, A.P., Jiang, D., and Aguiar, R.C. (2012). MicroRNAs miR-125a and miR-125b constitutively activate the NF-kappaB pathway by targeting the tumor necrosis factor alpha-induced protein 3 (TNFAIP3, A20). Proc Natl Acad Sci U S A *109*, 7865-7870.
38. Kiss, T. (2001). Small nucleolar RNA-guided post-transcriptional modification of cellular RNAs. EMBO J *20*, 3617-3622.
39. Kopp, F., and Mendell, J.T. (2018). Functional Classification and Experimental Dissection of Long Noncoding RNAs. Cell *172*, 393-407.
40. Kozomara, A., and Griffiths-Jones, S. (2014). miRBase: annotating high confidence microRNAs using deep sequencing data. Nucleic Acids Res *42*, D68-73.
41. Kumar, S., and Hedges, S.B. (1998). A molecular timescale for vertebrate evolution. Nature *392*, 917-920.
42. Lai, F., Damle, S.S., Ling, K.K., and Rigo, F. (2020). Directed RNase H Cleavage of Nascent Transcripts Causes Transcription Termination. Mol Cell *77*, 1032-1043 e1034.

43. Lai, F., Orom, U.A., Cesaroni, M., Beringer, M., Taatjes, D.J., Blobel, G.A., and Shiekhattar, R. (2013). Activating RNAs associate with Mediator to enhance chromatin architecture and transcription. Nature *494*, 497-501.

44. Lampert, F., Stafa, D., Goga, A., Soste, M.V., Gilberto, S., Olieric, N., Picotti, P., Stoffel, M., and Peter, M. (2018). The multi-subunit GID/CTLH E3 ubiquitin ligase promotes cell proliferation and targets the transcription factor Hbp1 for degradation. Elife *7*.

45. Lee, J.S., and Mendell, J.T. (2020). Antisense-Mediated Transcript Knockdown Triggers Premature Transcription Termination. Mol Cell *77*, 1044-1054 e1043.

46. Li, Q., Wang, Y., Wu, S., Zhou, Z., Ding, X., Shi, R., Thorne, R.F., Zhang, X.D., Hu, W., and Wu, M. (2019). CircACC1 Regulates Assembly and Activation of AMPK Complex under Metabolic Stress. Cell Metab *30*, 157-173 e157.

47. Li, W., Notani, D., Ma, Q., Tanasa, B., Nunez, E., Chen, A.Y., Merkurjev, D., Zhang, J., Ohgi, K., Song, X.*, et al.* (2013). Functional roles of enhancer RNAs for oestrogen-dependent transcriptional activation. Nature *498*, 516-520.

48. Li, Y., Zheng, Q., Bao, C., Li, S., Guo, W., Zhao, J., Chen, D., Gu, J., He, X., and Huang, S. (2015). Circular RNA is enriched and stable in exosomes: a promising biomarker for cancer diagnosis. Cell Res *25*, 981-984.

49. Liao, Y., Smyth, G.K., and Shi, W. (2014). featureCounts: an efficient general purpose program for assigning sequence reads to genomic features. Bioinformatics *30*, 923-930.

50. Liu, S.J., Horlbeck, M.A., Cho, S.W., Birk, H.S., Malatesta, M., He, D., Attenello, F.J., Villalta, J.E., Cho, M.Y., Chen, Y.*, et al.* (2017). CRISPRi-based genome-scale identification of functional long noncoding RNA loci in human cells. Science *355*.

51. Liu, S.J., Nowakowski, T.J., Pollen, A.A., Lui, J.H., Horlbeck, M.A., Attenello, F.J., He, D., Weissman, J.S., Kriegstein, A.R., Diaz, A.A.*, et al.* (2016). Single-cell analysis of long non-coding RNAs in the developing human neocortex. Genome Biol *17*, 67.

52. Loven, J., Hoke, H.A., Lin, C.Y., Lau, A., Orlando, D.A., Vakoc, C.R., Bradner, J.E., Lee, T.I., and Young, R.A. (2013). Selective inhibition of tumor oncogenes by disruption of super-enhancers. Cell *153*, 320-334.

53. Lu, Y., Zhao, X., Liu, Q., Li, C., Graves-Deal, R., Cao, Z., Singh, B., Franklin, J.L., Wang, J., Hu, H.*, et al.* (2017). lncRNA MIR100HG-derived miR-100 and miR-125b mediate cetuximab resistance via Wnt/beta-catenin signaling. Nat Med *23*, 1331-1341.

54. Luo, S., Lu, J.Y., Liu, L., Yin, Y., Chen, C., Han, X., Wu, B., Xu, R., Liu, W., Yan, P.*, et al.* (2016). Divergent lncRNAs Regulate Gene Expression and Lineage Differentiation in Pluripotent Cells. Cell Stem Cell *18*, 637-652.

55. Marin-Bejar, O., Mas, A.M., Gonzalez, J., Martinez, D., Athie, A., Morales, X., Galduroz, M., Raimondi, I., Grossi, E., Guo, S.*, et al.* (2017). The human lncRNA LINC-PINT inhibits tumor cell invasion through a highly conserved sequence element. Genome Biol *18*, 202.

56. Melo, C.A., Drost, J., Wijchers, P.J., van de Werken, H., de Wit, E., Oude Vrielink, J.A., Elkon, R., Melo, S.A., Leveille, N., Kalluri, R.*, et al.* (2013). eRNAs are required for p53-dependent enhancer activity and gene transcription. Mol Cell *49*, 524-535.

57. Memczak, S., Jens, M., Elefsinioti, A., Torti, F., Krueger, J., Rybak, A., Maier, L., Mackowiak, S.D., Gregersen, L.H., Munschauer, M.*, et al.* (2013). Circular RNAs are a large class of animal RNAs with regulatory potency. Nature *495*, 333-338.

58. Nagano, T., Varnai, C., Schoenfelder, S., Javierre, B.M., Wingett, S.W., and Fraser, P. (2015). Comparison of Hi-C results using in-solution versus in-nucleus ligation. Genome Biol *16*, 175.

59. Nam, J., Dong, P., Tarpine, R., Istrail, S., and Davidson, E.H. (2010). Functional cis-regulatory genomics for systems biology. Proc Natl Acad Sci U S A *107*, 3930-3935.

60. Naumova, N., Smith, E.M., Zhan, Y., and Dekker, J. (2012). Analysis of long-range chromatin interactions using Chromosome Conformation Capture. Methods *58*, 192-203.

61. Ng, S.Y., Bogu, G.K., Soh, B.S., and Stanton, L.W. (2013). The long noncoding RNA RMST interacts with SOX2 to regulate neurogenesis. Mol Cell *51*, 349-359.

62. Nord, H., Hartmann, C., Andersson, R., Menzel, U., Pfeifer, S., Piotrowski, A., Bogdan, A., Kloc, W., Sandgren, J., Olofsson, T.*, et al.* (2009). Characterization of novel and complex genomic aberrations in glioblastoma using a 32K BAC array. Neuro Oncol *11*, 803-818.

63. Orom, U.A., Derrien, T., Beringer, M., Gumireddy, K., Gardini, A., Bussotti, G., Lai, F., Zytnicki, M., Notredame, C., Huang, Q.*, et al.* (2010). Long noncoding RNAs with enhancer-like function in human cells. Cell *143*, 46-58.

64. Papagregoriou, G., Erguler, K., Dweep, H., Voskarides, K., Koupepidou, P., Athanasiou, Y., Pierides, A., Gretz, N., Felekkis, K.N., and Deltas, C. (2012). A miR-1207-5p binding site polymorphism abolishes regulation of HBEGF and is associated with disease severity in CFHR5 nephropathy. PLoS One *7*, e31021.

65. Park, S.Y., Lee, J.H., Ha, M., Nam, J.W., and Kim, V.N. (2009). miR-29 miRNAs activate p53 by targeting p85 alpha and CDC42. Nat Struct Mol Biol *16*, 23-29.

66. Pekarsky, Y., Santanam, U., Cimmino, A., Palamarchuk, A., Efanov, A., Maximov, V., Volinia, S., Alder, H., Liu, C.G., Rassenti, L.*, et al.* (2006). Tcl1 expression in chronic lymphocytic leukemia is regulated by miR-29 and miR-181. Cancer Res *66*, 11590-11593.

67. Phillips, J.E., and Corces, V.G. (2009). CTCF: master weaver of the genome. Cell *137*, 1194-1211.

68. Piwecka, M., Glazar, P., Hernandez-Miranda, L.R., Memczak, S., Wolf, S.A., Rybak-Wolf, A., Filipchyk, A., Klironomos, F., Cerda Jara, C.A., Fenske, P.*, et al.* (2017). Loss of a mammalian circular RNA locus causes miRNA deregulation and affects brain function. Science *357*.

69. Pomerantz, M.M., Li, F., Takeda, D.Y., Lenci, R., Chonkar, A., Chabot, M., Cejas, P., Vazquez, F., Cook, J., Shivdasani, R.A.*, et al.* (2015). The androgen receptor cistrome is extensively reprogrammed in human prostate tumorigenesis. Nat Genet *47*, 1346-1351.

70. Pons-Espinal, M., Gasperini, C., Marzi, M.J., Braccia, C., Armirotti, A., Potzsch, A., Walker, T.L., Fabel, K., Nicassio, F., Kempermann, G.*, et al.* (2019). MiR-135a-5p Is Critical for Exercise-Induced Adult Neurogenesis. Stem Cell Reports *12*, 1298-1312.

71. Profumo, V., Forte, B., Percio, S., Rotundo, F., Doldi, V., Ferrari, E., Fenderico, N., Dugo, M., Romagnoli, D., Benelli, M.*, et al.* (2019). LEADeR role of miR-205 host gene as long noncoding RNA in prostate basal cell differentiation. Nat Commun *10*, 307.

72. Pulido-Quetglas, C., Aparicio-Prat, E., Arnan, C., Polidori, T., Hermoso, T., Palumbo, E., Ponomarenko, J., Guigo, R., and Johnson, R. (2017). Scalable Design of Paired CRISPR Guide RNAs for Genomic Deletion. PLoS Comput Biol *13*, e1005341.

73. Qi, L.S., Larson, M.H., Gilbert, L.A., Doudna, J.A., Weissman, J.S., Arkin, A.P., and Lim, W.A. (2013). Repurposing CRISPR as an RNA-guided platform for sequence-specific control of gene expression. Cell *152*, 1173-1183.

74. Quinn, J.J., and Chang, H.Y. (2016). Unique features of long non-coding RNA biogenesis and function. Nat Rev Genet *17*, 47-62.

75. Rahl, P.B., Lin, C.Y., Seila, A.C., Flynn, R.A., McCuine, S., Burge, C.B., Sharp, P.A., and Young, R.A. (2010). c-Myc regulates transcriptional pause release. Cell *141*, 432-445.

76. Rao, S.S., Huntley, M.H., Durand, N.C., Stamenova, E.K., Bochkov, I.D., Robinson, J.T., Sanborn, A.L., Machol, I., Omer, A.D., Lander, E.S.*, et al.* (2014). A 3D map of the human genome at kilobase resolution reveals principles of chromatin looping. Cell *159*, 1665-1680.

77. Ron, G., Globerson, Y., Moran, D., and Kaplan, T. (2017). Promoter-enhancer interactions identified from Hi-C data using probabilistic models and hierarchical topological domains. Nat Commun *8*, 2237.

78. Roush, S., and Slack, F.J. (2008). The let-7 family of microRNAs. Trends Cell Biol *18*, 505-516.

79. Ru, P., Hu, P., Geng, F., Mo, X., Cheng, C., Yoo, J.Y., Cheng, X., Wu, X., Guo, J.Y., Nakano, I., *et al.* (2016). Feedback Loop Regulation of SCAP/SREBP-1 by miR-29 Modulates EGFR Signaling-Driven Glioblastoma Growth. Cell Rep *16*, 1527-1535.

80. Sanger, H.L., Klotz, G., Riesner, D., Gross, H.J., and Kleinschmidt, A.K. (1976). Viroids are single-stranded covalently closed circular RNA molecules existing as highly base-paired rod-like structures. Proc Natl Acad Sci U S A *73*, 3852-3856.

81. Sengupta, S., den Boon, J.A., Chen, I.H., Newton, M.A., Stanhope, S.A., Cheng, Y.J., Chen, C.J., Hildesheim, A., Sugden, B., and Ahlquist, P. (2008). MicroRNA 29c is down-regulated in nasopharyngeal carcinomas, up-regulating mRNAs encoding extracellular matrix proteins. Proc Natl Acad Sci U S A *105*, 5874-5878.

82. Sloan, K.E., Leisegang, M.S., Doebele, C., Ramirez, A.S., Simm, S., Safferthal, C., Kretschmer, J., Schorge, T., Markoutsa, S., Haag, S., *et al.* (2015). The association of late-acting snoRNPs with human pre-ribosomal complexes requires the RNA helicase DDX21. Nucleic Acids Res *43*, 553-564.

83. Sonoda, Y., Ozawa, T., Hirose, Y., Aldape, K.D., McMahon, M., Berger, M.S., and Pieper, R.O. (2001). Formation of intracranial tumors by genetically modified human astrocytes defines four pathways critical in the development of human anaplastic astrocytoma. Cancer Res *61*, 4956-4960.

84. Stadhouders, R., Kolovos, P., Brouwer, R., Zuin, J., van den Heuvel, A., Kockx, C., Palstra, R.J., Wendt, K.S., Grosveld, F., van Ijcken, W., *et al.* (2013). Multiplexed chromosome conformation capture sequencing for rapid genome-scale high-resolution detection of long-range chromatin interactions. Nat Protoc *8*, 509-524.

85. Stewart, S.A., Dykxhoorn, D.M., Palliser, D., Mizuno, H., Yu, E.Y., An, D.S., Sabatini, D.M., Chen, I.S., Hahn, W.C., Sharp, P.A., *et al.* (2003). Lentivirus-delivered stable gene silencing by RNAi in primary cells. RNA *9*, 493-501.

86. Sun, Q., Tripathi, V., Yoon, J.H., Singh, D.K., Hao, Q., Min, K.W., Davila, S., Zealy, R.W., Li, X.L., Polycarpou-Schwarz, M.*, et al.* (2018). MIR100 host gene-encoded lncRNAs regulate cell cycle by modulating the interaction between HuR and its target mRNAs. Nucleic Acids Res *46*, 10405-10416.

87. Treiber, T., Treiber, N., and Meister, G. (2019). Regulation of microRNA biogenesis and its crosstalk with other cellular pathways. Nat Rev Mol Cell Biol *20*, 5-20.

88. Tseng, Y.Y., Moriarity, B.S., Gong, W., Akiyama, R., Tiwari, A., Kawakami, H., Ronning, P., Reuland, B., Guenther, K., Beadnell, T.C.*, et al.* (2014). PVT1 dependence in cancer with MYC copy-number increase. Nature *512*, 82-86.

89. Ulitsky, I., and Bartel, D.P. (2013). lincRNAs: genomics, evolution, and mechanisms. Cell *154*, 26-46.

90. Vicens, Q., and Westhof, E. (2014). Biogenesis of Circular RNAs. Cell *159*, 13-14.

91. Wang, K.C., Yang, Y.W., Liu, B., Sanyal, A., Corces-Zimmerman, R., Chen, Y., Lajoie, B.R., Protacio, A., Flynn, R.A., Gupta, R.A.*, et al.* (2011). A long noncoding RNA maintains active chromatin to coordinate homeotic gene expression. Nature *472*, 120-124.

92. Wang, Y., Medvid, R., Melton, C., Jaenisch, R., and Blelloch, R. (2007). DGCR8 is essential for microRNA biogenesis and silencing of embryonic stem cell self-renewal. Nat Genet *39*, 380-385.

93. Won, H., de la Torre-Ubieta, L., Stein, J.L., Parikshak, N.N., Huang, J., Opland, C.K., Gandal, M.J., Sutton, G.J., Hormozdiari, F., Lu, D.*, et al.* (2016). Chromosome conformation elucidates regulatory relationships in developing human brain. Nature *538*, 523-527.

94. Wu, H., Yang, L., and Chen, L.L. (2017). The Diversity of Long Noncoding RNAs and Their Generation. Trends Genet *33*, 540-552.

95. Wysocka, J., Reilly, P.T., and Herr, W. (2001). Loss of HCF-1-chromatin association precedes temperature-induced growth arrest of tsBN67 cells. Mol Cell Biol *21*, 3820-3829.

96. Xing, Y.H., Yao, R.W., Zhang, Y., Guo, C.J., Jiang, S., Xu, G., Dong, R., Yang, L., and Chen, L.L. (2017). SLERT Regulates DDX21 Rings Associated with Pol I Transcription. Cell *169*, 664-678 e616.

97. Xu, H., Sun, J., Shi, C., Sun, C., Yu, L., Wen, Y., Zhao, S., Liu, J., Xu, J., Li, H.*, et al.* (2015). miR-29s inhibit the malignant behavior of U87MG glioblastoma cell line by targeting DNMT3A and 3B. Neurosci Lett *590*, 40-46.

98. Yan, C., Chen, Y., Kong, W., Fu, L., Liu, Y., Yao, Q., and Yuan, Y. (2017). PVT1-derived miR-1207-5p promotes breast cancer cell growth by targeting STAT6. Cancer Sci *108*, 868-876.

99. Yanaihara, N., Caplen, N., Bowman, E., Seike, M., Kumamoto, K., Yi, M., Stephens, R.M., Okamoto, A., Yokota, J., Tanaka, T.*, et al.* (2006). Unique microRNA molecular profiles in lung cancer diagnosis and prognosis. Cancer Cell *9*, 189-198.

100. Yang, L., Duff, M.O., Graveley, B.R., Carmichael, G.G., and Chen, L.L. (2011). Genomewide characterization of non-polyadenylated RNAs. Genome Biol *12*, R16.

101. Yeo, G.W., Coufal, N.G., Liang, T.Y., Peng, G.E., Fu, X.D., and Gage, F.H. (2009). An RNA code for the FOX2 splicing regulator revealed by mapping RNA-protein interactions in stem cells. Nat Struct Mol Biol *16*, 130-137.

102. Yin, Q.F., Yang, L., Zhang, Y., Xiang, J.F., Wu, Y.W., Carmichael, G.G., and Chen, L.L. (2012). Long noncoding RNAs with snoRNA ends. Mol Cell *48*, 219-230.

103. Zhang, H., Deng, T., Ge, S., Liu, Y., Bai, M., Zhu, K., Fan, Q., Li, J., Ning, T., Tian, F.*, et al.* (2019a). Exosome circRNA secreted from adipocytes promotes the growth of hepatocellular carcinoma by targeting deubiquitination-related USP7. Oncogene *38*, 2844-2859.

104. Zhang, H., Zhu, L., Bai, M., Liu, Y., Zhan, Y., Deng, T., Yang, H., Sun, W., Wang, X., Zhu, K.*, et al.* (2019b). Exosomal circRNA derived from gastric tumor promotes white adipose browning by targeting the miR-133/PRDM16 pathway. Int J Cancer *144*, 2501-2515.

105. Zhang, Y., Zhang, X.O., Chen, T., Xiang, J.F., Yin, Q.F., Xing, Y.H., Zhu, S., Yang, L., and Chen, L.L. (2013). Circular intronic long noncoding RNAs. Mol Cell *51*, 792-806.

Publishing Agreement

It is the policy of the University to encourage open access and broad distribution of all theses, dissertations, and manuscripts. The Graduate Division will facilitate the distribution of UCSF theses, dissertations, and manuscripts to the UCSF Library for open access and distribution. UCSF will make such theses, dissertations, and manuscripts accessible to the public and will take reasonable steps to preserve these works in perpetuity.

I hereby grant the non-exclusive, perpetual right to The Regents of the University of California to reproduce, publicly display, distribute, preserve, and publish copies of my thesis, dissertation, or manuscript in any form or media, now existing or later derived, including access online for teaching, research, and public service purposes.

DocuSigned by:
Daniel He
0C112F97A1F64A1...
Author Signature

3/9/2021
Date